Technische Universität München

The key role of Satellite Laser Ranging towards the integrated estimation of geometry, rotation and gravitational field of the Earth

Dissertation
von

Mathis Bloßfeld

Fachgebiet Satellitengeodäsie

Ingenieurfakultät Bau Geo Umwelt

Ingenieurfakultät Bau Geo Umwelt

Fachgebiet Satellitengeodäsie

The key role of Satellite Laser Ranging towards the integrated estimation of geometry, rotation and gravitational field of the Earth

Mathis Bloßfeld

Vollständiger Abdruck der von der Ingenieurfakultät Bau Geo Umwelt der Technischen Universität München zur Erlangung des akademischen Grades eines

Doktor - Ingenieurs

genehmigten Dissertation.

Vorsitzende(r):	Univ.-Prof. Dr. rer. nat. T. Kolbe
Prüfer der Dissertation:	1. Univ.-Prof. Dr. phil. nat. U. Hugentobler
	2. Univ.-Prof. Dr.-Ing. F. Seitz
	3. Univ.-Prof. Dr. phil. nat. habil. M. Rothacher, Eidgenössische Technische Universität Zürich, Schweiz

Die Dissertation wurde am 24.09.2014 bei der Technischen Universität München eingereicht und durch die Ingenieurfakultät Bau Geo Umwelt am 22.01.2015 angenommen.

Kurzfassung

Im Jahr 2007 wurde das Globale Geodätische Beobachtungssystem GGOS als eine vollwertige Komponente der Internationalen Assoziation für Geodäsie (IAG) eingerichtet. Ein primäres Ziel von GGOS ist die Integration von geometrischen und gravimetrischen Beobachtungsverfahren zur konsistenten Bestimmung geodätisch-geophysikalischer Parameter. Dabei stützt sich GGOS auf die Daten und Services der IAG. Um dieses Ziel zu erreichen ist neben der Kombination unterschiedlicher Beobachtungstypen auch eine gemeinsame Schätzung von Stationskoordinaten (TRF), Erdorientierungsparametern (EOP) und Koeffizienten des Erdschwerefelds (Stokes-Koeffizienten) nötig. Bis jetzt wurde diese Kombination von geometrischen und gravimetrischen Beobachtungen aber noch nicht vollständig realisiert.

Diese Dissertation untersucht die bestehenden Korrelationen zwischen den oben genannten Parametergruppen und stellt damit einen wichtigen Schritt im Hinblick auf den Integrationsgedanken von GGOS dar. Eine Möglichkeit dazu bietet die Laserentfernungsmessung zu Satelliten (SLR), die in dieser Arbeit innerhalb einer inter-technischen (SLR kombiniert mit GNSS und VLBI) und einer intra-technischen Kombination (SLR zu mehreren Satelliten) untersucht wird. SLR bietet aufgrund der hohen Sensitivität für die oben genannten Parameter (TRF, EOP, Stokes-Koeffizienten) die Möglichkeit, bestehende Parameterabhängigkeiten in einer gemeinsamen Schätzung zu untersuchen.

Die vorliegende Arbeit basiert im Wesentlichen auf fünf Hauptautor-Publikationen, deren Ergebnisse durch vier Koautor-Publikationen ergänzt werden. Zum ersten Mal wird die Berechnung so genannter Epochenreferenzrahmen (ERFs) vorgestellt, die eine gute Approximation von nicht modellierten nicht-linearen Stationsbewegungen erlauben. Im Gegensatz zu dem konventionellen linearen Modell der Stationsbewegungen realisieren die ERFs eine zeitlich-hochaufgelöste Schätzung der Stationspositionen. Dabei kommt SLR eine wesentliche Rolle zu, da die zeitlich hoch aufgelösten Referenzrahmen ihre Ursprungsinformation von SLR erhalten. Im Gegensatz zu den ERFs werden die vernachlässigten Stationsbewegungen im linearen Ansatz durch Parameterabhängigkeiten von Translationen und Rotationen (aufgrund einer nicht-optimalen Verteilung von Bodenstationen) in zeitgleich mitbestimmte Parameter wie z.B. die Polkoordinaten gezwungen. Allerdings weisen die ERFs aufgrund des variablen Stationsnetzes ein instabileres geodätisches Datum auf als die konventionellen Referenzrahmen. Eine Möglichkeit, die Datumsstabilität zu erhöhen, ist die Vergrößerung des Kombinationsintervalls (z.B. von einer auf vier Wochen) was jedoch eine Verschlechterung der Approximationsgenauigkeit zur Folge hat.

Neben den Polkoordinaten ist die Tageslänge (engl. Length Of Day; LOD), die über Satellitenbeobachtungen bestimmt wird, durch große Systematiken beeinflusst. Der Grund für diese Systematiken wird in dieser Arbeit mit Hilfe von SLR-Beobachtungen untersucht. Dabei werden die theoretischen Beziehungen zwischen der Satellitenbahn, LOD und dem Stokes-Koeffizienten C_{20} hergeleitet. Für eine quantitative Abschätzung dieser Parameterbeziehung werden LOD-Zeitreihen mit verschiedenen Erdschwerefeldmodellen und Satellitenkonstellationen berechnet und verglichen. Zudem werden säkulare Effekte der Knotendrehung, hervorgerufen durch relativistische und empirische Beschleunigungen, diskutiert.

Neben der separaten Schätzung von Stationskoordinaten und EOP wird auch die Schätzung von Stokes-Koeffizienten analysiert. Um die Parameterabhängigkeit der Satellitenbahn von den Stokes-Koeffizienten 2. Grades weiter zu reduzieren, werden SLR-Beobachtungen von bis zu zehn Satelliten miteinander kombiniert. Dabei wird der Einfluss jedes Satelliten auf die kombinierte Lösung über die Dekorrelation von Satellitenbahnparametern und C_{20} bestimmt. Die geschätzten Koeffizienten werden anschließend durch externe Daten validiert und diskutiert (z. B. äquatoriale Anregungsfunktionen von Polkoordinaten und antarktische Eismassentrends).

Der letzte Teil dieser Dissertation beschäftigt sich mit den Parameterabhängigkeiten, die bei einer gemeinsamen Schätzung aller genannten Parameter berücksichtigt werden müssen. Das Verständnis und die Behandlung dieser Abhängigkeiten ist grundlegend für eine integrierte Schätzung. Durch die Untersuchung der SLR-Multisatellitenlösung, bei der alle Parameter gleichzeitig geschätzt werden, wird ein vertieftes Verständnis der Parameterabhängigkeiten erreicht, das anschließend auch auf andere Beobachtungsverfahren übertragen werden kann. Diese Erkenntnisse tragen zu einer Kombination von geometrischen und gravimetrischen Beobachtungsverfahren bei.

Abstract

In 2007, the Global Geodetic Observing System (GGOS) was installed as a full component of the International Association of Geodesy (IAG). One primary goal of GGOS is the integration of geometric and gravimetric observation techniques to estimate consistent geodetic-geophysical parameters. Thereby, GGOS is based on the data and services of the IAG. Besides the combination of different geodetic techniques, also the common estimation of the station coordinates (TRF), Earth Orientation Parameters (EOP) and coefficients of the Earth's gravitational field (Stokes coefficients) is necessary in order to reach this goal. However, the combination of all geometric and gravimetric observation techniques is not yet fully realized.

A major step towards the GGOS idea of parameter integration would be the understanding of the existing correlations between the above mentioned fundamental geodetic parameter groups. This topic is the major objective of this thesis. One possibility to study the interactions is the use of Satellite Laser Ranging (SLR) in an inter-technique combination with Global Navigation Satellite Systems (GNSS) and Very Long Baseline Interferometry (VLBI) or the intra-technique combination of multiple SLR-tracked satellites. SLR plays a key role in this thesis since it is the unique technique which is sensitive to all parameter groups and allows an integrated parameter estimation with very high accuracy.

The present work is based on five first-author publications which are supplemented by four co-author publications. In this framework, for the first time an extensive discussion of a refined global Terrestrial Reference Frame (TRF) estimation procedure, the estimation of so-called Epoch Reference Frames (ERFs) is presented. In contrast to the conventional linear station motion model, the ERFs provide frequently estimated station coordinates and Earth Orientation Parameters (EOP) which allow to approximate not modeled non-linear station motions very accurately. Thereby, SLR provides the origin information for the frequently estimated ERFs. The neglected non-linear station motions in the conventional TRF realizations are forced via the correlation of translations and rotations (due to a non-optimal ground station network) into the terrestrial pole coordinates. In contrast to this, the pole coordinates of the Epoch Reference Frame (ERF)s are only partly biased. However, due to the sparse and varying ground station network, the ERFs have a more unstable datum than the conventional TRFs. One possibility to improve the ERF datum stability is to enlarge the sampling interval (e.g., from one week to four weeks) which results in a decreased ability of the ERFs to monitor short-term station motions.

Besides the pole coordinates, also significantly corrupted satellite-derived Length Of Day (LOD) values have been found. The reason for this systematic error is investigated in this thesis on the basis of SLR estimates. The theoretical relationship between the orbital elements, LOD and the Stokes coefficient C_{20} is worked out. To quantify this interaction, several time series using different a priori models for the Earth's gravitational field and different satellite constellations have been computed and compared. Furthermore, secular effects on the nodal precession due to relativistic effects and empirical accelerations are analyzed.

In addition to the separate estimation of station coordinates and EOP, also the estimation of Stokes coefficients is analyzed. In order to further decorrelate the orbital elements and Stokes coefficients, the combination of up to ten different SLR-tracked satellites have been studied. Thereby, the impact of each satellite on the decorrelation of satellite orbit parameters and C_{20} is investigated. Afterwards, the resulting second-degree Stokes coefficients are validated w.r.t. other external state-of-the-art time series and datasets (e.g., equatorial excitation functions of polar motion, Antarctic ice mass trends).

The last part of this thesis discusses in detail the interactions and correlations which have to be considered if the fundamental geodetic parameters are estimated in one common adjustment. The understanding and correct handling of these interactions is essential for the integrated estimation. Based on the findings of the SLR single-technique multi-parameter solution, the achieved understandings of the parameter interactions can be transferred to other geodetic space techniques and might support the combination of geometric and gravimetric observations in future.

Preface (Reader's guide)

This cumulative dissertation is primarily based on the following five first-author publications:

P-I Bloßfeld M., Seitz M., Angermann D. (2014) Non-linear station motions in epoch and multi-year reference frames, In: J Geodesy 88(1), pp: 45-63, DOI: 10.1007/s00190-013-0668-6

P-II Bloßfeld M., Gerstl M., Hugentobler U., Angermann D., Müller H. (2014) Systematic effects in LOD from SLR observations, In: Adv Space Res 54, pp: 1049–1063, DOI: 10.1016/j.asr.2014.06.009

P-III Bloßfeld M., Müller H., Gerstl M., Štefka V., Bouman J., Göttl F., Horwath M. (2015) Second-degree Stokes coefficients from multi-satellite SLR, In: J Geodesy, in review

P-IV Bloßfeld M., Seitz M., Angermann D. (2015) Epoch reference frames as short-term realizations of the ITRS, In: IAG Symposia Series 143, in press

P-V Bloßfeld M., Štefka V., Müller H., Gerstl M. (2015) Satellite Laser Ranging – A tool to realize GGOS?, In: IAG Symposia Series 143, in press

Within this dissertation, the papers are cited using the abbreviation 'P' for 'publication' and a Roman number for the number of the paper.

This dissertation is split into two parts:

The first part comprises the scope of the thesis, the introduction, a description of the applied methodology, a short introduction of the used software, the theoretical foundations of the estimated fundamental geodetic parameters, discussions of parameter limitations and strategies to resolve them. Finally, the first-author publications are summarized and the first-author's own contributions to each publication are described. In the "Abbreviations and Nomenclature" chapter, the used abbreviations and parameter/variable definitions are summarized.

The second part of this dissertation contains full-text reformatted versions of the published, accepted or submitted first-author publications.

In addition to the first-author publications, the following four co-author publications supplement the results of this dissertation:

P-A Seitz M., Angermann D., Bloßfeld M., Drewes H., Gerstl M. (2012) The 2008 DGFI Realization of the ITRS: DTRF2008. In: J Geodesy 86(12), pp: 1097–1123, DOI: 10.1007/s00190-012-0567-2

P-B Rodriguez-Solano C. J., Hugentobler U., Steigenberger P., Bloßfeld M., Fritsche M. (2014) Reducing the draconitic errors in GNSS geodetic products, In: J Geodesy 88(6), pp: 559–574, DOI: 10.1007/s00190-014-0704-1

P-C Haberkorn C., Bloßfeld M., Bouman J., Fuchs M., Schmidt M. (2015) Combined estimation of the Earth's gravity field using SLR and GRACE data, In: IAG Symposia Series 143, in press

P-D Göttl F., Schmidt M., Seitz F., Bloßfeld M. (2015) Separation of atmospheric, oceanic and hydrological polar motion excitation mechanisms by a combination of geometric and gravimetric space observations, In: J Geodesy, online first, DOI: 10.1007/s00190-014-0782-0

Contents

1 Introduction

The scope of geodesy has changed during the past two decades. 20 years ago, geodesy was the discipline of measuring the shape, rotation and gravitational field of the Earth. Nowadays, this is only one part since geodesy turned into the multidisciplinary science of providing reliable and accurate measurements of a highly dynamic and complex system Earth including the discussion of causes for the observed changes (Plag and Pearlman, 2009). Due to the increased observation accuracy, former disturbances have changed into target values (e.g., physical atmospheric and ionospheric parameters; Dettmering et al., 2010). The foundations for this development are the significant technological improvements of the geodetic space techniques, namely the Global Navigation Satellite Systems (GNSS), Lunar and Satellite Laser Ranging (LLR, SLR), Very Long Baseline Interferometry (VLBI), Doppler Orbithography and Radiopositioning Integrated by Satellite (DORIS), and the launch of a wide range of Earth observing satellites such as, e.g., the altimeter missions Topex/Poseidon, Jason 1/2 or the gravimetric missions CHAllenging Minisatellite Payload (CHAMP), GRAvity recovery and Climate Experiment (GRACE) and Gravity field and steady-state Ocean Circulation Explorer (GOCE) in the last 20 years.

Using this variety of sensor systems, geodesy is able to provide a significant contribution to the monitoring and understanding of global change. In 1999, the geodetic community, organized under the umbrella of the IAG, recognized the need to integrate this unique constellation of measurement techniques into one observation system (Rummel et al., 2005). Therefore, in 2003, the International Union of Geodesy and Geophysics (IUGG) is considering (IUGG Resolution 3, 2003)

"*That the International Association of Geodesy (IAG) has taken an initiative towards the realization of the IUGG Resolution no.1 adopted at the 22nd General Assembly in Birmingham 1999 by installing the Integrated Global Geodetic Observing System (IGGOS);*"

At the IUGG General Assembly in Perugia (Italy), the IUGG Resolution 3 (2007) recognizes the significant progress of the IGGOS project since 2003 (the project was renamed to GGOS in 2005) and considers that the IAG elevates the status of GGOS from a project to a full component of the IAG.

The scope of GGOS is the use of observations to provide the spatial and temporal changes of surface dynamics on a global scale plus an assessment of mass anomalies, mass transports and mass exchange processes (Rummel et al., 2005). The observations which are incorporated in GGOS serve as a basis for the so-called "three pillars" of geodesy (Plag and Pearlman, 2009). These pillars are the Earth's time-dependent **geometric shape**, **rotation** and **gravitational field**. Terrestrial Reference Frames (TRFs) and satellite orbits act as the connection between the pillars. The fundamental geodetic parameters associated to the three pillars are the station coordinates, the Earth Orientation Parameters (EOP) and the Stokes coefficients.

The International Terrestrial Reference Frame (ITRF) plays a fundamental role in geodesy. The prerequisite for the geodetic detection of climate change impacts is a long-term stable, globally uniform and universally available reference frame (Rummel, 2014). The EOP are necessary to transform the observations based on satellite missions from the celestial reference system into an Earth-fixed reference system. The Stokes coefficients can be used to describe mass-related phenomena in the Earth interior and in its non-rigid envelope (Torge, 2001). As a qualitative goal, Gross et al. (2009) formulate a user requirement of 1 mm accuracy and 0.1 mm/y stability for all parameters. This accuracy can only be achieved if current limitations are resolved and if the strengths of different observation techniques are combined.

The integration of different observation systems and satellite constellations into one observing system results in the integrated estimation of the fundamental geodetic parameters in one common adjustment. However, the combination of all geometric and gravimetric observation techniques is still not well addressed in the current literature. Physical interactions and parameter correlations have been studied using simulations or test cases. An example for the inter-technique combination of GNSS, VLBI and SLR is the "Global Geodetic Observing System – Deutschland (GGOS-D)" project (Rothacher et al., 2011). The authors show that a homogeneous reprocessing plus a rigorous combination lead to a TRF which significantly improves the combined EOP.

Since SLR is the only technique that provides information with very high accuracy to all three pillars of GGOS, the technique is used in this thesis in order to study parameter interactions and correlations. Within this thesis, **the key role of SLR towards the integrated estimation of geometry, rotation and gravitational field of the Earth** is outlined. The thesis provides the framework for the following five first-author publications:

P-I Bloßfeld M., Seitz M., Angermann D. (2014) Non-linear station motions in epoch and multi-year reference frames, In: J Geodesy 88(1), pp: 45-63, DOI: 10.1007/s00190-013-0668-6

P-II Bloßfeld M., Gerstl M., Hugentobler U., Angermann D., Müller H. (2014) Systematic effects in LOD from SLR observations, In: Adv Space Res 54, pp: 1049–1063, DOI: 10.1016/j.asr.2014.06.009

P-III Bloßfeld M., Müller H., Gerstl M., Štefka V., Bouman J., Göttl F., Horwath M. (2015) Second-degree Stokes coefficients from multi-satellite SLR, In: J Geodesy, in review

P-IV Bloßfeld M., Seitz M., Angermann D. (2015) Epoch reference frames as short-term realizations of the ITRS, In: IAG Symposia Series 143, in press

P-V Bloßfeld M., Štefka V., Müller H., Gerstl M. (2015) Satellite Laser Ranging – A tool to realize GGOS?, In: IAG Symposia Series 143, in press

These publications focus on various aspects towards the integrated estimation of the mentioned parameters and the role of SLR within GGOS. Therefore, the characteristics of SLR in the inter- and intra-technique combination are studied. Furthermore, possibilities to fully exploit the potential of SLR to contribute to the determination of TRF, EOP and Stokes coefficients are revealed. Figure 1.1 shows the three pillars and the main achievements of the five first-author publications to the fundamental associated parameters.

Starting from the combined multi-year reference frame (MRF) computation, the investigations published in P-I and P-IV lead to the combined Epoch Reference Frames (ERFs). As an output of the ERFs, improved terrestrial pole coordinates but still strongly corrupted Length Of Day (LOD) values have been obtained. The reason for this corruption is investigated in P-II. The output of P-II is the understanding of the correlations between LOD and the Stokes coefficient C_{20}. As a conclusion, the need for a higher decorrelation of these parameters (e.g., by using SLR orbits with different altitudes and inclinations) can be formulated. P-III describes in detail the SLR multi-satellite solution and presents an extensive validation of the obtained second-degree Stokes coefficients. Finally, in P-V all three parameter groups are estimated using multi-satellite SLR.

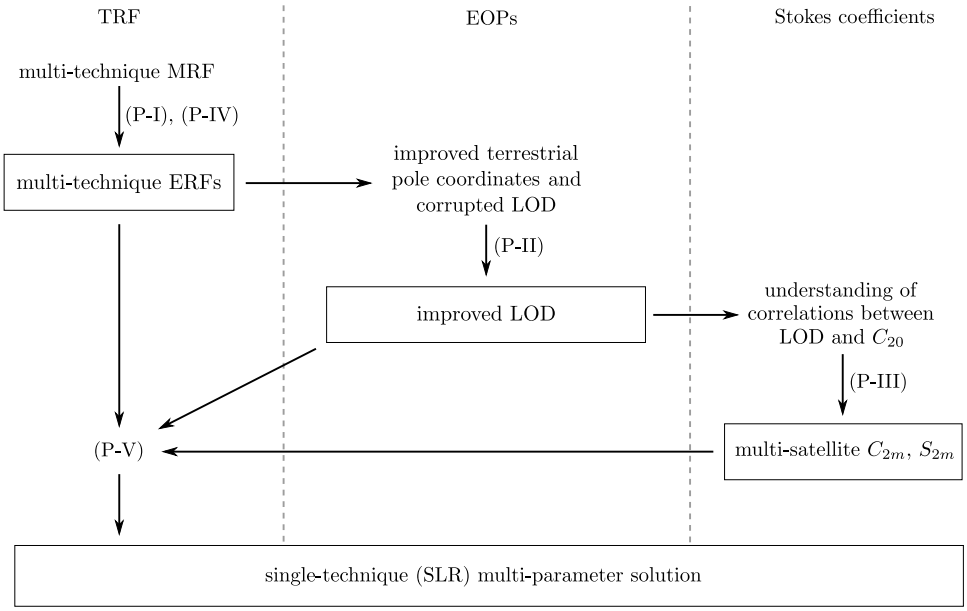

Figure 1.1: Causal coherence of first-author publications in relation to the geodetic parameters. The boxes indicate the main achievements of the publications.

The methodology to combine different SLR-tracked satellites (intra-technique combination) is presented in Chapter 2. The same formulas are used to combine SLR with other geometric observation techniques such as GNSS and VLBI (inter-technique combination). It has to be emphasized that all results discussed in this thesis and in the publications (P-I to P-V and P-A to P-D) are obtained by a combination of different techniques or satellites. Hence, Chapter 2 provides the fundamental basics to obtain the results addressed in Chapter 3 and in the publications. All matrix operations which are used in the analysis or combination process are derived for the three levels of the *Gauß-Markov* model, the observation equation, the Normal EQuation (NEQ) and the solution (parameter) level. A brief discussion of the pros and cons of the three levels is also included. At the end of Chapter 2, two libraries of the DGFI Orbit and Geodetic parameter estimation Software (DOGS) are described; the Orbit Computation library of DOGS (DOGS-OC) for the analysis of SLR observations and the Combination and Solution library of DOGS (DOGS-CS). Furthermore, a short summary of the software developments performed for DOGS-OC in the framework of this thesis is included.

The key topic of this thesis is addressed in Chapter 3. It describes the theoretical and computational foundations of the TRF, EOP and Stokes coefficients. Each section is related to one parameter group and is structured into a short description of the state-of-the-art, current parameter limitations and deficiencies, as well as strategies to resolve them. A special focus is on the estimation of Epoch Reference Frames (ERFs; P-I, P-IV), the reduction of systematics in the LOD estimates of SLR (P-II), and the improved estimation of second-degree Stokes coefficients using a multi-satellite SLR solution (P-III). The integrated estimation including a description of the existing interactions of all parameters is addressed in the last section of this chapter. As a case study, the SLR multi-satellite solution is used for the integrated estimation of the Earth's geometry, rotation and gravitational field (P-V).

The major findings of this thesis and the contributing publications are summarized in Chapter 4. Furthermore, an outlook on strategies to improve the multi-satellite (SLR-only) and multi-technique solutions and to extend the integrated approach to other space techniques is given. Finally, Chapter 5 summarizes the first- and co-author publications.

2 Combination theory

Nowadays, geodetic parameters are commonly estimated through a combination of different geodetic space techniques or observations. This chapter describes the methodology for the inter- and intra-technique combination as it is applied at the Deutsches Geodätisches Forschungsinstitut (DGFI) (see Figure 2.1). An example for an inter-technique combination is the combination of different geodetic space techniques such as GNSS, SLR, VLBI (P-I, P-IV) and DORIS (P-A) or the combination of SLR and GRACE (P-C). An example for the intra-technique combination is the combination of different SLR-tracked satellites (P-II, P-III and P-V).

Going into detail, the first part of this chapter describes the fundamental formulas of the least squares adjustment based on the *Gauß*[1]*-Markov*[2] model. The formulas and derivations are primarily based on Angermann et al. (2004), Koch (2004), Thaller (2008), Seitz M. (2009), Seitz M. (2015), Seitz M. et al. (2015), the description of the Solution INdependent EXchange format (SINEX)[3] and the manual of DOGS-CS 5.0 (Gerstl et al., 2001).

The second part of this chapter provides the formulas for different matrix operations which might be necessary for a combination at the three levels of the least squares adjustment (observation equation, NEQ and solution level). It may serve as a compendium for the intra- and inter-technique pre- and postprocessing (② and ⑤, ⑥, ⑦ in Figure 2.1). A short discussion of the pros and cons of each level is given at the beginning of Section 2.2. An overview of the different matrix operations is given in Table 2.1. Figure 2.1 shows exemplarily the processing procedure at the NEQ level in order to obtain an inter- or intra-technique combination.

The third part describes the combination of different techniques or satellites at the three levels of the least squares adjustment. It has to be pointed out here that at DGFI, only the combination at the NEQ level is performed to combine the four geodetic space techniques GNSS, SLR, VLBI and DORIS and to combine SLR and GRACE. Also the multi-satellite SLR solution is obtained from a combination at the NEQ level.

Section 2.4 provides the formulas for a Variance Component Estimation (VCE) at the NEQ level according to P-III, P-C, Koch (2004), Böckmann et al. (2010a), Böckmann et al. (2010b) and Bloßfeld and Seitz M. (2012).

The last section describes the software developed and used at DGFI to process SLR observations (DOGS-OC) and to perform an intra- or inter-technique combination at the NEQ level (DOGS-CS).

2.1 *Gauß-Markov* model

The functional part $f(\boldsymbol{x})$ of the *Gauß-Markov* model consists of n observation equations which contain u unknown parameters. These equations give the relationship between the observations $\boldsymbol{b}$ and the unknown parameters $\boldsymbol{x}$ which is based on mathematical and/or physical principles (quantitative relationship; Koch, 2004)

$$\boldsymbol{b} + \boldsymbol{v} = f(\boldsymbol{x}). \tag{2.1}$$

In Equation (2.1), $\boldsymbol{v}$ denotes a vector containing the errors of the functional model and the observations. In general, the number of observations is chosen to be larger than the number of unknowns ($n > u$) in order to minimize the impact of one single observation on the estimated parameters. If the relationship between the observations and the unknown parameters is not linear, a linearisation has to be performed. Therefore, the function $f(\boldsymbol{x})$ is expanded into a Taylor series. If a priori values $\boldsymbol{x_0}$ of the parameters $\boldsymbol{x}$ are known with sufficient accuracy, the Taylor series expansion could be terminated after the first order correction term $\boldsymbol{\Delta x}$:

$$f(\boldsymbol{x}) = f(\boldsymbol{x_0} + \boldsymbol{\Delta x}) = f(\boldsymbol{x_0}) + \left.\frac{\partial f}{\partial \boldsymbol{x}}\right|_{\boldsymbol{x}=\boldsymbol{x_0}} \cdot \boldsymbol{\Delta x} + O(\boldsymbol{x}^2) \tag{2.2}$$

[1] Carl Friedrich Gauß (Gauß, 1823)
[2] Andrei Andrejewitsch Markov (Markov, 1912)
[3] http://www.iers.org/IERS/EN/Organization/AnalysisCoordinator/SinexFormat/sinex_cont.html, (2014-08-09)

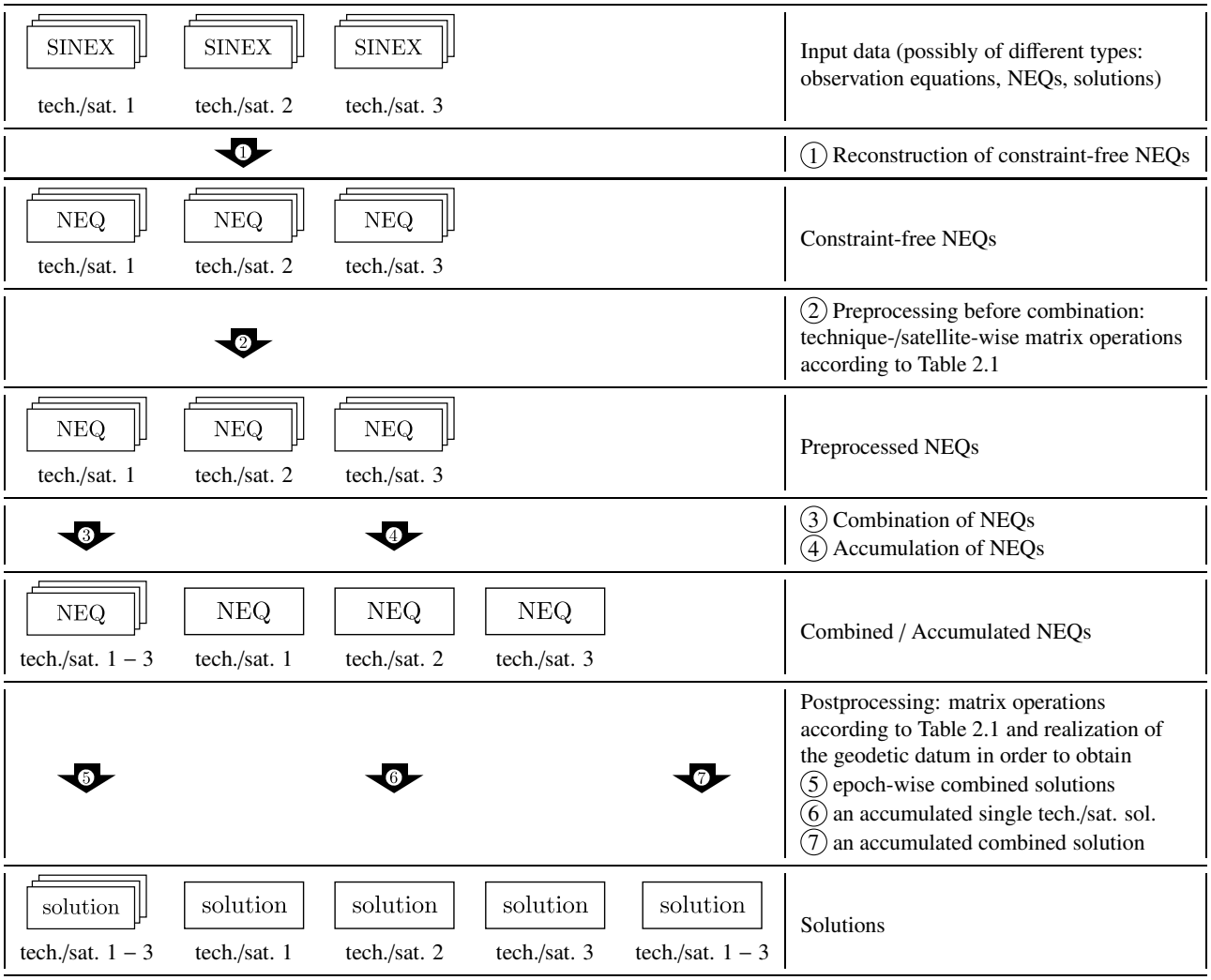

Figure 2.1: Example of a processing procedure for the inter- or intra-technique combination of three different techniques or three different SLR-tracked satellites. The example shows the combination procedure at the NEQ level applied at DGFI.

with an error of second order $O(\boldsymbol{x}^2)$ and the approximation of the unknowns

$$\boldsymbol{x} = \boldsymbol{x_0} + \boldsymbol{\Delta x}. \tag{2.3}$$

The new linearized equation system reads

$$\boldsymbol{b} + \boldsymbol{v} = f(\boldsymbol{x_0}) + \boldsymbol{A\Delta x} \tag{2.4}$$

with the vector of observations $\boldsymbol{b}$ and the matrix $\boldsymbol{A}$ which contains the partial derivatives of the functional model $f(\boldsymbol{x})$ with respect to the parameters $\boldsymbol{x}$. Neglecting the observation errors $\boldsymbol{v}$, Equation (2.4) would not be consistent. The expectation value of the observations $E(\boldsymbol{b} + \boldsymbol{v}) = E(\boldsymbol{b})$ using the assumption $E(\boldsymbol{v}) = 0$. Re-arranging Equation (2.4) leads to

$$\boldsymbol{v} = \boldsymbol{A\Delta x} - (\boldsymbol{b} - f(\boldsymbol{x_0})) = \boldsymbol{A\Delta x} - \boldsymbol{l} \tag{2.5}$$

wherein $\boldsymbol{l} = (\boldsymbol{b} - f(\boldsymbol{x_0}))$ is the vector called 'observed' minus 'computed with a priori values' (O-C). The stochastic part of the *Gauß-Markov* model is defined by

$$\boldsymbol{K_{ll}} = \sigma_0^2 \boldsymbol{P_{ll}^{-1}} = \sigma_0^2 \boldsymbol{Q_{ll}}. \tag{2.6}$$

Therein, $\boldsymbol{K_{ll}}$ is the variance-covariance matrix of the observations, σ_0^2 is the unknown variance factor and $\boldsymbol{P_{ll}}$ is the weighting matrix of the observations. The diagonal elements of the co-factor matrix $\boldsymbol{Q_{ll}}$ are called weight reciprocals. If the observations are uncorrelated and equally weighted, $\boldsymbol{P_{ll}}$ is a unit matrix $\boldsymbol{I_n}$ with dimension $[n \times n]$ and σ_0^2 is called variance of the weight unit. The aim of the least squares adjustment is to minimize the weighted square sum of the observation errors

$$S(\boldsymbol{\Delta x}) = ||\boldsymbol{v}||^2_{P_{ll}} = \boldsymbol{v}^T \boldsymbol{P_{ll}} \boldsymbol{v} \rightarrow min. \tag{2.7}$$

Inserting (2.5) into (2.7) leads to the equation

$$S(\boldsymbol{\Delta \hat{x}}) = \boldsymbol{\Delta \hat{x}}^T \boldsymbol{A}^T \boldsymbol{P_{ll}} \boldsymbol{A} \boldsymbol{\Delta \hat{x}} - 2\boldsymbol{A}^T \boldsymbol{P_{ll}} \boldsymbol{l} \boldsymbol{\Delta \hat{x}} + \boldsymbol{l}^T \boldsymbol{P_{ll}} \boldsymbol{l}. \tag{2.8}$$

The function $S(\boldsymbol{\Delta \hat{x}})$ has an extremum at the point where $\partial S(\boldsymbol{\Delta \hat{x}}) / \partial \boldsymbol{\Delta \hat{x}} = 0$. According to (Koch, 2004), this extremum is a minimum and leads to the NEQ system

$$\boldsymbol{A}^T \boldsymbol{P_{ll}} \boldsymbol{A} \boldsymbol{\Delta \hat{x}} = \boldsymbol{A}^T \boldsymbol{P_{ll}} \boldsymbol{l} \tag{2.9}$$

with the unique solution

$$\boldsymbol{\Delta \hat{x}} = \left(\boldsymbol{A}^T \boldsymbol{P_{ll}} \boldsymbol{A} \right)^{-1} \boldsymbol{A}^T \boldsymbol{P_{ll}} \boldsymbol{l}, \tag{2.10}$$

wherein the normal equation matrix is

$$\boldsymbol{N} = \boldsymbol{A}^T \boldsymbol{P_{ll}} \boldsymbol{A} \tag{2.11}$$

with the rank $rg(\boldsymbol{A}) = rg(\boldsymbol{N})$. If $rg(\boldsymbol{N}) = u$, the matrices $\boldsymbol{A}$ and $\boldsymbol{N}$ are of full rank which means that the u parameters are linear independent. The vector of the right hand side of the NEQ system reads

$$\boldsymbol{y} = \boldsymbol{A}^T \boldsymbol{P_{ll}} \boldsymbol{l}. \tag{2.12}$$

According to Equation (2.3), the corrected unknown parameters can be determined by

$$\boldsymbol{\hat{x}} = \boldsymbol{x_0} + \left(\boldsymbol{A}^T \boldsymbol{P_{ll}} \boldsymbol{A} \right)^{-1} \boldsymbol{A}^T \boldsymbol{P_{ll}} \boldsymbol{l} = \boldsymbol{x_0} + \boldsymbol{N}^{-1} \boldsymbol{y}. \tag{2.13}$$

The least squares adjustment according to *Gauß-Markov* yields the same estimates as the best linear unbiased estimation (Koch, 2004). The a posteriori variance factor $\hat{\sigma}_0^2$ is computed with

$$\hat{\sigma}_0^2 = \frac{\boldsymbol{\hat{v}}^T \boldsymbol{P_{ll}} \boldsymbol{\hat{v}}}{r}. \tag{2.14}$$

Therein, $\boldsymbol{\hat{v}}$ is the vector of the corrected errors which is obtained from minimizing the square sum of the observations errors using Equation (2.7) and $r = n - u$ is the redundancy (degree of freedom) of the equation system. The relationship between the weighted square sum of the observations and of the residuals can be written as

$$\boldsymbol{y^T} \boldsymbol{\Delta \hat{x}} = \boldsymbol{l}^T \boldsymbol{P_{ll}} \boldsymbol{l} - \boldsymbol{\hat{v}}^T \boldsymbol{P_{ll}} \boldsymbol{\hat{v}}. \tag{2.15}$$

The variance-covariance matrix of the estimated unknowns is derived from the variance-covariance matrix of the observations through error propagation

$$\boldsymbol{\hat{K}_{\hat{x}\hat{x}}} = \hat{\sigma}_0^2 \left(\boldsymbol{A}^T \boldsymbol{P_{ll}} \boldsymbol{A} \right)^{-1} = \hat{\sigma}_0^2 \boldsymbol{N}^{-1}. \tag{2.16}$$

In order to solve the NEQ with Equation (2.10), the matrix $\boldsymbol{N}$ which has to be inverted must be of full rank. This is usually not the case. To achieve a regular NEQ, constraints (named pseudo observations in this thesis) have to be added (see Section 2.2.5).

2.2 Matrix operations at observation, normal equation and parameter level

Using the *Gauß-Markov* model, a combination can be performed at three different levels of the least squares adjustment (Angermann et al., 2004; Seitz M., 2015; Seitz M. et al., 2015). Figure 2.2 illustrates the combination of different geodetic space techniques at the observation equation, normal equation and parameter (solution) level. The three levels are defined through the following quantities of the *Gauß-Markov* model:

observation equation level (Equation (2.5)): $\boldsymbol{A}, \boldsymbol{l}, \boldsymbol{P_{ll}}, \sigma_0^2, \boldsymbol{x_0}$

The combination at the observation equation level is the most rigorous combination model. The observation equations of different techniques / satellites are directly stored together in one equation system and the data preprocessing (editing, reduction, etc.) is done consistently for all techniques / satellites. If the observation equations are created with different software packages, it has to be ensured that common a priori models and standards are used. Nevertheless, the most rigorous combination at observation level might be realized, when all the different techniques or satellite observations are processed in one software package because identical routines are used for the preprocessing. Up to now, a software to combine all geometric and gravitmetric observations at the observation equation level is not available although some software packages already might combine the four geometric observations techniques at the observation level.

normal equation (NEQ) level (Equation (2.9)): $\boldsymbol{N}, \boldsymbol{y}, \boldsymbol{l^T P_{ll} l}, \sigma_0^2, \boldsymbol{x_0}$

The combination at the NEQ level is an alternative to the combination at observation equation level if the same parametrization and a priori models are used. The advantage of this type of combination is that NEQs which are processed with different software packages can be combined since an international conventional exchange format for normal equations and solutions exists (Solution INdependent EXchange format; SINEX). Thereby, it has to be ensured that the NEQs contain only non-distorting constraints (see 2.2.5), because otherwise, the NEQs are deformed and systematics affect the combined solution. The most important difference to the combination at observation level is the preprocessing separately performed for each technique/satellite and the assumption of uncorrelated observations (block-diagonal structure of $\boldsymbol{P_{ll}}$).

parameter (solution) level (Equation (2.13)): $\boldsymbol{N^{-1}}, \hat{\boldsymbol{x}}, \hat{\boldsymbol{v}}^{\boldsymbol{T}} \boldsymbol{P_{ll}} \hat{\boldsymbol{v}}, \hat{\sigma}_0^2, \boldsymbol{x_0}$

The combination at the parameter level cannot be considered as a straight-forward approach (Seitz M., 2015) since pseudo-observations are applied multiple times. In a first step, single-technique / single-satellite solutions are obtained by adding a minimum number of pseudo-observations. If more pseudo-observations are applied, the solution is over-constrained (deformed; Seitz M., 2015). In addition, the combined solution depends on the variance-covariance information of the input solutions which again depend on the pseudo-observations. In a second step, the solutions are combined in another least squares adjustment process. It is obvious that the new observation equations differ from the ones of the observation equation and NEQ approach. Furthermore, similarity transformation parameters have to be introduced for each technique/satellite in order to ensure that the datum of the combined solution can be obtained independently.

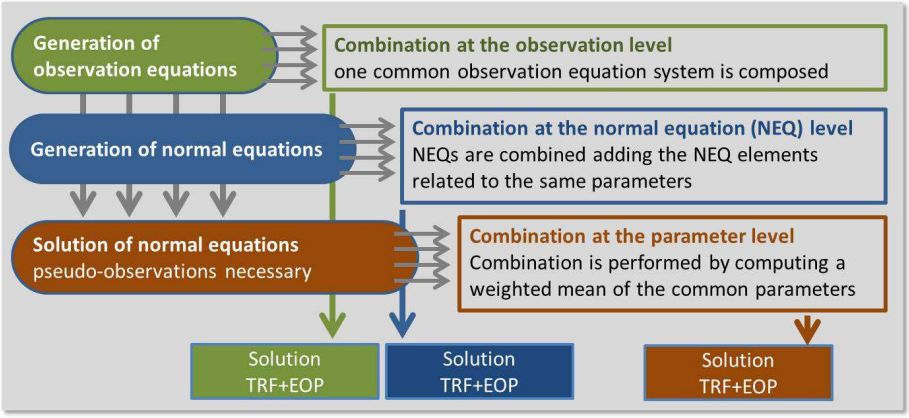

Figure 2.2: Combination of geodetic space techniques at observation equation, normal equation and parameter (solution) level of the *Gauß-Markov* model (taken from Seitz M. (2015); Seitz M. et al. (2015)). The gray arrows illustrate the four geodetic space techniques GNSS, SLR, VLBI and DORIS.

After the respective equation is reached in the processing chain of Equations (2.5) to (2.16), the different equation systems can be combined using the formulas provided in Section 2.3. In case of the combination at observation equation and NEQ level, the processing chain is completed by proceeding to Equation (2.16) to obtain a solution (see Figure 2.3). In case of the combination at solution level, the processing chain has to be restarted at Equation (2.5) with different observation equations (estimated parameters are used as new observations).

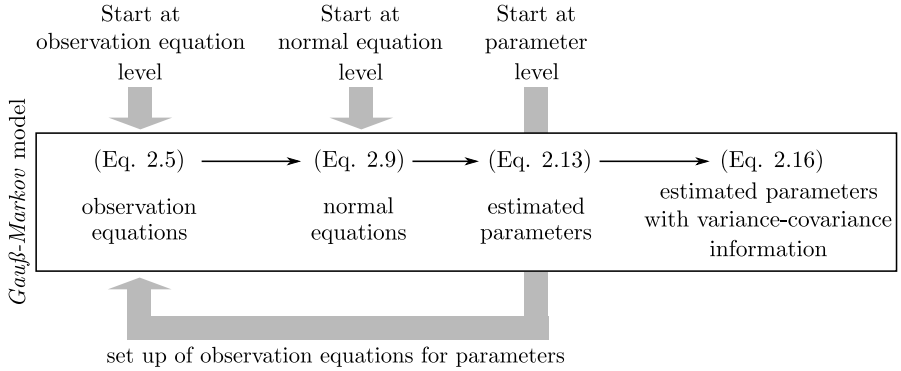

Figure 2.3: Processing chain for the combination at observation equation, normal equation and parameter level of the *Gauß-Markov* model.

An overview of the different parameter vector and matrix operations and the corresponding equations related to the three levels is presented in Table 2.1. Therein, the equations for the different transformations of the parameter vector and for the introduction, reduction and elimination of parameters are referenced. Additionally, the table provides the equations for the application of constraints and the reconstruction of constraint-free NEQs. Finally, the equations for the combination of observation equations, NEQs and solutions (Section 2.3) are given.

Table 2.1: Overview of parameter vector and matrix operations performed at different levels of the least squares adjustment.

Parameter vector/matrix manipulation	Observation equation level	Normal equation level	Parameter (solution) level
Transformation of a priori values	Eq. (2.28)	Eq. (2.29)	Eq. (2.30)
Scaling of parameters	Eq. (2.32)	Eq. (2.33)	Eq. (2.34)
Transformation of parametrization	Eq. (2.37) in Eq. (2.32)	Eq. (2.37) in Eq. (2.33)	Eq. (2.37) in Eq. (2.34)
Transformation of parametrization with regularization	Eq. (2.41) in Eq. (2.32)	Eq. (2.41) in Eq. (2.33)	Eq. (2.41) in Eq. (2.34)
Transformation of epoch	Eq. (2.44) in Eq. (2.32)	Eq. (2.44) in Eq. (2.33)	Eq. (2.44) in Eq. (2.34)
Introduction of linear station motion	Eq. (2.56)	Eq. (2.57)	Eq. (2.58)
Introduction of linear-trigonometric station motion	Eq. (2.60) in Eq. (2.56)	Eq. (2.60) in Eq. (2.57)	Eq. (2.60) in Eq. (2.58)
Introduction of infinitesimal similarity transformation parameters	Eq. (2.69) in Eq. (2.56)	Eq. (2.69) in Eq. (2.57)	Eq. (2.69) in Eq. (2.58)
Reduction of parameters	Eq. (2.75) (*Restitution-Eq.* (2.76))	Eq. (2.80) (*Restitution-Eq.* (2.79))	Eq. (2.83) (*Restitution-Eq.* (2.82))
Elimination of parameters	Eq. (2.90)	Eq. (2.91)	not possible
Application of constraints	Eq. (2.93)	Eq. (2.95)	not possible
Reconstruction of constraint-free NEQ systems	not possible	Eq. (2.99)	Eq. (2.100)
Combination of observation equations, NEQs and solutions	Eq. (2.105)	Eq. (2.107)	Eq. (2.109)

In the following, based on the development of the DOGS-CS software, the presented operations of the equation systems can generally be divided into a translation of a priori values (2.17) and an affine transformation of the parameter vector $\hat{\boldsymbol{x}}$ (2.18). The translation of a priori values is a special case of the affine transformation of the parameter vector.

$$\boldsymbol{x_0} \mapsto \boldsymbol{x_0} + \boldsymbol{t}, \quad \Delta\hat{\boldsymbol{x}} \mapsto \Delta\hat{\boldsymbol{x}} - \boldsymbol{t}, \tag{2.17}$$

$$\hat{\boldsymbol{x}} \mapsto \boldsymbol{R}\hat{\boldsymbol{x}} + \boldsymbol{d}. \tag{2.18}$$

With $\boldsymbol{T} := \boldsymbol{R}^{-1}$, the functional definition of this transformation yields

$$\hat{\tilde{\boldsymbol{x}}} = \boldsymbol{R}\hat{\boldsymbol{x}} + \boldsymbol{d}, \qquad \Delta\hat{\tilde{\boldsymbol{x}}} = \boldsymbol{R}(\Delta\hat{\boldsymbol{x}} - \boldsymbol{t}) \tag{2.19}$$

$$\hat{\boldsymbol{x}} = \boldsymbol{R}^{-1}(\hat{\tilde{\boldsymbol{x}}} - \boldsymbol{d}) = \boldsymbol{T}(\hat{\tilde{\boldsymbol{x}}} - \boldsymbol{d}), \qquad \Delta\hat{\boldsymbol{x}} = \boldsymbol{R}^{-1}\Delta\hat{\tilde{\boldsymbol{x}}} + \boldsymbol{t} = \boldsymbol{T}\Delta\hat{\tilde{\boldsymbol{x}}} + \boldsymbol{t} \tag{2.20}$$

For the transformation of the a priori values $\boldsymbol{x_0}$, we have to distinguish between two cases:

1. *conformal transformation of prescribed a priori values* (new introduced a priori values are transformed with the same functional model as the parameters)

$$\boldsymbol{x_0}, \tilde{\boldsymbol{x}}_\mathbf{0} = \text{defined}, \qquad \boldsymbol{t} = \boldsymbol{T}(\tilde{\boldsymbol{x}}_\mathbf{0} - \boldsymbol{d}) - \boldsymbol{x_0} \tag{2.21}$$

2. *conformal a priori values* (existing a priori values are transformed with the same functional model as the parameters)

$$\boldsymbol{x_0} = \boldsymbol{T}(\tilde{\boldsymbol{x}}_\mathbf{0} - \boldsymbol{d}), \qquad \tilde{\boldsymbol{x}}_\mathbf{0} = \boldsymbol{T}^{-1}\boldsymbol{x_0} + \boldsymbol{d} = \boldsymbol{R}\boldsymbol{x_0} + \boldsymbol{d}, \qquad \boldsymbol{t} = \mathbf{0} \tag{2.22}$$

This general functional definition gives at the observation equation level: $\{\boldsymbol{A}, \boldsymbol{l}, \boldsymbol{P_{ll}}, \boldsymbol{v}, \boldsymbol{x_0}\} \mapsto \{\tilde{\boldsymbol{A}}, \tilde{\boldsymbol{l}}, \tilde{\boldsymbol{P}}_{\boldsymbol{ll}}, \tilde{\boldsymbol{v}}, \tilde{\boldsymbol{x}}_\mathbf{0}\}$

$$\begin{aligned}
\tilde{\boldsymbol{A}} &= \boldsymbol{A}\boldsymbol{T}, \\
\tilde{\boldsymbol{l}} &= \boldsymbol{l} - \boldsymbol{A}\boldsymbol{t}, \\
\tilde{\boldsymbol{P}}_{\boldsymbol{ll}} &= \boldsymbol{P_{ll}}, \\
\tilde{\boldsymbol{v}} &= \boldsymbol{v}, \\
\boldsymbol{t} &= \boldsymbol{T}(\tilde{\boldsymbol{x}}_\mathbf{0} - \boldsymbol{d}) - \boldsymbol{x_0}, \quad \tilde{\boldsymbol{x}}_\mathbf{0} \text{ defined} \quad \text{(case 1)}, \\
\boldsymbol{t} &= \mathbf{0}, \qquad\qquad\qquad \tilde{\boldsymbol{x}}_\mathbf{0} = \boldsymbol{T}^{-1}\boldsymbol{x_0} + \boldsymbol{d} = \boldsymbol{R}\boldsymbol{x_0} + \boldsymbol{d} \quad \text{(case 2)}.
\end{aligned} \tag{2.23}$$

Applying the general functional definition to NEQ systems yields: $\{\boldsymbol{N}, \boldsymbol{y}, \boldsymbol{l}^\boldsymbol{T}\boldsymbol{P_{ll}}\boldsymbol{l}, \boldsymbol{x_0}\} \mapsto \{\tilde{\boldsymbol{N}}, \tilde{\boldsymbol{y}}, \tilde{\boldsymbol{l}}^\boldsymbol{T}\tilde{\boldsymbol{P}}_{\boldsymbol{ll}}\tilde{\boldsymbol{l}}, \tilde{\boldsymbol{x}}_\mathbf{0}\}$

$$\begin{aligned}
\tilde{\boldsymbol{N}} &= \boldsymbol{T}^T\boldsymbol{N}\boldsymbol{T}, \\
\tilde{\boldsymbol{y}} &= \boldsymbol{T}^T(\boldsymbol{y} - \boldsymbol{N}\boldsymbol{t}), \\
\tilde{\boldsymbol{l}}^\boldsymbol{T}\tilde{\boldsymbol{P}}_{\boldsymbol{ll}}\tilde{\boldsymbol{l}} &= \boldsymbol{l}^\boldsymbol{T}\boldsymbol{P_{ll}}\boldsymbol{l} - \boldsymbol{t}^T(2\boldsymbol{y} - \boldsymbol{N}\boldsymbol{t}), \\
\boldsymbol{t} &= \boldsymbol{T}(\tilde{\boldsymbol{x}}_\mathbf{0} - \boldsymbol{d}) - \boldsymbol{x_0}, \quad \tilde{\boldsymbol{x}}_\mathbf{0} \text{ defined} \quad \text{(case 1)}, \\
\boldsymbol{t} &= \mathbf{0}, \qquad\qquad\qquad \tilde{\boldsymbol{x}}_\mathbf{0} = \boldsymbol{T}^{-1}\boldsymbol{x_0} + \boldsymbol{d} = \boldsymbol{R}\boldsymbol{x_0} + \boldsymbol{d} \quad \text{(case 2)}.
\end{aligned} \tag{2.24}$$

At the solution (parameter) level, the general functional definition gives:
$\{\hat{\boldsymbol{x}}, \boldsymbol{N}^{-1}, \Delta\hat{\boldsymbol{x}}, \boldsymbol{l}^\boldsymbol{T}\boldsymbol{P_{ll}}\boldsymbol{l}, \hat{\boldsymbol{v}}^\boldsymbol{T}\boldsymbol{P_{ll}}\hat{\boldsymbol{v}}, \boldsymbol{x_0}\} \mapsto \{\hat{\tilde{\boldsymbol{x}}}, \tilde{\boldsymbol{N}}^{-1}, \Delta\hat{\tilde{\boldsymbol{x}}}, \tilde{\boldsymbol{l}}^\boldsymbol{T}\tilde{\boldsymbol{P}}_{\boldsymbol{ll}}\tilde{\boldsymbol{l}}, \hat{\tilde{\boldsymbol{v}}}^\boldsymbol{T}\tilde{\boldsymbol{P}}_{\boldsymbol{ll}}\hat{\tilde{\boldsymbol{v}}}, \tilde{\boldsymbol{x}}_\mathbf{0}\}$

$$\begin{aligned}
\hat{\tilde{\boldsymbol{x}}} &= \boldsymbol{R}\hat{\boldsymbol{x}} + \boldsymbol{d}, \\
\tilde{\boldsymbol{N}}^{-1} &= \boldsymbol{R}\boldsymbol{N}^{-1}\boldsymbol{R}^T, \\
\Delta\hat{\tilde{\boldsymbol{x}}} &= \boldsymbol{R}(\Delta\hat{\boldsymbol{x}} - \boldsymbol{t}), \\
\tilde{\boldsymbol{l}}^\boldsymbol{T}\tilde{\boldsymbol{P}}_{\boldsymbol{ll}}\tilde{\boldsymbol{l}} &= \boldsymbol{l}^\boldsymbol{T}\boldsymbol{P_{ll}}\boldsymbol{l} - \boldsymbol{t}^T\boldsymbol{N}(2\Delta\hat{\boldsymbol{x}} - \boldsymbol{t}), \\
\hat{\tilde{\boldsymbol{v}}}^\boldsymbol{T}\tilde{\boldsymbol{P}}_{\boldsymbol{ll}}\hat{\tilde{\boldsymbol{v}}} &= \hat{\boldsymbol{v}}^\boldsymbol{T}\boldsymbol{P_{ll}}\hat{\boldsymbol{v}}, \\
\boldsymbol{t} &= \boldsymbol{T}(\tilde{\boldsymbol{x}}_\mathbf{0} - \boldsymbol{d}) - \boldsymbol{x_0}, \quad \tilde{\boldsymbol{x}}_\mathbf{0} \text{ defined} \quad \text{(case 1)}, \\
\boldsymbol{t} &= \mathbf{0}, \qquad\qquad\qquad \tilde{\boldsymbol{x}}_\mathbf{0} = \boldsymbol{T}^{-1}\boldsymbol{x_0} + \boldsymbol{d} = \boldsymbol{R}\boldsymbol{x_0} + \boldsymbol{d} \quad \text{(case 2)}.
\end{aligned} \tag{2.25}$$

From Equation (2.23), (2.24) and (2.25), one can see that a transformation of the parameter vector at observation equation and NEQ level is only possible, if the transformation matrix $\boldsymbol{R}$ is regular. At solution level, this requirement is not necessary if the a priori values are conformal (case 2; see Eq. (2.22)). The two different cases (regular and irregular transformation matrix) are programmed in the TRAnsFOrmation routine of

DOGS-CS (CS-TRAFO) and the TRAnsformation with SIngluar transformation matrix routine of DOGS-CS (CS-TRASI). Examples for such transformations are given in the following section. Further details on the used software routines are presented in Section 2.5.2.

If the parameter vector contains different parameter groups, e.g., station coordinates and velocities, EOP, Stokes coefficients or orbit parameters, it can be divided into different parts $\hat{\boldsymbol{x}} = (\hat{\boldsymbol{x}}_1^T, \hat{\boldsymbol{x}}_2^T, \ldots, \hat{\boldsymbol{x}}_N^T)^T$ with $j = 1, 2, \ldots, N$ parameter groups, each with u_j parameters. Using this separation, the transformation of a single parameter group can be done with $\boldsymbol{R_j}, \boldsymbol{d_j}$ and $\boldsymbol{t_j}$. If a parameter group should remain constant, the respective part of the functional model reads $\boldsymbol{R_j} = \boldsymbol{I}_{u_t}, \boldsymbol{d_j} = \boldsymbol{0}$ and $\boldsymbol{t_j} = \boldsymbol{0}$. The transformation model extended to the complete parameter vector reads

$$\boldsymbol{R} = diag(\boldsymbol{R_1}, \boldsymbol{R_2}, \ldots, \boldsymbol{R_N}),\ \boldsymbol{d} = diag(\boldsymbol{d_1^T}, \boldsymbol{d_2^T}, \ldots, \boldsymbol{d_N^T})^T,\ \boldsymbol{t} = diag(\boldsymbol{t_1^T}, \boldsymbol{t_2^T}, \ldots, \boldsymbol{t_N^T})^T. \quad (2.26)$$

2.2.1 Transformation of the parameter vector

The transformations of the parameter vector described in this section are the transformation of the a priori values, the scaling of parameters, the change of the parametrization with and without regularization and the change of the parameter epoch.

a) Transformation of a priori values with equal epoch

An example for the transformation of the parameter vector is the transformation of the vector of a priori values $\boldsymbol{x_0} \mapsto \tilde{\boldsymbol{x}}_\boldsymbol{0}$ (case 1) in order to ensure that two NEQs have the same a priori values. The transformation of the vector of a priori values can be considered as a translation (special case of affine transformation; Seitz M., 2009). The general functional model of the transformation reads

$$\boldsymbol{R} = \boldsymbol{T} = \boldsymbol{I_u}, \qquad \boldsymbol{d} = \boldsymbol{0}, \qquad \boldsymbol{t} = \tilde{\boldsymbol{x}}_\boldsymbol{0} - \boldsymbol{x_0}. \quad (2.27)$$

Inserting (2.27) in (2.23), we get for the observation equation level

$$\tilde{\boldsymbol{A}} = \boldsymbol{A}, \qquad \tilde{\boldsymbol{l}} = \boldsymbol{l} - \boldsymbol{A}(\tilde{\boldsymbol{x}}_\boldsymbol{0} - \boldsymbol{x_0}), \qquad \tilde{\boldsymbol{P}}_{\boldsymbol{ll}} = \boldsymbol{P_{ll}}, \qquad \tilde{\boldsymbol{v}} = \boldsymbol{v}, \qquad \tilde{\boldsymbol{x}}_\boldsymbol{0} = \boldsymbol{t} + \boldsymbol{x_0}. \quad (2.28)$$

With (2.27) and (2.24), the transformation of the a priori values at the NEQ level yields

$$\begin{aligned} \tilde{\boldsymbol{N}} &= \boldsymbol{N}, \qquad \tilde{\boldsymbol{y}} = \boldsymbol{y} - \boldsymbol{N}(\tilde{\boldsymbol{x}}_\boldsymbol{0} - \boldsymbol{x_0}), \\ \tilde{\boldsymbol{l}}^T \tilde{\boldsymbol{P}}_{\boldsymbol{ll}} \tilde{\boldsymbol{l}} &= \boldsymbol{l}^T \boldsymbol{P_{ll}} \boldsymbol{l} - (\tilde{\boldsymbol{x}}_\boldsymbol{0} - \boldsymbol{x_0})^T (2\boldsymbol{y} - \boldsymbol{N}(\tilde{\boldsymbol{x}}_\boldsymbol{0} - \boldsymbol{x_0})), \qquad \tilde{\boldsymbol{x}}_\boldsymbol{0} = \boldsymbol{t} + \boldsymbol{x_0}. \end{aligned} \quad (2.29)$$

The transformation at the parameter (solution) level can be expressed with (2.27) and (2.25) as

$$\begin{aligned} \hat{\tilde{\boldsymbol{x}}} &= \hat{\boldsymbol{x}} \qquad \text{and} \\ \tilde{\boldsymbol{N}}^{-1} &= \boldsymbol{N}^{-1}, \qquad \Delta\hat{\tilde{\boldsymbol{x}}} = \Delta\hat{\boldsymbol{x}} - (\tilde{\boldsymbol{x}}_\boldsymbol{0} - \boldsymbol{x_0}), \\ \tilde{\boldsymbol{l}}^T \tilde{\boldsymbol{P}}_{\boldsymbol{ll}} \tilde{\boldsymbol{l}} &= \boldsymbol{l}^T \boldsymbol{P_{ll}} \boldsymbol{l} - (\tilde{\boldsymbol{x}}_\boldsymbol{0} - \boldsymbol{x_0})^T \boldsymbol{N}(2\Delta\hat{\boldsymbol{x}} - (\tilde{\boldsymbol{x}}_\boldsymbol{0} - \boldsymbol{x_0})), \\ \hat{\tilde{\boldsymbol{v}}}^T \tilde{\boldsymbol{P}}_{\boldsymbol{ll}} \hat{\tilde{\boldsymbol{v}}} &= \hat{\boldsymbol{v}}^T \boldsymbol{P_{ll}} \hat{\boldsymbol{v}}, \qquad \tilde{\boldsymbol{x}}_\boldsymbol{0} = \boldsymbol{t} + \boldsymbol{x_0}. \end{aligned} \quad (2.30)$$

As Equation (2.30) shows, the parameter estimates do not change if their a priori values are changed (only the estimated corrections to the a priori values change).

b) Scaling of parameters

The scaling of parameters can be necessary, if, for example, the unit of the x-component of terrestrial pole coordinates x_p should be changed from $[as]$ to $[mas]$ or the NEQ matrix rows and columns should be equilibrated. The scaled parameters read $\hat{\tilde{\boldsymbol{x}}}_j = 1000 \cdot \hat{\boldsymbol{x}}_\boldsymbol{j} = \lambda_j \hat{\boldsymbol{x}}_\boldsymbol{j} = \boldsymbol{R}\hat{\boldsymbol{x}}_\boldsymbol{j}$. The general functional model of the transformation of u_t parameters with $j = 1, 2, \ldots, u_t$ and conformal a priori values (case 2) is

$$\boldsymbol{R} = diag(\lambda_0, \lambda_1, \ldots, \lambda_{u_t}), \qquad \boldsymbol{d} = \boldsymbol{0}, \qquad \boldsymbol{t} = \boldsymbol{0}. \quad (2.31)$$

Equation (2.31) and (2.23) leads to the formula at the observation equation level

$$\tilde{\boldsymbol{A}} = \boldsymbol{A}\boldsymbol{T}, \qquad \tilde{\boldsymbol{l}} = \boldsymbol{l}, \qquad \tilde{\boldsymbol{P}}_{\boldsymbol{l}\boldsymbol{l}} = \boldsymbol{P}_{\boldsymbol{l}\boldsymbol{l}}, \qquad \tilde{\boldsymbol{v}} = \boldsymbol{v}, \qquad \tilde{\boldsymbol{x}}_{\boldsymbol{0}} = \boldsymbol{R}\boldsymbol{x}_{\boldsymbol{0}}. \tag{2.32}$$

The NEQ system reads

$$\tilde{\boldsymbol{N}} = \boldsymbol{T}^T\boldsymbol{N}\boldsymbol{T}, \qquad \tilde{\boldsymbol{y}} = \boldsymbol{T}^T\boldsymbol{y}, \qquad \tilde{\boldsymbol{l}}^T\tilde{\boldsymbol{P}}_{\boldsymbol{l}\boldsymbol{l}}\tilde{\boldsymbol{l}} = \boldsymbol{l}^T\boldsymbol{P}_{\boldsymbol{l}\boldsymbol{l}}\boldsymbol{l}, \qquad \tilde{\boldsymbol{x}}_{\boldsymbol{0}} = \boldsymbol{R}\boldsymbol{x}_{\boldsymbol{0}}. \tag{2.33}$$

using (2.31) and (2.24). The transformation at the parameter level by applying (2.31) to (2.25) yields

$$\begin{aligned} \hat{\tilde{\boldsymbol{x}}} &= \boldsymbol{R}\hat{\boldsymbol{x}} \qquad \text{and} \\ \tilde{\boldsymbol{N}}^{-1} &= \boldsymbol{R}\boldsymbol{N}^{-1}\boldsymbol{R}^T, \qquad \Delta\hat{\tilde{\boldsymbol{x}}} = \boldsymbol{R}\Delta\hat{\boldsymbol{x}}, \qquad \tilde{\boldsymbol{l}}^T\tilde{\boldsymbol{P}}_{\boldsymbol{l}\boldsymbol{l}}\tilde{\boldsymbol{l}} = \boldsymbol{l}^T\boldsymbol{P}_{\boldsymbol{l}\boldsymbol{l}}\boldsymbol{l}, \\ \hat{\tilde{\boldsymbol{v}}}^T\tilde{\boldsymbol{P}}_{\boldsymbol{l}\boldsymbol{l}}\hat{\tilde{\boldsymbol{v}}} &= \hat{\boldsymbol{v}}^T\boldsymbol{P}_{\boldsymbol{l}\boldsymbol{l}}\hat{\boldsymbol{v}}, \qquad \tilde{\boldsymbol{x}}_{\boldsymbol{0}} = \boldsymbol{R}\boldsymbol{x}_{\boldsymbol{0}}. \end{aligned} \tag{2.34}$$

c) Transformation of parametrization of terrestrial/celestial pole coordinates

If the functional model $f(\boldsymbol{x})$ should be changed or if different space techniques are combined (e.g., P-I, P-A), it could be necessary to transform the vector of unknowns $\hat{\boldsymbol{x}}$ together with its a priori values $\boldsymbol{x}_{\boldsymbol{0}}$ into a new vector $\hat{\tilde{\boldsymbol{x}}}$ with conformal a priori values $\tilde{\boldsymbol{x}}_{\boldsymbol{0}}$ (case 2). An example is the transformation of EOP which is described in the following:
The time dependency of EOP within the interval of one VLBI-only NEQ (usually 1 h or 24 h) is expressed by an offset at the reference epoch $p(t_i)$ (mid epoch of observation interval) and a drift $\dot{p}(t_i)$ (see Figure 2.4). In contrast to this, the Global Positioning System (GPS)-only or SLR-only EOP might be parametrized as a piece-wise linear (pwl) polygon with offsets at 0 h epochs (P-I). This parametrization has the advantages, that (i) continuity at the day boundaries is ensured and therefore less parameters are needed to express the time dependency within a time interval longer than one day and furthermore, (ii) the offsets can be determined more stably than the rates. Therefore, a more stable solution can be obtained (Thaller, 2008; Seitz M., 2009). For an n-day time interval, $2n$ parameters are necessary in the $(p(t_i),\, \dot{p}(t_i))^T$ parametrization and only $n+1$ parameters for the $(p(t_1),\, p(t_2))^T$ representation. The linear relationship between the two representations reads

$$\hat{\boldsymbol{x}}_{\boldsymbol{i}} = \begin{pmatrix} p(t_i) \\ \dot{p}(t_i) \end{pmatrix} = \begin{bmatrix} \frac{t_2 - t_i}{t_2 - t_1} & \frac{t_i - t_1}{t_2 - t_1} \\ \frac{-1}{t_2 - t_1} & \frac{1}{t_2 - t_1} \end{bmatrix} \begin{pmatrix} p(t_1) \\ p(t_2) \end{pmatrix} = \boldsymbol{T}_{\boldsymbol{i}}\hat{\tilde{\boldsymbol{x}}}_{\boldsymbol{i}} \qquad \text{or vice-versa} \tag{2.35}$$

$$\hat{\tilde{\boldsymbol{x}}}_{\boldsymbol{i}} = \begin{pmatrix} p(t_1) \\ p(t_2) \end{pmatrix} = \begin{bmatrix} 1 & t_1 - t_i \\ 1 & t_2 - t_i \end{bmatrix} \begin{pmatrix} p(t_i) \\ \dot{p}(t_i) \end{pmatrix} = \boldsymbol{T}_{\boldsymbol{i}}^{-1}\hat{\boldsymbol{x}}_{\boldsymbol{i}} = \boldsymbol{R}_{\boldsymbol{i}}\hat{\boldsymbol{x}}_{\boldsymbol{i}}. \tag{2.36}$$

For a parameter vector containing EOP and station coordinates, the general functional transformation model yields

$$\boldsymbol{R} = \begin{bmatrix} \boldsymbol{R}_{\boldsymbol{i}} & \boldsymbol{0} \\ \boldsymbol{0} & \boldsymbol{I}_{\boldsymbol{u}-\boldsymbol{2}} \end{bmatrix}, \qquad \boldsymbol{d} = \boldsymbol{0}, \qquad \boldsymbol{t} = \boldsymbol{0}. \tag{2.37}$$

The corresponding quantities at the three levels of the *Gauß-Markov* model can be computed by inserting Equation (2.37) into Equation (2.23), (2.24) and (2.25), respectively.

It is important to mention here, that the above described linear interpolation from an offset and drift representation to a piecewise-linear polygon with offsets at midnight epochs is not valid for all EOP. Besides the reduction of subdaily, daily and long-term effects due to ocean tides and libration for all EOP (see also Section 3.2.2), the interpolation of, e.g., Universal Time 1 (UT1) and LOD needs a reduction (and conversion afterwards) of well-known conventional correction terms caused by zonal tides which have periods between 5 days and 18.6 years in order to minimize the interpolation error. The transformation of parametrization using this so-called "regularization" (consideration of effects caused by zonal tides) is discussed in the next section. Nevertheless, the interpolation error for all EOP due to the linear interpolation is at the limit looking at today's accuracy of the geodetic space techniques.

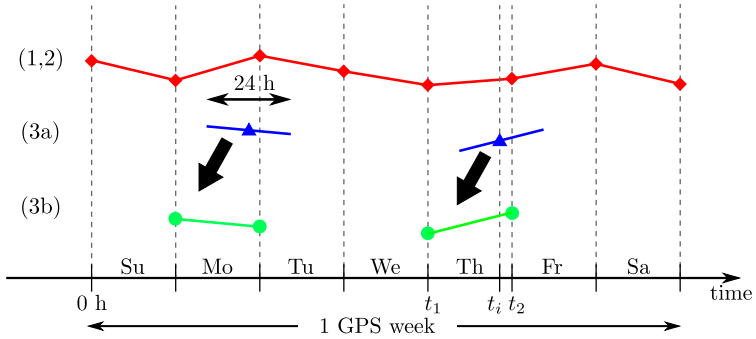

Figure 2.4: Different EOP parametrizations of (1) GPS-only, (2) SLR-only (red diamonds) and (3) VLBI-only input NEQs (3a) before the parameter transformation (blue triangles + line) and (3b) after the parameter transformation (green circles). The VLBI-only EOP are transformed into the starting day boundaries of each session.

d) Transformation of parametrization of UT1/LOD with regularization (consideration of zonal terms)

In case of UT1 and LOD, the change of the offset/drift parametrization cannot be done solely by linearly interpolating these quantities to midnight epochs due to the fact that the interpolation error due to the linear interpolation would be too large. Before interpolating, conventional correction terms $r(t_i)$, caused by the effect of zonal tides (tidal deformation of the Earth with a decoupled core, an elastic mantle and equilibrium oceans) on the Earth rotation have to be subtracted (Petit and Luzum, 2010). The advantage of such a "regularization" is, that the corrected time-dependent parameters $\bar{p}(t_i)$ and $\dot{\bar{p}}(t_i)$ can be approximated much better by a linear interpolation than the uncorrected parameters $p(t)$ (Gerstl et al., 2001). After the interpolation, the subtracted effects are restored again at the midnight epochs t_1 and t_2. Condensed, the interpolation of UT1 and LOD can be divided into three steps (P-I)

i reduction of [UT1(t_i), LOD(t_i)] to [UT1$_\mathrm{R}(t_i)$, LOD$_\mathrm{R}(t_i)$] by tidal signal corrections according to Petit and Luzum (2010)

ii linear parameter transformation with [UT1$_\mathrm{R}(t_i)$, LOD$_\mathrm{R}(t_i)$] to the midnight epochs t_1 and t_2 (like terrestrial pole coordinates)

iii conversion of UT1$_\mathrm{R}$ offsets at midnight epochs to UT1 offsets at midnight epochs (re-adding the respective tidal signal corrections at midnight epochs).

The regularization for a time-dependent parameter reads

$$p(t) = \bar{p}(t_i) + r(t_i) \qquad \text{and} \qquad \dot{p}(t_i) = \dot{\bar{p}}(t_i) + \dot{r}(t_i). \tag{2.38}$$

After replacing $p(t_i)$ and $\dot{p}(t_i)$ in Equation (2.35) with $\bar{p}(t_i)$ and $\dot{\bar{p}}(t_i)$ and applying Equation (2.38), the linear relationship between the two regularized parametrizations reads

$$\hat{\boldsymbol{x}}_{\boldsymbol{i}} = \begin{pmatrix} p(t_i) \\ \dot{p}(t_i) \end{pmatrix} = \begin{bmatrix} \frac{t_2-t_i}{t_2-t_1} & \frac{t_i-t_1}{t_2-t_1} \\ \frac{-1}{t_2-t_1} & \frac{1}{t_2-t_1} \end{bmatrix} \begin{pmatrix} p(t_1) \\ p(t_2) \end{pmatrix} + \begin{pmatrix} r(t_i) \\ \dot{r}(t_i) \end{pmatrix} - \begin{bmatrix} \frac{t_2-t_i}{t_2-t_1} & \frac{t_i-t_1}{t_2-t_1} \\ \frac{-1}{t_2-t_1} & \frac{1}{t_2-t_1} \end{bmatrix} \begin{pmatrix} r(t_1) \\ r(t_2) \end{pmatrix} = \boldsymbol{T_i}\hat{\bar{\boldsymbol{x}}}_{\boldsymbol{i}} - \boldsymbol{T_i}\boldsymbol{d_i}. \tag{2.39}$$

Re-arranging Equation (2.39) yields

$$\hat{\bar{\boldsymbol{x}}}_{\boldsymbol{i}} = \begin{pmatrix} p(t_1) \\ p(t_2) \end{pmatrix} = \begin{bmatrix} 1 & t_1 - t_i \\ 1 & t_2 - t_i \end{bmatrix} \begin{pmatrix} p(t_i) \\ \dot{p}(t_i) \end{pmatrix} + \begin{pmatrix} r(t_1) \\ r(t_2) \end{pmatrix} - \begin{bmatrix} 1 & t_1 - t_i \\ 1 & t_2 - t_i \end{bmatrix} \begin{pmatrix} r(t_i) \\ \dot{r}(t_i) \end{pmatrix} = \boldsymbol{R_i}\hat{\boldsymbol{x}}_i + \boldsymbol{d_i}. \tag{2.40}$$

Using Equation (2.40), we can derive the quantities

$$\boldsymbol{R_i} = \begin{bmatrix} 1 & t_1 - t_i \\ 1 & t_2 - t_i \end{bmatrix}, \qquad \boldsymbol{d_i} = \begin{pmatrix} r(t_1) - r(t_i) - (t_1 - t_i)\dot{r}(t_i) \\ r(t_2) - r(t_i) - (t_2 - t_i)\dot{r}(t_i) \end{pmatrix}, \qquad \boldsymbol{t_i} = \boldsymbol{0}. \tag{2.41}$$

The change of the mathematical model with regularization can be done at the three levels of the *Gauß-Markov* model by applying Equation (2.41) to Equation (2.23), (2.24) and (2.25), respectively.

e) Transformation of epoch

An example for the epoch transformation of parameters and their a priori values is the transformation of the coordinates of the j-th station with the corresponding velocities from a reference epoch t_1 to a new epoch t_2 of a TRF realization. This task is often done in order to compare different TRF realizations.

$$\hat{\boldsymbol{x}}_{\boldsymbol{i}} = \begin{pmatrix} p(t_1) \\ \dot{p}(t_1) \end{pmatrix} = \begin{bmatrix} 1 & t_1 - t_2 \\ 0 & 1 \end{bmatrix} \begin{pmatrix} p(t_2) \\ \dot{p}(t_2) \end{pmatrix} = \boldsymbol{T}_{\boldsymbol{i}} \hat{\tilde{\boldsymbol{x}}}_{\boldsymbol{i}} \qquad \text{or vice-versa} \tag{2.42}$$

$$\hat{\tilde{\boldsymbol{x}}}_{\boldsymbol{i}} = \begin{pmatrix} p(t_2) \\ \dot{p}(t_2) \end{pmatrix} = \begin{bmatrix} 1 & t_2 - t_1 \\ 0 & 1 \end{bmatrix} \begin{pmatrix} p(t_1) \\ \dot{p}(t_1) \end{pmatrix} = \boldsymbol{T}_{\boldsymbol{i}}^{-1} \hat{\boldsymbol{x}}_{\boldsymbol{i}} = \boldsymbol{R}_{\boldsymbol{j}} \hat{\boldsymbol{x}}_{\boldsymbol{i}} \qquad \text{with} \qquad \dot{p}(t_1) = \dot{p}(t_2). \tag{2.43}$$

The general functional model of the epoch transformation for a parameter vector containing EOP, station coordinates and velocities yields

$$\boldsymbol{R} = \begin{bmatrix} \boldsymbol{I}_{\boldsymbol{u-2}} & \boldsymbol{0} \\ \boldsymbol{0} & \boldsymbol{R}_{\boldsymbol{i}} \end{bmatrix}, \qquad \boldsymbol{d} = \boldsymbol{0}, \qquad \boldsymbol{t} = \boldsymbol{0}. \tag{2.44}$$

As it was the case for the transformation of parametrization (Section 2.2.1), the quantities at the three levels of the *Gauß-Markov* model can be computed by inserting Equation (2.44) in Equation (2.32), (2.33) and (2.34), respectively.

2.2.2 Introduction of additional parameters

This section provides the formula for the extension of a parameter vector $\hat{\boldsymbol{x}}$ by a vector of u_a additional parameters $\hat{\boldsymbol{q}}$ which are in affine relation to u_t parameters of $\hat{\boldsymbol{x}}$. The dimension of $\hat{\boldsymbol{q}}$ is $[u_a \times 1]$. This means, the vector $\hat{\boldsymbol{x}}$ with the dimension $[u \times 1]$ consists of $u - u_t$ parameters which are in non-affine relation to $\hat{\boldsymbol{q}}$ and u_t parameters which are in affine relation to $\hat{\boldsymbol{q}}$. If all parameters $\hat{\boldsymbol{q}}$ are non-affine to $\hat{\boldsymbol{x}}$, $u_t = 0$ and $\hat{\boldsymbol{q}}$ can be added like an independent equation system (see Section 2.3). Using the affine relation, the parameter vector $\hat{\boldsymbol{x}}$ can be extended using the transformation

$$\begin{pmatrix} \hat{\tilde{\boldsymbol{x}}} \\ \hat{\boldsymbol{q}} \end{pmatrix} \mapsto \hat{\boldsymbol{x}}. \tag{2.45}$$

Since the vector $\begin{pmatrix} \hat{\tilde{\boldsymbol{x}}} & \hat{\boldsymbol{q}} \end{pmatrix}^T$ has the dimension $[(u + u_a) \times 1]$ and $\hat{\boldsymbol{x}}$ has $[u \times 1]$, this mapping can be defined uniquely only in the shown direction. Similar to the functional transformation model (2.19), the extension reads

$$\hat{\boldsymbol{x}} = \boldsymbol{T}(\hat{\tilde{\boldsymbol{x}}} - \boldsymbol{d}) + \boldsymbol{S}\hat{\boldsymbol{q}} = \begin{bmatrix} \boldsymbol{T} & \boldsymbol{S} \end{bmatrix} \begin{pmatrix} \hat{\tilde{\boldsymbol{x}}} \\ \hat{\boldsymbol{q}} \end{pmatrix} - \boldsymbol{T}\boldsymbol{d}, \tag{2.46}$$

$$\Delta\hat{\boldsymbol{x}} = \boldsymbol{T}\Delta\hat{\tilde{\boldsymbol{x}}} + \boldsymbol{S}\Delta\hat{\boldsymbol{q}} + \boldsymbol{t} = \begin{bmatrix} \boldsymbol{T} & \boldsymbol{S} \end{bmatrix} \begin{pmatrix} \Delta\hat{\tilde{\boldsymbol{x}}} \\ \Delta\hat{\boldsymbol{q}} \end{pmatrix} + \boldsymbol{t}. \tag{2.47}$$

As it was the case for the transformation of the a priori values $\boldsymbol{x_0}$ in Equation (2.21) and (2.22), we have to distinguish between two cases:

1. *conformal transformation of prescribed a priori values* (new introduced a priori values are transformed with the same functional model as the parameters)

$$\boldsymbol{x_0}, \tilde{\boldsymbol{x}}_{\boldsymbol{0}} = \text{defined}, \qquad \boldsymbol{t} = \boldsymbol{T}(\tilde{\boldsymbol{x}}_{\boldsymbol{0}} - \boldsymbol{d}) + \boldsymbol{S}\boldsymbol{q_0} - \boldsymbol{x_0} \tag{2.48}$$

2. *conformal a priori values* (existing a priori values are transformed with the same functional model as the parameters)

$$\boldsymbol{x_0} = \boldsymbol{T}(\tilde{\boldsymbol{x}}_\mathbf{0} - \boldsymbol{d}) + \boldsymbol{S}\boldsymbol{q_0}, \qquad \tilde{\boldsymbol{x}}_\mathbf{0} = \boldsymbol{T}^{-1}(\boldsymbol{x_0} - \boldsymbol{S}\boldsymbol{q_0}) + \boldsymbol{d}, \qquad \boldsymbol{t} = \mathbf{0} \tag{2.49}$$

According to Equation (2.26), the parameter subvector $\hat{\boldsymbol{x}}_\boldsymbol{j}$ with $j = 2, 3, \ldots, N$ is extended by new parameters $\hat{\boldsymbol{q}}_\boldsymbol{j}$ to a new parameter vector $\begin{pmatrix}\hat{\tilde{\boldsymbol{x}}}_\boldsymbol{j} & \hat{\boldsymbol{q}}_\boldsymbol{j}\end{pmatrix}^T$ through a transformation defined by $\boldsymbol{R_j}, \boldsymbol{S_j}, \boldsymbol{d_j}, \boldsymbol{t_j}$. The non-transformed parameters (e.g., EOP) are stored in the subvector $\hat{\boldsymbol{x}}_\mathbf{1}$ (dimension: $[(u - u_t - u_a) \times 1]$). This means, the new complete parameter vector reads $\begin{pmatrix}\hat{\boldsymbol{x}}_\mathbf{1} & \hat{\tilde{\boldsymbol{x}}}_\boldsymbol{j} & \hat{\boldsymbol{q}}_\boldsymbol{j}\end{pmatrix}^T$ with the dimension $[(u + u_a) \times 1]$. The transformation of the complete system (2.46) is done with

$$\boldsymbol{T} = \begin{bmatrix} \boldsymbol{I}_{[u-u_t-u_a]} & \mathbf{0} & \cdots & \mathbf{0} \\ \mathbf{0} & \boldsymbol{T_1} & & \\ \vdots & & \ddots & \\ \mathbf{0} & & & \boldsymbol{T_N} \end{bmatrix}, \qquad \boldsymbol{S} = \begin{bmatrix} \mathbf{0} & \cdots & \mathbf{0} \\ \boldsymbol{S_1} & & \\ & \ddots & \\ & & \boldsymbol{S_N} \end{bmatrix}, \qquad \boldsymbol{d} = \begin{pmatrix} \mathbf{0} \\ \boldsymbol{d_1} \\ \vdots \\ \boldsymbol{d_N} \end{pmatrix}, \qquad \boldsymbol{t} = \begin{pmatrix} \mathbf{0} \\ \boldsymbol{t_1} \\ \vdots \\ \boldsymbol{t_N} \end{pmatrix}. \tag{2.50}$$

The identity matrix $\boldsymbol{I}$ and the quadratic zero matrices $\mathbf{0}$ in Equation (2.50) have the dimension $[u - u_t - u_a]$ and correspond to the non-transformed parameters of the original equation system. The matrix $\boldsymbol{T}$ (dimension: $[u \times u]$) has always the form of a block-diagonal matrix whereas the form of $\boldsymbol{S}$ (dimension: $[(u + u_a) \times u_a]$) may vary (Gerstl et al., 2001). Using Equation (2.5) and (2.47), the general functional model at the observation equation level yields

$$\begin{aligned}
\tilde{\boldsymbol{A}} &= \begin{bmatrix}\boldsymbol{A}\boldsymbol{T} & \boldsymbol{A}\boldsymbol{S}\end{bmatrix}, \\
\tilde{\boldsymbol{l}} &= \boldsymbol{l} - \boldsymbol{A}\boldsymbol{t}, \\
\tilde{\boldsymbol{P}}_{\boldsymbol{ll}} &= \boldsymbol{P}_{\boldsymbol{ll}}, \\
\tilde{\boldsymbol{v}} &= \boldsymbol{v}, \\
\boldsymbol{t} &= \boldsymbol{T}(\tilde{\boldsymbol{x}}_\mathbf{0} - \boldsymbol{d}) + \boldsymbol{S}\boldsymbol{q_0} - \boldsymbol{x_0}, \ \tilde{\boldsymbol{x}}_\mathbf{0} \text{ defined} \quad \text{(case 1)}, \\
\tilde{\boldsymbol{x}}_\mathbf{0} &= \boldsymbol{T}^{-1}(\boldsymbol{x_0} - \boldsymbol{S}\boldsymbol{q_0}) + \boldsymbol{d} = \boldsymbol{R}(\boldsymbol{x_0} - \boldsymbol{S}\boldsymbol{q_0}) + \boldsymbol{d} \quad \text{(case 2)}.
\end{aligned} \tag{2.51}$$

At the NEQ level, the functional model reads

$$\begin{aligned}
\tilde{\boldsymbol{N}} &= \begin{bmatrix}\boldsymbol{T}^T\boldsymbol{N}\boldsymbol{T} & \boldsymbol{T}^T\boldsymbol{N}\boldsymbol{S} \\ \boldsymbol{S}^T\boldsymbol{N}\boldsymbol{T} & \boldsymbol{S}^T\boldsymbol{N}\boldsymbol{S}\end{bmatrix}, \\
\tilde{\boldsymbol{y}} &= \begin{pmatrix}\boldsymbol{T}^T(\boldsymbol{y} - \boldsymbol{N}\boldsymbol{t}) \\ \boldsymbol{S}^T(\boldsymbol{y} - \boldsymbol{N}\boldsymbol{t})\end{pmatrix}, \\
\tilde{\boldsymbol{l}}^T\tilde{\boldsymbol{P}}_{\boldsymbol{ll}}\tilde{\boldsymbol{l}} &= \boldsymbol{l}^T\boldsymbol{P}_{\boldsymbol{ll}}\boldsymbol{l} - \boldsymbol{t}^T(2\boldsymbol{y} - \boldsymbol{N}\boldsymbol{t}), \\
\boldsymbol{t} &= \boldsymbol{T}(\tilde{\boldsymbol{x}}_\mathbf{0} - \boldsymbol{d}) + \boldsymbol{S}\boldsymbol{q_0} - \boldsymbol{x_0}, \ \tilde{\boldsymbol{x}}_\mathbf{0} \text{ defined} \quad \text{(case 1)}, \\
\tilde{\boldsymbol{x}}_\mathbf{0} &= \boldsymbol{T}^{-1}(\boldsymbol{x_0} - \boldsymbol{S}\boldsymbol{q_0}) + \boldsymbol{d} = \boldsymbol{R}(\boldsymbol{x_0} - \boldsymbol{S}\boldsymbol{q_0}) + \boldsymbol{d} \quad \text{(case 2)}.
\end{aligned} \tag{2.52}$$

If $\boldsymbol{q_0}$ and $\hat{\boldsymbol{q}}$ are given, the general functional model at the solution level is

$$\hat{\tilde{\boldsymbol{x}}} = \boldsymbol{R}\hat{\boldsymbol{x}} + \boldsymbol{d} - \boldsymbol{R}\boldsymbol{S}\hat{\boldsymbol{q}}, \qquad \text{or}$$

$$\begin{aligned}
\tilde{\boldsymbol{N}}^{-1} &= \begin{bmatrix}\tilde{\boldsymbol{N}}_{\mathbf{11}} & \tilde{\boldsymbol{N}}_{\mathbf{12}} \\ \tilde{\boldsymbol{N}}_{\mathbf{21}} & \tilde{\boldsymbol{N}}_{\mathbf{22}}\end{bmatrix}^{-1} = \begin{bmatrix}\boldsymbol{T}^T\boldsymbol{N}\boldsymbol{T} & \boldsymbol{T}^T\boldsymbol{N}\boldsymbol{S} \\ \boldsymbol{S}^T\boldsymbol{N}\boldsymbol{T} & \boldsymbol{S}^T\boldsymbol{N}\boldsymbol{S}\end{bmatrix}^{-1} = \\
&= \begin{bmatrix} (\tilde{\boldsymbol{N}}_{\mathbf{11}} - \tilde{\boldsymbol{N}}_{\mathbf{12}}\tilde{\boldsymbol{N}}_{\mathbf{22}}^{-1}\tilde{\boldsymbol{N}}_{\mathbf{21}})^{-1} & -\tilde{\boldsymbol{N}}_{\mathbf{11}}^{-1}\tilde{\boldsymbol{N}}_{\mathbf{12}}(\tilde{\boldsymbol{N}}_{\mathbf{22}} - \tilde{\boldsymbol{N}}_{\mathbf{21}}\tilde{\boldsymbol{N}}_{\mathbf{11}}^{-1}\tilde{\boldsymbol{N}}_{\mathbf{12}})^{-1} \\ -\tilde{\boldsymbol{N}}_{\mathbf{22}}^{-1}\tilde{\boldsymbol{N}}_{\mathbf{21}}(\tilde{\boldsymbol{N}}_{\mathbf{11}} - \tilde{\boldsymbol{N}}_{\mathbf{12}}\tilde{\boldsymbol{N}}_{\mathbf{22}}^{-1}\tilde{\boldsymbol{N}}_{\mathbf{21}})^{-1} & (\tilde{\boldsymbol{N}}_{\mathbf{22}} - \tilde{\boldsymbol{N}}_{\mathbf{21}}\tilde{\boldsymbol{N}}_{\mathbf{11}}^{-1}\tilde{\boldsymbol{N}}_{\mathbf{12}})^{-1} \end{bmatrix} \\
\Delta\hat{\tilde{\boldsymbol{x}}} &= \boldsymbol{R}(\Delta\hat{\boldsymbol{x}} - \boldsymbol{S}\Delta\hat{\boldsymbol{q}} - \boldsymbol{t}), \\
\tilde{\boldsymbol{l}}^T\tilde{\boldsymbol{P}}_{\boldsymbol{ll}}\tilde{\boldsymbol{l}} &= \boldsymbol{l}^T\boldsymbol{P}_{\boldsymbol{ll}}\boldsymbol{l} - \boldsymbol{t}^T\boldsymbol{N}(2\Delta\hat{\boldsymbol{x}} - \boldsymbol{t}), \\
\hat{\tilde{\boldsymbol{v}}}^T\tilde{\boldsymbol{P}}_{\boldsymbol{ll}}\hat{\tilde{\boldsymbol{v}}} &= \hat{\boldsymbol{v}}^T\boldsymbol{P}_{\boldsymbol{ll}}\hat{\boldsymbol{v}} \\
\boldsymbol{t} &= \boldsymbol{T}(\tilde{\boldsymbol{x}}_\mathbf{0} - \boldsymbol{d}) + \boldsymbol{S}\boldsymbol{q_0} - \boldsymbol{x_0}, \ \tilde{\boldsymbol{x}}_\mathbf{0} \text{ defined} \quad \text{(case 1)}, \\
\tilde{\boldsymbol{x}}_\mathbf{0} &= \boldsymbol{T}^{-1}(\boldsymbol{x_0} - \boldsymbol{S}\boldsymbol{q_0}) + \boldsymbol{d} = \boldsymbol{R}(\boldsymbol{x_0} - \boldsymbol{S}\boldsymbol{q_0}) + \boldsymbol{d} \quad \text{(case 2)}.
\end{aligned} \tag{2.53}$$

a) Introduction of linear station motions

The station coordinates $\boldsymbol{x_j}(t_i)$ of the j-th station ($1 \leq j \leq N$) can be represented through a linear model relative to t_0 as

$$\boldsymbol{x_j}(t_i) = \boldsymbol{x_j}(t_0) + (t_i - t_0)\dot{\boldsymbol{x}}_{\boldsymbol{j}}(t_0). \tag{2.54}$$

Thereby, the parameter vector is extended by the 3-dimensional station velocities $\dot{\boldsymbol{x}}_{\boldsymbol{j}}(t_0)$. The a priori values $\boldsymbol{x_{j,0}}(t_i)$ of the coordinates of the j-th station at the i-th epoch ($1 \leq i \leq T$) are kept (which means that $\boldsymbol{x_{j,0}}(t_i) = \boldsymbol{x_{j,0}}(t_0)$ is assumed) and new a priori values $\boldsymbol{q_{j,0}}(t_0)$ are introduced into the a priori vector $\tilde{\boldsymbol{x}}_{\boldsymbol{0}}(t_0)$. Using Equation (2.54), the general functional model for the epoch t_i yields $\boldsymbol{d} = \boldsymbol{0}, \boldsymbol{t} = \boldsymbol{0}$ and

$$\boldsymbol{T} = \boldsymbol{I_u}, \qquad \boldsymbol{q_0} = \begin{pmatrix} \dot{\boldsymbol{x}}_{\boldsymbol{1,0}} \\ \vdots \\ \dot{\boldsymbol{x}}_{\boldsymbol{N,0}} \end{pmatrix}, \qquad \boldsymbol{S} = \begin{bmatrix} \boldsymbol{0} & \cdots & \boldsymbol{0} \\ \boldsymbol{S_1} & & \\ & \ddots & \\ & & \boldsymbol{S_N} \end{bmatrix}, \qquad \text{with} \qquad \boldsymbol{S_j} = (t_i - t_0)\boldsymbol{I_3}. \tag{2.55}$$

For a detailed description of the above matrices and its structure, please see Equation (2.50) and its description.

At the observation equation level, Equation (2.55) and (2.51) result in

$$\tilde{\boldsymbol{A}} = \begin{bmatrix} \boldsymbol{A} & \boldsymbol{AS} \end{bmatrix}, \qquad \tilde{\boldsymbol{l}} = \boldsymbol{l}, \qquad \tilde{\boldsymbol{P}}_{\boldsymbol{ll}} = \boldsymbol{P_{ll}}, \qquad \tilde{\boldsymbol{v}} = \boldsymbol{v}, \qquad \tilde{\boldsymbol{x}}_{\boldsymbol{0}} = \boldsymbol{x_0} - \boldsymbol{Sq_0}. \tag{2.56}$$

At the NEQ level, applying Equation (2.55) to (2.52) gives

$$\tilde{\boldsymbol{N}} = \begin{bmatrix} \boldsymbol{N} & \boldsymbol{NS} \\ \boldsymbol{S^T N} & \boldsymbol{S^T NS} \end{bmatrix}, \qquad \tilde{\boldsymbol{y}} = \begin{pmatrix} \boldsymbol{y} \\ \boldsymbol{S^T y} \end{pmatrix}, \qquad \tilde{\boldsymbol{l}}^T \tilde{\boldsymbol{P}}_{\boldsymbol{ll}} \tilde{\boldsymbol{l}} = \boldsymbol{l}^T \boldsymbol{P_{ll}} \boldsymbol{l}, \qquad \tilde{\boldsymbol{x}}_{\boldsymbol{0}} = \boldsymbol{x_0} - \boldsymbol{Sq_0}. \tag{2.57}$$

The transformed quantities of the solution level with Equation (2.55) and (2.53) are

$$\begin{aligned}
\hat{\tilde{\boldsymbol{x}}} &= \hat{\boldsymbol{x}} - \boldsymbol{S}\hat{\boldsymbol{q}}, \qquad \text{and} \\
\tilde{\boldsymbol{N}}^{-1} &= \begin{bmatrix} \boldsymbol{N} & \boldsymbol{NS} \\ \boldsymbol{S^T N} & \boldsymbol{S^T NS} \end{bmatrix}^{-1} = \begin{bmatrix} \tilde{\boldsymbol{N}}_{\boldsymbol{11}} & \tilde{\boldsymbol{N}}_{\boldsymbol{12}} \\ \tilde{\boldsymbol{N}}_{\boldsymbol{21}} & \tilde{\boldsymbol{N}}_{\boldsymbol{22}} \end{bmatrix}^{-1} = \\
&= \begin{bmatrix} (\tilde{\boldsymbol{N}}_{\boldsymbol{11}} - \tilde{\boldsymbol{N}}_{\boldsymbol{12}}\tilde{\boldsymbol{N}}_{\boldsymbol{22}}^{-1}\tilde{\boldsymbol{N}}_{\boldsymbol{21}})^{-1} & -\tilde{\boldsymbol{N}}_{\boldsymbol{11}}^{-1}\tilde{\boldsymbol{N}}_{\boldsymbol{12}}(\tilde{\boldsymbol{N}}_{\boldsymbol{22}} - \tilde{\boldsymbol{N}}_{\boldsymbol{21}}\tilde{\boldsymbol{N}}_{\boldsymbol{11}}^{-1}\tilde{\boldsymbol{N}}_{\boldsymbol{12}})^{-1} \\ -\tilde{\boldsymbol{N}}_{\boldsymbol{22}}^{-1}\tilde{\boldsymbol{N}}_{\boldsymbol{21}}(\tilde{\boldsymbol{N}}_{\boldsymbol{11}} - \tilde{\boldsymbol{N}}_{\boldsymbol{12}}\tilde{\boldsymbol{N}}_{\boldsymbol{22}}^{-1}\tilde{\boldsymbol{N}}_{\boldsymbol{21}})^{-1} & (\tilde{\boldsymbol{N}}_{\boldsymbol{22}} - \tilde{\boldsymbol{N}}_{\boldsymbol{21}}\tilde{\boldsymbol{N}}_{\boldsymbol{11}}^{-1}\tilde{\boldsymbol{N}}_{\boldsymbol{12}})^{-1} \end{bmatrix} \\
\Delta\hat{\tilde{\boldsymbol{x}}} &= \Delta\hat{\boldsymbol{x}} - \boldsymbol{S}\Delta\hat{\boldsymbol{q}}, \\
\tilde{\boldsymbol{l}}^{\boldsymbol{T}} \tilde{\boldsymbol{P}}_{\boldsymbol{ll}} \tilde{\boldsymbol{l}} &= \boldsymbol{l}^{\boldsymbol{T}} \boldsymbol{P_{ll}} \boldsymbol{l}, \\
\hat{\tilde{\boldsymbol{v}}}^{\boldsymbol{T}} \tilde{\boldsymbol{P}}_{\boldsymbol{ll}} \hat{\tilde{\boldsymbol{v}}} &= \hat{\boldsymbol{v}}^{\boldsymbol{T}} \boldsymbol{P_{ll}} \hat{\boldsymbol{v}}, \\
\tilde{\boldsymbol{x}}_{\boldsymbol{0}} &= \boldsymbol{x_0} - \boldsymbol{Sq_0}.
\end{aligned} \tag{2.58}$$

b) Introduction of linear-trigonometric station motion

A refined mathematical approach for modeling the motion of a station $\boldsymbol{x_j}$ is the linear-trigonometric representation relative to t_0

$$\boldsymbol{x_j}(t_i) = \boldsymbol{x_j}(t_0) + (t_i - t_0)\dot{\boldsymbol{x}}_{\boldsymbol{j}}(t_0) + \boldsymbol{c_j}(t_0)\cos((t_i - t_0)\omega) + \boldsymbol{s_j}(t_0)\sin((t_i - t_0)\omega). \tag{2.59}$$

In this case, the parameter vector is extended by the 3-dimensional station velocities $\dot{\boldsymbol{x}}_{\boldsymbol{j}}(t_0)$ and the amplitudes of the sine- and cosine-terms $\boldsymbol{s_j}(t_0)$ and $\boldsymbol{c_j}(t_0)$. The frequency ω can be arbitrarily chosen (e.g., $\omega = \frac{2\pi}{1\,yr}$). This leads to the general functional model with $\Delta t_i = (t_i - t_0)$

$$\boldsymbol{T} = \boldsymbol{I_u}, \qquad \boldsymbol{q_0} = \begin{pmatrix} \dot{\boldsymbol{x}}_{\boldsymbol{1,0}} \\ \boldsymbol{c}_{\boldsymbol{1,0}} \\ \boldsymbol{s}_{\boldsymbol{1,0}} \\ \vdots \\ \dot{\boldsymbol{x}}_{\boldsymbol{N,0}} \\ \boldsymbol{c}_{\boldsymbol{N,0}} \\ \boldsymbol{s}_{\boldsymbol{N,0}} \end{pmatrix}, \qquad \boldsymbol{S} = \begin{bmatrix} \boldsymbol{0} & \cdots & \boldsymbol{0} \\ \boldsymbol{S_1} & & \\ & \ddots & \\ & & \boldsymbol{S_N} \end{bmatrix}, \qquad \boldsymbol{d} = \boldsymbol{0}, \qquad \boldsymbol{t} = \boldsymbol{0} \qquad \text{with} \tag{2.60}$$

$$\boldsymbol{S_1} = \begin{bmatrix} \Delta t_i \boldsymbol{I_3} & \cos(\Delta t_i \omega)\boldsymbol{I_3} & \sin(\Delta t_i \omega)\boldsymbol{I_3} \end{bmatrix}.$$

For a detailed description of the structure of $\boldsymbol{S}$, please see Equation (2.50) and its description. The introduction of a linear-trigonometric station motion model at the three levels of the *Gauß-Markov* model can be done by inserting Equation (2.60) in Equation (2.56), (2.57) and (2.58), respectively.

c) Introduction of infinitesimal similarity transformation parameters

If k different equation systems with j stations $\hat{\boldsymbol{x}}_{\boldsymbol{j}}^{\boldsymbol{k}}$ at the same epoch are given and should be combined to common unknown station coordinates $\hat{\boldsymbol{x}}_{\boldsymbol{j}}$, it is important that they have a common geodetic datum. Therefore, sometimes it is necessary to transform the datum of one equation system to another or to remove undocumented constraints from it. In case of Cartesian coordinates, a 7-parameter similarity (Helmert) transformation ($u_a = 7$) or in case of Cartesian coordinates and velocities, a 14-parameter similarity transformation ($u_a = 14$) can be used for k different equation systems. The seven parameters are

$$\begin{aligned} &\mu = \mu(t) \in \mathbb{R}: && \text{the scale parameter,} \\ &\boldsymbol{\alpha} = \begin{bmatrix} \alpha & \beta & \gamma \end{bmatrix}^T = \begin{bmatrix} \alpha(t) & \beta(t) & \gamma(t) \end{bmatrix}^T \in \mathbb{R}^3: && \text{the three Cardan angles or rotations,} \\ &\boldsymbol{h} = \begin{bmatrix} h^1 & h^2 & h^3 \end{bmatrix}^T = \begin{bmatrix} h^1(t) & h^2(t) & h^3(t) \end{bmatrix}^T \in \mathbb{R}^3: && \text{the 3-dimensional translation vector of origin.} \end{aligned}$$

The 14 parameters are the above described seven parameters plus their rates. The vector of additional unknowns of the k-th equation system in case of the ($u_a = 7$)-parameter similarity transformation reads

$$\begin{aligned} \hat{\boldsymbol{q}}_{\boldsymbol{k}}^{\boldsymbol{i}} &= \left(\hat{q}_k^1 \dots \hat{q}_k^{u_a}\right)^T = \left(q_0^1 + \Delta\hat{q}_k^1 \dots q_0^{u_a} + \Delta\hat{q}_k^{u_a}\right)^T = \begin{pmatrix} \mu_k & \boldsymbol{\alpha}_{\boldsymbol{k}}^T & \boldsymbol{h}_{\boldsymbol{k}}^T \end{pmatrix}^T \qquad \text{and} \\ \hat{\boldsymbol{q}}_{\boldsymbol{k}}^{\boldsymbol{i}} &= \left(\hat{q}_k^1 \dots \hat{q}_k^{u_a}\right)^T = \left(q_0^1 + \Delta\hat{q}_k^1 \dots q_0^{u_a} + \Delta\hat{q}_k^{u_a}\right)^T = \begin{pmatrix} \mu_k & \boldsymbol{\alpha}_{\boldsymbol{k}}^T & \boldsymbol{h}_{\boldsymbol{k}}^T & \dot{\mu}_k & \dot{\boldsymbol{\alpha}}_{\boldsymbol{k}}^T & \dot{\boldsymbol{h}}_{\boldsymbol{k}}^T \end{pmatrix}^T \end{aligned} \tag{2.61}$$

in case of the ($u_a = 14$)-parameter transformation, respectively. The 7-parameter similarity transformation of a station j with $1 \le j \le N$ of the k-th equation system can be written as

$$\hat{\tilde{\boldsymbol{x}}}_{\boldsymbol{j}}^{\boldsymbol{k}} = (1 + \mu_k)\boldsymbol{D}_k \hat{\boldsymbol{x}}_{\boldsymbol{j}}^{\boldsymbol{k}} + \boldsymbol{h_k} = \boldsymbol{H}_{\boldsymbol{j}}^{\boldsymbol{7}}(\hat{\boldsymbol{x}}_{\boldsymbol{j}}^{\boldsymbol{k}}, \hat{\boldsymbol{q}}_{\boldsymbol{k}}) \qquad \text{with} \qquad \boldsymbol{D_k} = \boldsymbol{D}_{\boldsymbol{k}}^{\boldsymbol{1}}(\alpha_k)\boldsymbol{D}_{\boldsymbol{k}}^{\boldsymbol{2}}(\beta_k)\boldsymbol{D}_{\boldsymbol{k}}^{\boldsymbol{3}}(\gamma_k) \tag{2.62}$$

using the elementary three dimensional rotation matrices $\boldsymbol{D}_{\boldsymbol{k}}^{\boldsymbol{1}}$, $\boldsymbol{D}_{\boldsymbol{k}}^{\boldsymbol{2}}$ and $\boldsymbol{D}_{\boldsymbol{k}}^{\boldsymbol{3}}$ around the $x-$, $y-$ and $z-$axis

$$\boldsymbol{D}_{\boldsymbol{k}}^{\boldsymbol{1}}(\alpha_k) = \begin{bmatrix} 1 & 0 & 0 \\ 0 & \cos\alpha_k & \sin\alpha_k \\ 0 & -\sin\alpha_k & \cos\alpha_k \end{bmatrix}, \; \boldsymbol{D}_{\boldsymbol{k}}^{\boldsymbol{2}}(\beta_k) = \begin{bmatrix} \cos\beta_k & 0 & -\sin\beta_k \\ 0 & 1 & 0 \\ \sin\beta_k & 0 & \cos\beta_k \end{bmatrix}, \; \boldsymbol{D}_{\boldsymbol{k}}^{\boldsymbol{3}}(\gamma_k) = \begin{bmatrix} \cos\gamma_k & \sin\gamma_k & 0 \\ -\sin\gamma_k & \cos\gamma_k & 0 \\ 0 & 0 & 1 \end{bmatrix}. \tag{2.63}$$

The inverse transformation with respect to Equation (2.62) yields

$$\hat{\boldsymbol{x}}_{\boldsymbol{j}}^{\boldsymbol{k}} = \boldsymbol{H}_{\boldsymbol{j}}^{\boldsymbol{u_a=7}}(\hat{\tilde{\boldsymbol{x}}}_{\boldsymbol{j}}^{\boldsymbol{k}}, \hat{\boldsymbol{q}}_{\boldsymbol{k}}) = \frac{1}{(1 + \mu_k)}\boldsymbol{D}_{\boldsymbol{k}}^T(\boldsymbol{\alpha_k})(\hat{\tilde{\boldsymbol{x}}}_{\boldsymbol{j}}^{\boldsymbol{k}} - \boldsymbol{h_k}). \tag{2.64}$$

Since only small datum differences between two equation systems are assumed, infinitesimal similarity transformation parameters are computed through a Taylor series expansion (terminated after the first order correction

term) of $\boldsymbol{H}_j^{u_a}(\hat{\tilde{\boldsymbol{x}}}_j^k, \hat{\boldsymbol{q}}_k)$ using $\tilde{\boldsymbol{x}}_j^k$ as starting points and assuming common a priori values for the unknowns $\boldsymbol{q_0} = \boldsymbol{0}$ for all k equation systems (see also Gerstl et al., 2001):

$$\boldsymbol{H}_j^{u_a}(\hat{\tilde{\boldsymbol{x}}}_j^k, \hat{\boldsymbol{q}}_k) = \boldsymbol{H}_j^{u_a}(\hat{\tilde{\boldsymbol{x}}}_j^k, \boldsymbol{q_0} + \Delta\hat{\boldsymbol{q}}_k) = \boldsymbol{H}_j^{u_a}(\hat{\tilde{\boldsymbol{x}}}_j^k, \boldsymbol{0}) + \sum_{i=1}^{u_a} \frac{\partial \boldsymbol{H}_j^{u_a}(\hat{\tilde{\boldsymbol{x}}}_j^k, \boldsymbol{0})}{\partial \hat{\boldsymbol{q}}_k^i} \cdot \Delta\hat{\boldsymbol{q}}_k^i + O(\Delta\hat{\boldsymbol{q}}^2). \tag{2.65}$$

By inserting the partial derivatives of Equation (2.64) into Equation (2.65), the transformation reads

$$\hat{\boldsymbol{x}}_j^k = \hat{\tilde{\boldsymbol{x}}}_j^k + \sum_{i=1}^{u_a=7} \frac{\partial \boldsymbol{H}_j^{u_a}(\hat{\tilde{\boldsymbol{x}}}_j^k, \boldsymbol{0})}{\partial \hat{\boldsymbol{q}}_k^i} \cdot \Delta\hat{\boldsymbol{q}}_k = \hat{\tilde{\boldsymbol{x}}}_j^k + \begin{bmatrix} \tilde{x}_j^k & 0 & -\tilde{z}_j^k & \tilde{y}_j^k & 1 & 0 & 0 \\ \tilde{y}_j^k & \tilde{z}_j^k & 0 & -\tilde{x}_j^k & 0 & 1 & 0 \\ \tilde{z}_j^k & -\tilde{y}_j^k & \tilde{x}_j^k & 0 & 0 & 0 & 1 \end{bmatrix} \cdot \begin{pmatrix} -\Delta\mu_k \\ -\Delta\boldsymbol{\alpha_k} \\ -\Delta\boldsymbol{h_k} \end{pmatrix}. \tag{2.66}$$

The negative signs of the unknown transformation parameters are caused by the inverse transformation of Equation (2.64) compared to Equation (2.62) (see Gerstl et al., 2001). If the equation system contains coordinates and velocities, $u_a = 14$ and $\partial \boldsymbol{H}_j^{u_a}(\hat{\tilde{\boldsymbol{x}}}_j^k, \boldsymbol{0})/\partial\hat{\boldsymbol{q}}_k$ reads

$$\frac{\partial \boldsymbol{H}_j^{14}(\hat{\tilde{\boldsymbol{x}}}_j^k, \boldsymbol{0})}{\partial \hat{\boldsymbol{q}}_k} = \begin{bmatrix} \frac{\partial \boldsymbol{H}_j^7(\hat{\tilde{\boldsymbol{x}}}_j^k, \boldsymbol{0})}{\partial \hat{\boldsymbol{q}}_k} & \boldsymbol{0} \\ \frac{\partial \dot{\boldsymbol{H}}_j^7(\hat{\tilde{\boldsymbol{x}}}_j^k, \boldsymbol{0})}{\partial \hat{\boldsymbol{q}}_k} & \frac{\partial \boldsymbol{H}_j^7(\hat{\tilde{\boldsymbol{x}}}_j^k, \boldsymbol{0})}{\partial \hat{\boldsymbol{q}}_k} \end{bmatrix} \quad \text{with} \quad \frac{\partial \dot{\boldsymbol{H}}_j^7(\hat{\tilde{\boldsymbol{x}}}_j^k, \boldsymbol{0})}{\partial \hat{\boldsymbol{q}}_k} = \begin{bmatrix} \dot{\tilde{x}}_j^k & 0 & -\dot{\tilde{z}}_j^k & \dot{\tilde{y}}_j^k & 0 & 0 & 0 \\ \dot{\tilde{y}}_j^k & \dot{\tilde{z}}_j^k & 0 & -\dot{\tilde{x}}_j^k & 0 & 0 & 0 \\ \dot{\tilde{z}}_j^k & -\dot{\tilde{y}}_j^k & \dot{\tilde{x}}_j^k & 0 & 0 & 0 & 0 \end{bmatrix}. \tag{2.67}$$

The Equations (2.66) and (2.67) can now be used to define the mapping of j stations of the k-th equation system on the combined solution as

$$\begin{aligned} \hat{\boldsymbol{x}}_j^k &= \boldsymbol{T}_k(\hat{\tilde{\boldsymbol{x}}}_j^k - \boldsymbol{d}_j^k) + \boldsymbol{S}_k\Delta\hat{\boldsymbol{q}}_k, \\ \Delta\hat{\boldsymbol{x}}_j^k &= \boldsymbol{T}_k\Delta\hat{\tilde{\boldsymbol{x}}}_j^k + \boldsymbol{S}_k\Delta\hat{\boldsymbol{q}}_k + \boldsymbol{t}_j^k, \end{aligned} \tag{2.68}$$

with

$$\boldsymbol{T}_k = \begin{bmatrix} \boldsymbol{I}_{u-u_t-u_a} & \boldsymbol{0} & \cdots & \boldsymbol{0} \\ \boldsymbol{0} & \boldsymbol{T}_1 & & \\ \vdots & & \ddots & \\ \boldsymbol{0} & & & \boldsymbol{T}_N \end{bmatrix} = \boldsymbol{I_u}, \quad \boldsymbol{S}_k = \begin{bmatrix} \boldsymbol{0} \\ \frac{\partial \boldsymbol{H}_1^{u_a}(\hat{\tilde{\boldsymbol{x}}}_1^k, \boldsymbol{0})}{\partial \hat{\boldsymbol{q}}_k} \\ \vdots \\ \frac{\partial \boldsymbol{H}_N^{u_a}(\hat{\tilde{\boldsymbol{x}}}_N^k, \boldsymbol{0})}{\partial \hat{\boldsymbol{q}}_k} \end{bmatrix}, \quad \boldsymbol{d}_j^k = \boldsymbol{0} \quad \text{and} \quad \boldsymbol{t}_j^k = \boldsymbol{0} \tag{2.69}$$

for the (u_a)-parameter transformation. In Equation (2.69), u_t is the number of transformed coordinates (and velocities). The corrections for the unknowns of the $(u_a = 7)$-parameter transformation as well as of the $(u_a = 14)$-parameter transformation are explained in Equation (2.61) with $\boldsymbol{q_0} = \boldsymbol{0}$. The introduction of infinitesimal similarity transformation parameters at the three levels of the *Gauß-Markov* model can be done by inserting Equation (2.69) in Equation (2.56), (2.57) and (2.58), respectively.

2.2.3 Reduction of parameters

In order to keep the NEQs easy to handle (limited dimension of NEQs), technique-specific parameters might be reduced from a NEQ system. The reduction of u_r parameters $\Delta\boldsymbol{x_1}$ can be performed at each level of the *Gauß-Markov* model. The reduction at the observation equation and the NEQ level is based on the partial inversion of the Jacobian matrix $\boldsymbol{A}$ and the NEQ matrix $\boldsymbol{N}$. Thereby, the part of $\boldsymbol{A}$ and $\boldsymbol{N}$ associated with the unknowns $\Delta\boldsymbol{x_1}$ ($\boldsymbol{A_1}$, $\boldsymbol{N_{11}}$) must be regular and of full rank.

To reduce the unknowns $\Delta\boldsymbol{x_1}$ at the observation equation level, the n observation equations are reordered in such a way that the unknowns to be reduced are stored at the beginning of the equation system

$$\Delta\boldsymbol{x} = \begin{pmatrix} \Delta\boldsymbol{x_1} \\ \Delta\boldsymbol{x_2} \end{pmatrix} \Leftrightarrow \begin{bmatrix} \boldsymbol{A_1} & \boldsymbol{A_2} \end{bmatrix} \begin{pmatrix} \Delta\boldsymbol{x_1} \\ \Delta\boldsymbol{x_2} \end{pmatrix} = \boldsymbol{A_1}\Delta\boldsymbol{x_1} + \boldsymbol{A_2}\Delta\boldsymbol{x_2} = \boldsymbol{b} + \boldsymbol{v}. \tag{2.70}$$

Using Cholesky decomposition, the positive definite weight matrix $\boldsymbol{P_{ll}}$ is split up into $\boldsymbol{R^T R}$. With $\boldsymbol{R}$ being the 'root of $\boldsymbol{P_{ll}}$', Equation (2.70) is 'homogenized' and changes to

$$\boldsymbol{RA_1\Delta x_1 + RA_2\Delta x_2 = Rl + Rv} \Leftrightarrow \boldsymbol{\bar{A}_1\Delta x_1 + \bar{A}_2\Delta x_2 = \bar{l} + \bar{v}}. \tag{2.71}$$

For the reduction of unknowns at the observation equation level, the non-quadratic Jacobian matrix $\boldsymbol{A_1}$ has to be inverted. If $rg(\boldsymbol{A_1}) = u_r\ (\leq u)$, the pseudoinverse matrix

$$\boldsymbol{\bar{A}_1^+ = (\bar{A}_1^T \bar{A}_1)^{-1} \bar{A}_1^T} \qquad \text{with} \qquad \boldsymbol{\bar{A}_1^+ \bar{A}_1 = I_{u_r}} \tag{2.72}$$

can be used. Multiplying Equation (2.71) with $\boldsymbol{\bar{A}_1^+}$ from the left leads to the so-called *Restitution-Equation*

$$\boldsymbol{\Delta x_1 = \bar{A}_1^+(\bar{l} + \bar{v}) - \bar{A}_1^+ \bar{A}_2 \Delta x_2}. \tag{2.73}$$

With this equation, the reduced unknowns $\boldsymbol{\Delta x_1}$ can be restored again in the observation equations. Multiplying Equation (2.71) with $(\boldsymbol{I_{[n]} - \bar{A}_1 \bar{A}_1^+})$ from the left leads to the reduced observation equation

$$\boldsymbol{(I_{[n]} - \bar{A}_1 \bar{A}_1^+)\bar{A}_2 \Delta x_2 = (I_{[n]} - \bar{A}_1 \bar{A}_1^+)(\bar{l} + \bar{v})}. \tag{2.74}$$

Back-substituting $\boldsymbol{\bar{A}_1 = RA_1}$ and $\boldsymbol{\bar{A}_2 = RA_2}$ in Equation (2.74) yields to

$$\begin{aligned} \boldsymbol{\tilde{A}} &= \boldsymbol{(I_{[n]} - A_1(A_1^T P_{ll} A_1)^{-1} A_1^T P_{ll})A_2}, \\ \boldsymbol{\tilde{l}} &= \boldsymbol{(I_{[n]} - A_1(A_1^T P_{ll} A_1)^{-1} A_1^T P_{ll})l}, \\ \boldsymbol{\tilde{P}_{ll}} &= \boldsymbol{P_{ll}}, \\ \boldsymbol{\tilde{v}} &= \boldsymbol{(I_{[n]} - A_1(A_1^T P_{ll} A_1)^{-1} A_1^T P_{ll})v} \end{aligned} \tag{2.75}$$

at the observation equation level. The *Restitution-Equation* reads

$$\boldsymbol{\Delta x_1 = (A_1^T P_{ll} A_1)^{-1} A_1^T P_{ll}(l + v) - (A_1^T P_{ll} A_1)^{-1} A_1^T P_{ll} A_2 \Delta x_2}. \tag{2.76}$$

If we assume that $rg(\boldsymbol{A}) = rg([\boldsymbol{A_1}\ \boldsymbol{A_2}]) = u$ and $rg(\boldsymbol{A_1}) = u_r$, it follows that $rg(\boldsymbol{\tilde{A}}) = u - u_r$ (Gerstl et al., 2001). Since Equation (2.75) has the dimension n (linear independent observation equations), the first u_r observation equations (rows of the equation system) disappear in the reduced observation equation system. For the redundancy of the reduced observation equation system $\tilde{r}$, it follows

$$\tilde{r} = \tilde{n} - \tilde{u} = (n - u_r) - (u - u_r) = n - u = r. \tag{2.77}$$

In the same way as it was done at the observation equation level, the reduction of unknowns at the NEQ level starts with a symmetric sorting of unknowns

$$\begin{pmatrix} \boldsymbol{y_1} \\ \boldsymbol{y_2} \end{pmatrix} = \begin{bmatrix} \boldsymbol{N_{11}} & \boldsymbol{N_{12}} \\ \boldsymbol{N_{12}^T} & \boldsymbol{N_{22}} \end{bmatrix} \begin{pmatrix} \boldsymbol{\Delta\hat{x}_1} \\ \boldsymbol{\Delta\hat{x}_2} \end{pmatrix}. \tag{2.78}$$

Using Gaussian elimination method, Equation (2.78) changes to

$$\begin{pmatrix} \boldsymbol{N_{11}^{-1} y_1} \\ \boldsymbol{y_2 - N_{12}^T N_{11}^{-1} y_1} \end{pmatrix} = \begin{bmatrix} \boldsymbol{I_{u_r}} & \boldsymbol{N_{11}^{-1} N_{12}} \\ \boldsymbol{0} & \boldsymbol{N_{22} - N_{12}^T N_{11}^{-1} N_{12}} \end{bmatrix} \begin{pmatrix} \boldsymbol{\Delta\hat{x}_1} \\ \boldsymbol{\Delta\hat{x}_2} \end{pmatrix}. \tag{2.79}$$

The first row of Equation (2.79) is the *Restitution-Equation* at the NEQ level. The second row provides

$$\begin{aligned} \boldsymbol{\tilde{N}} &= \boldsymbol{N_{22} - N_{12}^T N_{11}^{-1} N_{12}}, \\ \boldsymbol{\tilde{y}} &= \boldsymbol{y_2 - N_{12}^T N_{11}^{-1} y_1}, \\ \boldsymbol{\tilde{l}^T \tilde{P}_{ll} \tilde{l}} &= \boldsymbol{\left((I_n - A_1(A_1^T P_{ll} A_1)^{-1} A_1^T P_{ll})l\right)^T P_{ll} \left((I_n - A_1(A_1^T P_{ll} A_1)^{-1} A_1^T P_{ll})l\right)} \\ &= \boldsymbol{l^T P_{ll} l - y_1^T N_{11}^{-1} y_1}. \end{aligned} \tag{2.80}$$

The reduction of unknowns at the parameter (solution) level is trivial. Since no partial inversion of $\boldsymbol{A}$ or $\boldsymbol{N}$ is necessary, the remaining unknowns can simply be extracted from the sorted solution system

$$\begin{aligned} \hat{\boldsymbol{x}} &= \begin{pmatrix} \hat{\boldsymbol{x}}_1 \\ \hat{\boldsymbol{x}}_2 \end{pmatrix} = \begin{pmatrix} \boldsymbol{x}_{0,1} \\ \boldsymbol{x}_{0,2} \end{pmatrix} + \begin{pmatrix} \boldsymbol{\Delta}\hat{\boldsymbol{x}}_1 \\ \boldsymbol{\Delta}\hat{\boldsymbol{x}}_2 \end{pmatrix} \qquad \text{with} \\ \begin{pmatrix} \boldsymbol{\Delta}\hat{\boldsymbol{x}}_1 \\ \boldsymbol{\Delta}\hat{\boldsymbol{x}}_2 \end{pmatrix} &= \begin{bmatrix} \boldsymbol{N}_{11} & \boldsymbol{N}_{12} \\ \boldsymbol{N}_{12}^T & \boldsymbol{N}_{22} \end{bmatrix}^{-1} \begin{pmatrix} \boldsymbol{y}_1 \\ \boldsymbol{y}_2 \end{pmatrix} = \begin{bmatrix} (\boldsymbol{N}^{-1})_{11} & (\boldsymbol{N}^{-1})_{12} \\ (\boldsymbol{N}^{-1})_{12}^T & (\boldsymbol{N}^{-1})_{22} \end{bmatrix} \begin{pmatrix} \boldsymbol{y}_1 \\ \boldsymbol{y}_2 \end{pmatrix} = \begin{bmatrix} \boldsymbol{M}_{11} & \boldsymbol{M}_{12} \\ \boldsymbol{M}_{12}^T & \boldsymbol{M}_{22} \end{bmatrix} \begin{pmatrix} \boldsymbol{y}_1 \\ \boldsymbol{y}_2 \end{pmatrix}. \end{aligned} \tag{2.81}$$

In Equation (2.81), the first row is the *Restitution-Equation* at the parameter level

$$\boldsymbol{\Delta}\hat{\boldsymbol{x}}_1 = \boldsymbol{M}_{11}\boldsymbol{y}_1 + \boldsymbol{M}_{12}\boldsymbol{y}_2. \tag{2.82}$$

The second row of Equation (2.81) provides the quantities of the reduced equation system at the parameter level:

$$\begin{aligned} \hat{\tilde{\boldsymbol{x}}} &= \hat{\boldsymbol{x}}_2, \qquad \text{and} \\ \tilde{\boldsymbol{N}}^{-1} &= \boldsymbol{M}_{22} = (\boldsymbol{N}^{-1})_{22}, \\ \boldsymbol{\Delta}\hat{\tilde{\boldsymbol{x}}} &= \boldsymbol{\Delta}\hat{\boldsymbol{x}}_2, \\ \tilde{\boldsymbol{l}}^T \tilde{\boldsymbol{P}}_{ll} \tilde{\boldsymbol{l}} &= \hat{\boldsymbol{v}}^T \boldsymbol{P}_{ll} \hat{\boldsymbol{v}} + \boldsymbol{\Delta}\hat{\boldsymbol{x}}_2^T \boldsymbol{M}_{22}^{-1} \boldsymbol{\Delta}\hat{\boldsymbol{x}}_2, \\ \hat{\tilde{\boldsymbol{v}}}^T \tilde{\boldsymbol{P}}_{ll} \hat{\tilde{\boldsymbol{v}}} &= \tilde{\boldsymbol{l}}^T \tilde{\boldsymbol{P}}_{ll} \tilde{\boldsymbol{l}} - \tilde{\boldsymbol{y}}^T \boldsymbol{\Delta}\hat{\tilde{\boldsymbol{x}}} = \hat{\boldsymbol{v}}^T \boldsymbol{P}_{ll} \hat{\boldsymbol{v}} \qquad \text{with Equation (2.79) and (2.80).} \end{aligned} \tag{2.83}$$

2.2.4 Elimination of parameters

The elimination of u_e parameters has two main applications:

(i) Fix parameters $\hat{\boldsymbol{x}}_1$ to the values $\boldsymbol{z}_1$. Thus, the corrections read $\boldsymbol{\Delta}\hat{\boldsymbol{x}}_1 = \boldsymbol{z}_1 - \boldsymbol{x}_{0,1}$. If the parameters are fixed to their a priori values, the corrections are zero. This application is a possibility to fix the geodetic datum if, e.g., the latitude and longitude of one station and the longitude of another station (in total three conditions) are fixed to its a priori value. Then, no additional constraints are necessary (see also Section 2.2.5).

(ii) Equalize parameters $\hat{\boldsymbol{x}}_1$ and $\hat{\boldsymbol{x}}_2$ (e.g., EOP offsets at day boundaries). This application is not really an elimination, but a transformation. As a result, the restriction equation $\boldsymbol{\Delta}\hat{\boldsymbol{x}}_1 - \boldsymbol{\Delta}\hat{\boldsymbol{x}}_2 = \boldsymbol{x}_{0,2} - \boldsymbol{x}_{0,1}$ can be formulated.

Both applications can be expressed through the generalized linear equation

$$\boldsymbol{C}_1\boldsymbol{\Delta}\hat{\boldsymbol{x}}_1 + \boldsymbol{C}_2\boldsymbol{\Delta}\hat{\boldsymbol{x}}_2 = \boldsymbol{z} \quad \text{with} \begin{cases} \boldsymbol{C}_1 = \boldsymbol{I}_{[u_e]},\ \boldsymbol{C}_2 = \boldsymbol{0} & \text{and } \boldsymbol{z} = \boldsymbol{z}_1 - \boldsymbol{x}_{0,1} + \boldsymbol{d}, \\ \boldsymbol{C}_1 = \boldsymbol{I}_{[u_e]},\ \boldsymbol{C}_{2_{[u_e \times (u-u_e)]}} & \text{and } \boldsymbol{z} = \boldsymbol{x}_{0,2} - \boldsymbol{x}_{0,1} + \boldsymbol{d}. \end{cases} \tag{2.84}$$

Therein, $\boldsymbol{\Delta}\hat{\boldsymbol{x}}_1$ are the parameters to be eliminated and $\boldsymbol{\Delta}\hat{\boldsymbol{x}}_2$ are the parameters which remain in the equation system. The matrix $\boldsymbol{C}_1$ must be a quadratic (regular) matrix. The structure of the matrix $\boldsymbol{C}_2$ depends on where the second group of parameters $\hat{\boldsymbol{x}}_2$ is stored in the equation system. If it is stored at the beginning of the remaining $(u - u_e)$ equations, $\boldsymbol{C}_2$ would have the structure $\left[-\boldsymbol{I}_{[u_e]} \quad \boldsymbol{0}_{[u_e \times (u-2u_e)]}\right]$. Multiplying Equation (2.84) with $\boldsymbol{C}_1^{-1}$ yields

$$\boldsymbol{\Delta}\hat{\boldsymbol{x}}_1 = \boldsymbol{C}_1^{-1}\boldsymbol{z} - \boldsymbol{C}_1^{-1}\boldsymbol{C}_2\boldsymbol{\Delta}\hat{\boldsymbol{x}}_2. \tag{2.85}$$

With Equation (2.85), the general transformation function can be expressed as

$$\boldsymbol{\Delta}\hat{\boldsymbol{x}} = \begin{pmatrix} \boldsymbol{\Delta}\hat{\boldsymbol{x}}_1 \\ \boldsymbol{\Delta}\hat{\boldsymbol{x}}_2 \end{pmatrix} \mapsto \boldsymbol{\Delta}\hat{\tilde{\boldsymbol{x}}} = \boldsymbol{\Delta}\hat{\boldsymbol{x}}_2 \tag{2.86}$$

$$\begin{pmatrix}\Delta\hat{\boldsymbol{x}}_1\\ \Delta\hat{\boldsymbol{x}}_2\end{pmatrix} = \underbrace{\begin{bmatrix}-\boldsymbol{C}_1^{-1}\boldsymbol{C}_2\\ \boldsymbol{I}_{[u-u_e]}\end{bmatrix}}_{=:\boldsymbol{T},} \Delta\hat{\tilde{\boldsymbol{x}}} + \underbrace{\begin{pmatrix}\boldsymbol{C}_1^{-1}\boldsymbol{z}\\ \boldsymbol{0}\end{pmatrix}}_{=:\boldsymbol{t},} \qquad \boldsymbol{d} = \boldsymbol{0} \tag{2.87}$$

After separating the parameters $\Delta\hat{\boldsymbol{x}}_2$, the observation equations and the NEQ system read

$$\boldsymbol{b} + \boldsymbol{v} = \begin{bmatrix}\boldsymbol{A}_1 & \boldsymbol{A}_2\end{bmatrix}\begin{pmatrix}\Delta\boldsymbol{x}_1\\ \Delta\boldsymbol{x}_2\end{pmatrix}, \tag{2.88}$$

$$\begin{pmatrix}\boldsymbol{y}_1\\ \boldsymbol{y}_2\end{pmatrix} = \begin{bmatrix}\boldsymbol{N}_{11} & \boldsymbol{N}_{12}\\ \boldsymbol{N}_{21} & \boldsymbol{N}_{22}\end{bmatrix}\begin{pmatrix}\Delta\hat{\boldsymbol{x}}_1\\ \Delta\hat{\boldsymbol{x}}_2\end{pmatrix}. \tag{2.89}$$

At the observation equation level, Equation (2.87) and (2.23) result in

$$\begin{aligned}\tilde{\boldsymbol{A}} &= \boldsymbol{A}\boldsymbol{T} = \begin{bmatrix}\boldsymbol{A}_1 & \boldsymbol{A}_2\end{bmatrix}\begin{bmatrix}-\boldsymbol{C}_1^{-1}\boldsymbol{C}_2\\ \boldsymbol{I}_{u-u_e}\end{bmatrix} = \boldsymbol{A}_2 - \boldsymbol{A}_1\boldsymbol{C}_1^{-1}\boldsymbol{C}_2,\\ \tilde{\boldsymbol{l}} &= \boldsymbol{l} - \boldsymbol{A}\boldsymbol{t} = l - \begin{bmatrix}\boldsymbol{A}_1 & \boldsymbol{A}_2\end{bmatrix}\begin{bmatrix}\boldsymbol{C}_1^{-1}\boldsymbol{z}\\ \boldsymbol{0}\end{bmatrix} = \boldsymbol{l} - \boldsymbol{A}_1\boldsymbol{C}_1^{-1}\boldsymbol{z},\\ \tilde{\boldsymbol{P}}_{ll} &= \boldsymbol{P}_{ll},\\ \tilde{\boldsymbol{v}} &= \boldsymbol{v}.\end{aligned} \tag{2.90}$$

At the NEQ level, applying Equation (2.87) to (2.24) gives

$$\begin{aligned}\tilde{\boldsymbol{N}} &= \boldsymbol{T}^T\boldsymbol{N}\boldsymbol{T} = (\boldsymbol{N}_{22} - \boldsymbol{N}_{12}\boldsymbol{C}_1^{-1}\boldsymbol{C}_2) - (\boldsymbol{C}_1^{-1}\boldsymbol{C}_2)^T(\boldsymbol{N}_{12} - \boldsymbol{N}_{11}\boldsymbol{C}_1^{-1}\boldsymbol{C}_2),\\ \tilde{\boldsymbol{y}} &= \boldsymbol{T}^T(\boldsymbol{y} - \boldsymbol{N}\boldsymbol{t}) = (\boldsymbol{y}_2 - (\boldsymbol{C}_1^{-1}\boldsymbol{C}_2)^T\boldsymbol{y}_1) - (\boldsymbol{N}_{12}^T\boldsymbol{C}_1^{-1}\boldsymbol{z}) + (\boldsymbol{C}_1^{-1}\boldsymbol{C}_2)^T\boldsymbol{N}_{11}\boldsymbol{C}_1^{-1}\boldsymbol{z},\\ \tilde{\boldsymbol{l}}^T\tilde{\boldsymbol{P}}_{ll}\tilde{\boldsymbol{l}} &= \boldsymbol{l}^T\boldsymbol{P}_{ll}\boldsymbol{l} - \boldsymbol{t}^T(2\boldsymbol{y} - \boldsymbol{N}\boldsymbol{t}) =\\ &= \boldsymbol{l}^T\boldsymbol{P}_{ll}\boldsymbol{l} - 2(\boldsymbol{C}_1^{-1}\boldsymbol{z})^T\boldsymbol{y}_1 + (\boldsymbol{C}_1^{-1}\boldsymbol{z})^T\boldsymbol{N}_{11}(\boldsymbol{C}_1^{-1}\boldsymbol{z}).\end{aligned} \tag{2.91}$$

According to Equation (2.25), the transformation matrix $\boldsymbol{R} = \boldsymbol{T}^{-1}$ is used at the solution level. Since $\boldsymbol{T}$ is not a quadratic matrix (dimension is $[u \times (u - u_e)]$) and therefore not invertible, the elimination of parameters at the solution level is not possible. A possibility to eliminate parameters from a given solution system would be the reconstruction of the NEQ system (see Section 2.2.6) and the application of Equation (2.91). Afterwards, a solution can be computed again using Equation (2.13).

If solutions are combined, the estimated parameters are used to built new observation equations and start a second least squares adjustment process (see Figure 2.3). Therein, the elimination of parameters is possible.

2.2.5 Application of constraints on equation systems

In Section 2.1, the NEQ matrix has the rank $rg(\boldsymbol{N}) = u$. If the NEQ matrix has a rank deficiency of $n_c = u - rg(\boldsymbol{N})$ with $rg(\boldsymbol{N}) < u$, this singularity can be removed by introducing appropriate and sufficient constraints. The constraints can be introduced as additional observations $\boldsymbol{c}$ with the standard deviations $\boldsymbol{\sigma_c}$ in an independent ($\boldsymbol{l}$ and $\boldsymbol{c}$ uncorrelated) linear equation system

$$\boldsymbol{v_c} = \boldsymbol{C}\Delta\boldsymbol{x} - \boldsymbol{c}. \tag{2.92}$$

This kind of observations is called 'pseudo observations' hereafter. If $\boldsymbol{\sigma_c}$ is infinitely small, the equations of conditions have to be exactly fulfilled within the adjustment. Otherwise, the impact of the pseudo observations can be varied.

At the observation equation level, the new observation vector $\tilde{\boldsymbol{l}}$ and the new weight matrix $\tilde{\boldsymbol{P}}_{\boldsymbol{ll}}$ using the Jacobian matrix $\boldsymbol{C}$ of the pseudo observations read

$$\begin{aligned} \tilde{\boldsymbol{A}} &= \begin{bmatrix} \boldsymbol{A} \\ \boldsymbol{C} \end{bmatrix}, \qquad \tilde{\boldsymbol{l}} = \begin{pmatrix} \boldsymbol{l} \\ \boldsymbol{c} \end{pmatrix}, \qquad \tilde{\boldsymbol{v}} = \begin{pmatrix} \boldsymbol{v} \\ \boldsymbol{v_c} \end{pmatrix}, \\ \tilde{\boldsymbol{P}}_{\boldsymbol{ll}} &= \begin{bmatrix} \boldsymbol{P}_{\boldsymbol{ll}} & 0 \\ 0 & \boldsymbol{P}_{\boldsymbol{cc}} \end{bmatrix} \qquad \text{with } \boldsymbol{P}_{\boldsymbol{cc}} = diag(\boldsymbol{\sigma_c}). \end{aligned} \tag{2.93}$$

The pseudo observations $\boldsymbol{c}$ are transformed to a NEQ system of constraints with

$$\boldsymbol{C}^T \boldsymbol{P}_{\boldsymbol{cc}} \boldsymbol{C} \Delta\hat{\boldsymbol{x}} = \boldsymbol{C}^{\boldsymbol{T}} \boldsymbol{P}_{\boldsymbol{cc}} \boldsymbol{c}. \tag{2.94}$$

If the matrix $\boldsymbol{C}$ has the rank $rg(\boldsymbol{C}) = n_c = u - rg(\boldsymbol{N})$ and $rg(\tilde{\boldsymbol{N}}) = u$, the applied constraints are called 'minimum constraints'.

The constrained NEQ system is

$$\begin{aligned} \tilde{\boldsymbol{N}} &= (\boldsymbol{N} + \boldsymbol{C}^T \boldsymbol{P}_{\boldsymbol{cc}} \boldsymbol{C}), \\ \tilde{\boldsymbol{y}} &= \boldsymbol{y} + \boldsymbol{C}^T \boldsymbol{P}_{\boldsymbol{cc}} \boldsymbol{c}, \\ \tilde{\boldsymbol{l}}^{\boldsymbol{T}} \tilde{\boldsymbol{P}}_{\boldsymbol{ll}} \tilde{\boldsymbol{l}} &= \boldsymbol{l}^{\boldsymbol{T}} \boldsymbol{P}_{\boldsymbol{ll}} \boldsymbol{l} + \boldsymbol{c}^{\boldsymbol{T}} \boldsymbol{P}_{\boldsymbol{cc}} \boldsymbol{c}. \end{aligned} \tag{2.95}$$

The variance-covariance matrix of the pseudo observations reads

$$\boldsymbol{K}_{\boldsymbol{cc}} = \sigma_0^2 \boldsymbol{P}_{\boldsymbol{cc}}^{-1}. \tag{2.96}$$

The above discussed constraints are used to remove the rank deficiency of a NEQ system. Therefore, an application at the solution level is not necessary since the NEQ have already been inverted at this level. If the constrained solution fulfills the requirements based on Equation (2.7),

$$\tilde{\boldsymbol{v}}^T \tilde{\boldsymbol{P}}_{\boldsymbol{ll}} \tilde{\boldsymbol{v}} = \begin{pmatrix} \boldsymbol{v}^T & \boldsymbol{v}_{\boldsymbol{c}}^T \end{pmatrix} \begin{bmatrix} \boldsymbol{P}_{\boldsymbol{ll}} & \boldsymbol{0} \\ \boldsymbol{0} & \boldsymbol{P}_{\boldsymbol{cc}} \end{bmatrix} \begin{pmatrix} \boldsymbol{v} \\ \boldsymbol{v_c} \end{pmatrix} = \boldsymbol{v}^T \boldsymbol{P}_{\boldsymbol{ll}} \boldsymbol{v} + \boldsymbol{v}_{\boldsymbol{c}}^T \boldsymbol{P}_{\boldsymbol{ll}} \boldsymbol{v}_{\boldsymbol{c}} \rightarrow min, \tag{2.97}$$

it can be concluded that the weighted square sum of the residuals of the constrained solution reads

$$\hat{\tilde{\boldsymbol{v}}}^T \tilde{\boldsymbol{P}}_{\boldsymbol{ll}} \hat{\tilde{\boldsymbol{v}}} = \hat{\boldsymbol{v}}^T \boldsymbol{P}_{\boldsymbol{ll}} \hat{\boldsymbol{v}}, \tag{2.98}$$

and $\boldsymbol{\Delta\tilde{x}}$ solves the unconstrained NEQ system $\boldsymbol{N}^{-1}\boldsymbol{y}$ (Gerstl et al., 2001). This kind of constraints is called "non-distorting" constraints. Minimum constraints are always non-distorting constraints. In contrast, non-distorting constraints are not always minimum constraints. An example for problem-specific minimum constraints are the No-Net-Rotation (NNR) conditions for positions and velocities which are used to remove the rank deficiency w.r.t. the orientation of a NEQ. NNR means that a network of stations is not allowed to show any rotations around the coordinate axes of a previously and arbitrarily defined station network. This constraint is addressed in more detail in Section 3.1 and P-I. The formalism of the NNR conditions is described in Angermann et al. (2004). Besides the NNR conditions, the No-Net-Translation (NNT) conditions and the No-Net-Scale (NNS) conditions are used to remove rank deficiencies for the origin and the scale, respectively.

Loose constraints are non-minimum constraints which have a non-distorting character. Their weight (2.93) is chosen so small that their distorting impact on the equations or on the solution may be neglected (Angermann et al., 2004).

Another group of constraints are conditions for stabilizing weak parameters, e.g. conditions for satellite orbit parameters, clock jumps or tropospheric parameters (stabilizing constraints). An Analysis Center (AC) might apply these conditions and reduce the technique-specific parameters afterwards. The last group of constraints are real constraints such as Lagrange scaling factors for perturbing accelerations.

2.2.6 Reconstruction of constraint-free NEQ systems

For various combination studies at DGFI, input data of external institutions, software packages or users might be necessary. Therefore, the exchange of data which are usually stored in SINEX files is required. A detailed description of the SINEX format can be found in the SINEX format description[4]. Examples for such input data are the contributions for the computation of the ITRF which are provided by the four Technique Center (TC)s of the International Earth Rotation and Reference Systems Service (IERS). The TCs of the International GNSS Service (IGS), International Laser Ranging Service (ILRS), International VLBI Service for Geodesy and Astrometry (IVS) and International DORIS Service (IDS) are asked[5] to provide (i) solutions with removable constraints, (ii) loosely constrained solutions (constraint level: $\sigma > 1$ m) or (iii) constraint-free NEQ systems, which are used by the DGFI Combination Center (CC) to compute a TRF solution.

In the case of the ITRF2008, constrained-free NEQ systems (VLBI) and solutions (GPS, SLR and DORIS) had been provided for the combination (P-A). If any constraints have been applied on the input NEQ matrices to remove the rank deficiency and to achieve a solution, the constraint-free NEQs have to be reconstructed. Otherwise, the applied constraints will impact the combined solution. This step is necessary for the computation at DGFI since the used combination software realizes a combination at the NEQ level. In general, two different types of equation systems are stored in the SINEX files:

- NEQ system with stabilizing constraints $\{\boldsymbol{N}, \boldsymbol{y}, \boldsymbol{l}^T\boldsymbol{P}_{ll}\boldsymbol{l}, \boldsymbol{x_0}, n, u\}$,
- solution with minimum constraints $\{\hat{\tilde{\boldsymbol{K}}}_{\hat{\boldsymbol{x}}\hat{\boldsymbol{x}}}, \boldsymbol{K}_{\boldsymbol{cc}}, \hat{\tilde{\boldsymbol{x}}}, \hat{\tilde{\boldsymbol{v}}}^T\tilde{\boldsymbol{P}}_{ll}\hat{\tilde{\boldsymbol{v}}}, \hat{\sigma}_0^2, \boldsymbol{x_0}, n + n_c, u\}$.

For a constraint-free NEQ system, the corresponding right-hand side and the weighted square sum of O-C can be reconstructed by using Equation (2.95)

$$\begin{aligned} \boldsymbol{N} &= \tilde{\boldsymbol{N}} - \boldsymbol{C}^T\boldsymbol{P}_{\boldsymbol{cc}}\boldsymbol{C}, \\ \boldsymbol{y} &= \tilde{\boldsymbol{y}} - \boldsymbol{C}^T\boldsymbol{P}_{\boldsymbol{cc}}\boldsymbol{c}, \\ \boldsymbol{l}^T\boldsymbol{P}_{ll}\boldsymbol{l} &= \tilde{\boldsymbol{l}}^T\tilde{\boldsymbol{P}}_{ll}\tilde{\boldsymbol{l}} - \boldsymbol{c}^T\boldsymbol{P}_{\boldsymbol{cc}}\boldsymbol{c}. \end{aligned} \tag{2.99}$$

Usually, the quantities $\boldsymbol{c}$ and $\boldsymbol{P}_{\boldsymbol{cc}}$ are not stored in the SINEX files. In addition, stabilizing constraints of reduced parameters are also not stored in the SINEX files. Thus, the constrained NEQ systems has to be used for the combination.

Starting from the parameter level, the reconstruction of a constraint-free NEQ system by using Equation (2.98) and assuming $\hat{\tilde{\boldsymbol{x}}} = \hat{\boldsymbol{x}}$ (non-distorting constraints) reads

$$\begin{aligned} \boldsymbol{N} &= \hat{\sigma}_0^2\hat{\tilde{\boldsymbol{K}}}_{\hat{\boldsymbol{x}}\hat{\boldsymbol{x}}}^{-1} - \sigma_0^2\boldsymbol{K}_{\boldsymbol{cc}}^{-1}, \\ \boldsymbol{y} &= \boldsymbol{N}\Delta\hat{\boldsymbol{x}} = \boldsymbol{N}\Delta\hat{\tilde{\boldsymbol{x}}} = \left(\hat{\sigma}_0^2\hat{\boldsymbol{K}}_{\hat{\boldsymbol{x}}\hat{\boldsymbol{x}}}^{-1} - \sigma_0^2\boldsymbol{K}_{\boldsymbol{cc}}^{-1}\right)(\hat{\tilde{\boldsymbol{x}}} - \boldsymbol{x_0}), \\ \boldsymbol{l}^T\boldsymbol{P}_{ll}\boldsymbol{l} &= \boldsymbol{y}^T\Delta\hat{\boldsymbol{x}} + \hat{\boldsymbol{v}}^T\boldsymbol{P}_{ll}\hat{\boldsymbol{v}} = \boldsymbol{y}^T\Delta\hat{\tilde{\boldsymbol{x}}} + \hat{\tilde{\boldsymbol{v}}}^T\tilde{\boldsymbol{P}}_{ll}\hat{\tilde{\boldsymbol{v}}}. \end{aligned} \tag{2.100}$$

A critical issue in the reconstruction of constraint-free NEQs is the lack of $\boldsymbol{l}^T\boldsymbol{P}_{ll}\boldsymbol{l}$ or $\hat{\boldsymbol{v}}^T\boldsymbol{P}_{ll}\hat{\boldsymbol{v}}$ since these quantities are needed for the correct stochastic part of the NEQ system. In Equation (2.100), the reconstructed NEQs are assumed to have an a priori variance factor which is equal to $\hat{\sigma}_0^2$. If an a priori variance factor of 1.0 is required, the NEQs have to be rescaled. This leads to

$$\begin{aligned} \boldsymbol{N}' &= \hat{\tilde{\boldsymbol{K}}}_{\hat{\boldsymbol{x}}\hat{\boldsymbol{x}}}^{-1} - \frac{\sigma_0^2}{\hat{\sigma}_0^2}\boldsymbol{K}_{\boldsymbol{cc}}^{-1}, \\ \boldsymbol{y}' &= \boldsymbol{N}'\Delta\hat{\boldsymbol{x}}, \\ (\boldsymbol{l}^T\tilde{\boldsymbol{P}}_{ll}\boldsymbol{l})' &= \boldsymbol{y}'^T\Delta\hat{\boldsymbol{x}} + \frac{1}{\hat{\sigma}_0^2}\hat{\boldsymbol{v}}^T\boldsymbol{P}_{ll}\hat{\boldsymbol{v}}. \end{aligned} \tag{2.101}$$

[4] http://www.iers.org/IERS/EN/Organization/AnalysisCoordinator/SinexFormat/sinex_cont.html (2014-08-09)

[5] IERS Message No. 137: ITRF2008 Call for Participation, http://datacenter.iers.org/eop/-/somos/5Rgv/getMeta/2/message_137.txt, (2014-08-09)

If the applied constraints are not documented in the SINEX file, the free NEQ cannot be reconstructed using Equation (2.99) or (2.100). To remove the datum definition, infinitesimal similarity transformation parameters $\hat{\boldsymbol{q}}$ have to be introduced (see Section 2.2.2) using all station coordinates stored in the NEQ system. In contrast to this, the datum was fixed by using only a subset of station coordinates (see Section 2.2.5). Figure 2.5 compares the two possibilities to create a free NEQ.

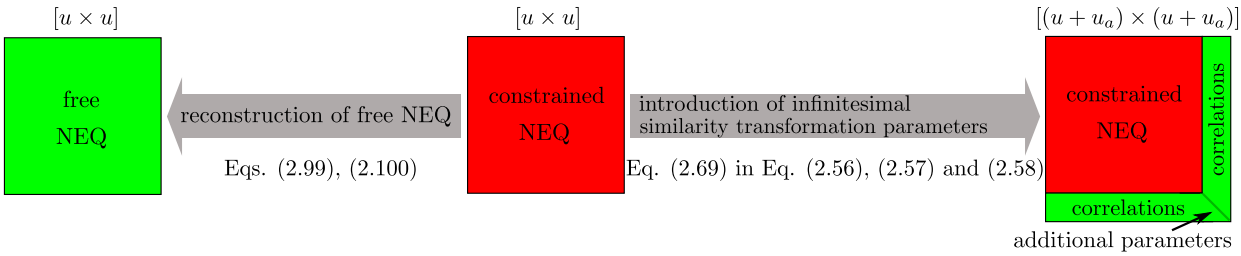

Figure 2.5: Comparison of reconstruction of a constraint-free NEQ system and introduction of infinitesimal similarity transformation parameters to restore the NEQ matrix singularity.

To test the datum information of the input data, Sillard and Boucher (2001) developed a strategy based on an S-transformation (similarity-linked transformation) to split the covariance matrix into (1) a part related to the internal noise in the observations and (2) a part related to the geodetic datum of the covariance matrix. Thereby, the internal part must be independent from the chosen reference system. Using the approach of Sillard and Boucher (2001), a given covariance matrix $\hat{\boldsymbol{K}}_{\hat{\boldsymbol{x}}\hat{\boldsymbol{x}}}$ can be split up into

$$\hat{\boldsymbol{K}}_{\hat{\boldsymbol{x}}\hat{\boldsymbol{x}}} = \hat{\boldsymbol{K}}_{\hat{\boldsymbol{x}}\hat{\boldsymbol{x}}} - \boldsymbol{S}(\boldsymbol{S}^T\hat{\boldsymbol{K}}_{\hat{\boldsymbol{x}}\hat{\boldsymbol{x}}}^{-1}\boldsymbol{S})^{-1}\boldsymbol{S}^T + \boldsymbol{S}(\boldsymbol{S}^T\hat{\boldsymbol{K}}_{\hat{\boldsymbol{x}}\hat{\boldsymbol{x}}}^{-1}\boldsymbol{S})^{-1}\boldsymbol{S}^T = \hat{\tilde{\boldsymbol{K}}}_{\hat{\boldsymbol{x}}\hat{\boldsymbol{x}}} + \boldsymbol{S}\hat{\boldsymbol{K}}_{\hat{\boldsymbol{q}}\hat{\boldsymbol{q}}}\boldsymbol{S}^T. \tag{2.102}$$

Therein, $\hat{\tilde{\boldsymbol{K}}}_{\hat{\boldsymbol{x}}\hat{\boldsymbol{x}}}$ is the part related to the internal noise in the observations and $\boldsymbol{S}\hat{\boldsymbol{K}}_{\hat{\boldsymbol{q}}\hat{\boldsymbol{q}}}\boldsymbol{S}^T$ is the part related to the geodetic datum of the covariance matrix. From this it follows that the covariance matrix of the u_a datum parameters $\hat{\boldsymbol{q}}$ is equal to

$$\hat{\boldsymbol{K}}_{\hat{\boldsymbol{q}}\hat{\boldsymbol{q}}} = (\boldsymbol{S}^T\hat{\boldsymbol{K}}_{\hat{\boldsymbol{x}}\hat{\boldsymbol{x}}}^{-1}\boldsymbol{S})^{-1} \qquad \text{with} \qquad \boldsymbol{S} = \begin{bmatrix} \boldsymbol{H}_1^{u_a} \\ \vdots \\ \boldsymbol{H}_N^{u_a} \end{bmatrix}. \tag{2.103}$$

For the definition of the matrices $\boldsymbol{H}_j^{u_a}$ with $1 \leq j \leq N$, please see Section 2.2.2. An example for the datum test can be found, e.g. for GPS, in Sillard and Boucher (2001) and for SLR in Angermann and Müller (2009). It is important to mention, that the matrix $\hat{\boldsymbol{K}}_{\hat{\boldsymbol{x}}\hat{\boldsymbol{x}}}$ should contain only station coordinates, since otherwise, the $\boldsymbol{S}$ matrix has the wrong dimension. Furthermore, if $\hat{\boldsymbol{K}}_{\hat{\boldsymbol{x}}\hat{\boldsymbol{x}}}$ has a rank deficiency, the matrix $\boldsymbol{S}^T\hat{\boldsymbol{K}}_{\hat{\boldsymbol{x}}\hat{\boldsymbol{x}}}^{-1}\boldsymbol{S}$ cannot be inverted. Therefore, loose constraints have to be added before the datum test.

2.3 Combination at observation, normal equation and parameter level

Based on Equation (2.5) and (2.6), the linearized observation equation system for the k-th technique with $1 \leq k \leq m$, each containing n_k observation equations and u_k unknowns, reads

$$\begin{aligned} \boldsymbol{v_k} &= \boldsymbol{A_k}\Delta\boldsymbol{x_k} - \boldsymbol{l_k}, \\ \boldsymbol{K_{ll,k}} &= \sigma_{0,k}^2(\boldsymbol{P_{ll,k}})^{-1} = \sigma_{0,k}^2\boldsymbol{Q_{ll,k}}. \end{aligned} \tag{2.104}$$

If all observation equations are related to the same parameters $\Delta\boldsymbol{x}$ and the same a priori reduction models and a priori values are used for the preprocessing, the combined equation system at the observation level is

$$\begin{pmatrix} \boldsymbol{v_1} \\ \vdots \\ \boldsymbol{v_m} \end{pmatrix} = \begin{bmatrix} \boldsymbol{A_1} \\ \vdots \\ \boldsymbol{A_m} \end{bmatrix}\Delta\boldsymbol{x} - \begin{pmatrix} \boldsymbol{l_1} \\ \vdots \\ \boldsymbol{l_m} \end{pmatrix}, \quad \boldsymbol{P_{ll}} = \sigma_0^2\begin{bmatrix} \boldsymbol{P_{ll,1}} & \boldsymbol{0} & \boldsymbol{0} \\ \boldsymbol{0} & \ddots & \boldsymbol{0} \\ \boldsymbol{0} & \boldsymbol{0} & \boldsymbol{P_{ll,m}} \end{bmatrix}. \tag{2.105}$$

This kind of combination is called “combination on the observation level”.

The advantage of a combination at the observation level is that a common preprocessing (data editing, outlier detection) can be performed. In contrast to the combination at the NEQ level, the weighting of single observations or the weighting of groups of observations can be done at the combination at the observation level. Furthermore, the combination might be realized in a much more efficient way (w.r.t. computation time) than a combination at the NEQ level.

As an example, the combination of GNSS clock parameters clearly identify this advantage. When GNSS observation equations are combined, the clock parameters can be reduced after the data editing. As a consequence, already reduced equation systems are combined. When GNSS NEQs are combined, the clock parameters must be still stored in the NEQ. This fact leads to huge NEQ systems where the combination needs a long computation time. After the combination, the clock parameters can be reduced.

Using Equation (2.105), the solution of the combined observation equation system can be computed according to Equations (2.7) to (2.16). The k-th NEQ system reads according to Equation (2.9)

$$\boldsymbol{N_k}\,\boldsymbol{\Delta x_k} = \boldsymbol{y_k}\,. \tag{2.106}$$

The NEQ systems can be combined by adding the elements which correspond to the same parameters. If the equation systems have different dimensions u_k, rows and columns with zero elements have to be inserted in the NEQ matrices $\boldsymbol{N_k}$ and zero elements in the NEQ vectors $\boldsymbol{y_k}$. Afterwards, a common sorting of all NEQ systems is done.

The combined NEQ system $\boldsymbol{N_c}$ with the a priori variance factor σ_0^2 can then be written as

$$\begin{aligned}
\boldsymbol{N_c} &= \lambda_1 \frac{\sigma_0^2}{\sigma_{0,1}^2}\boldsymbol{N_1} + \cdots + \lambda_m \frac{\sigma_0^2}{\sigma_{0,m}^2}\boldsymbol{N_m} = \sum_{k=1}^{m} \lambda_k \frac{\sigma_0^2}{\sigma_{0,k}^2}\boldsymbol{N_k}\,,\\
\boldsymbol{y_c} &= \lambda_1 \frac{\sigma_0^2}{\sigma_{0,1}^2}\boldsymbol{y_1} + \cdots + \lambda_m \frac{\sigma_0^2}{\sigma_{0,m}^2}\boldsymbol{y_m} = \sum_{k=1}^{m} \lambda_k \frac{\sigma_0^2}{\sigma_{0,k}^2}\boldsymbol{y_k}\,,\\
(\boldsymbol{l}^T\boldsymbol{P_{ll}}\boldsymbol{l})_c &= \lambda_1 \frac{\sigma_0^2}{\sigma_{0,1}^2}\boldsymbol{l_1}^T\boldsymbol{P_{ll,1}}\boldsymbol{l_1} + \cdots + \lambda_m \frac{\sigma_0^2}{\sigma_{0,1}^2}\boldsymbol{l_m}^T\boldsymbol{P_{ll,m}}\boldsymbol{l_m} = \sum_{k=1}^{m} \lambda_k \frac{\sigma_0^2}{\sigma_{0,k}^2}\boldsymbol{l_k}^T\boldsymbol{P_{ll,k}}\boldsymbol{l_k}\,.
\end{aligned} \tag{2.107}$$

The coefficients λ_k in Equation (2.107) are the individual weighting factors of the NEQs. This kind of combination is called "combination on the normal equation level". The solution of the combined NEQ system can be computed according to Equations (2.13) to (2.16).

At DGFI, the intra- and inter-technique combination of geodetic space techniques is performed at the NEQ level (P-I, P-A, Gerstl et al., 2001; Angermann et al., 2004).

The following paragraph briefly describes, for completeness, the "combination at parameter (solution) level" which is used by, e.g., the Institute Nationale de l'Information Géographique et Forestière (IGN) to combine different geodetic space techniques. The software used is called Combination and Analysis of Terrestrial REference Frames (CATREF; Altamimi et al., 2011). The individual technique solutions are obtained by using Equations (2.5) to (2.16). Therefore, individual minimum constraints to remove the rank deficiencies of the m NEQ matrices are applied. This step results in the NEQ matrix $(\boldsymbol{N_k} + \boldsymbol{C_k}^T\boldsymbol{P_{cc,k}}\boldsymbol{C_k})$ of the k-th equation system. The combination of the technique-dependent solutions is done afterwards by setting up a second least squares adjustment where the individual solutions are used as new observations ($\boldsymbol{l_k} = \hat{\boldsymbol{x}}_{\boldsymbol{k}}$) with the $\boldsymbol{A_k}$-matrix containing only zeros and ones

$$\begin{aligned}
\boldsymbol{A_{k_{[n_k \times u_k]}}}\boldsymbol{\Delta x_k} &= \hat{\boldsymbol{x}}_{\boldsymbol{k}} + \boldsymbol{v_k}\,,\\
\boldsymbol{K_{ll,k}} &= \sigma_{0,k}^2\boldsymbol{P_{ll,k}}^{-1} = \sigma_{0,k}^2(\boldsymbol{N_k} + \boldsymbol{C_k}^T\boldsymbol{P_{cc,k}}\boldsymbol{C_k})^{-1}.
\end{aligned} \tag{2.108}$$

In this equation system, individual infinitesimal similarity transformation parameters have to be introduced in order to ensure that the datum of the combined solution can be realized independently from the individual input solutions.

With Equation (2.108) and the assumption that all m equation systems are related to the same parameters $\boldsymbol{\Delta x}$ (ensured through expansion with zero elements and common a priori sorting), the combined equation system at the solution level reads

$$\begin{pmatrix} \boldsymbol{v_1} \\ \vdots \\ \boldsymbol{v_m} \end{pmatrix} = \begin{bmatrix} \boldsymbol{A_{1}}_{[n_1 \times u]} \\ \vdots \\ \boldsymbol{A_{m}}_{[n_m \times u]} \end{bmatrix} \boldsymbol{\Delta x} - \begin{pmatrix} \hat{\boldsymbol{x}}_\mathbf{1} \\ \vdots \\ \hat{\boldsymbol{x}}_\boldsymbol{m} \end{pmatrix}, \quad \boldsymbol{P_{ll}} = \sigma_0^2 \begin{bmatrix} (\boldsymbol{N_1} + \boldsymbol{C_1^T P_{cc,k} C_1}) & \mathbf{0} & \mathbf{0} \\ \mathbf{0} & \ddots & \mathbf{0} \\ \mathbf{0} & \mathbf{0} & (\boldsymbol{N_m} + \boldsymbol{C_m^T P_{cc,m} C_m}) \end{bmatrix}. \tag{2.109}$$

In this combined equation system, the individual solution vectors are assumed to be uncorrelated (block-diagonal structure of $\boldsymbol{P_{ll}}$). Using Equation (2.109), the solution of the combined observation equation system can be computed according to Equations (2.7) to (2.16).

2.4 Variance Component Estimation (VCE) at normal equation level

When combining the NEQs, the weighting of the different techniques can be done by, e.g., using equal weights, empirically derived weights (P-A) or by using an iteratively performed VCE (Koch and Kusche, 2002; Koch, 2004; Böckmann et al., 2010a; Bloßfeld and Seitz M., 2012; P-III). In this section, the iterative VCE algorithm based on a posteriori variance factors for NEQs is explained in detail.

Based on Equation (2.107), the combined NEQ system $\boldsymbol{N_c^{(j)}}$ of the (j)-th iteration step reads

$$\begin{aligned} \boldsymbol{N_c^{(j)}} &= \sum_{k=1}^{m} \frac{1}{\hat{\sigma}_{0,k}^{2(j)}} \boldsymbol{N_k}, \\ \boldsymbol{y_c^{(j)}} &= \sum_{k=1}^{m} \frac{1}{\hat{\sigma}_{0,k}^{2(j)}} \boldsymbol{y_k}, \\ (\boldsymbol{l^T P_{ll} l})_c^{(j)} &= \sum_{k=1}^{m} \frac{1}{\hat{\sigma}_{0,k}^{2(j)}} (\boldsymbol{l_k^T P_{ll,k} l_k}) \end{aligned} \tag{2.110}$$

with the a priori variance factor of the combined NEQ $\sigma_0^2 = 1$ and $\lambda_k = 1$ for $1 \leq k \leq m$. The solution of the NEQ system of the (j)-th iteration step is computed with Equation (2.13). The a posteriori variance factor of each NEQ of the first iteration is computed according to Equation (2.14). This means, the relative weighting factors of the NEQs depend on the a priori standard deviations of each individual NEQ system.

For the (j)-th iteration step, the weighted square sum of the residuals w.r.t. the combined parameter vector $\hat{\boldsymbol{x}}_\boldsymbol{c}$ and the partial redundancy of each of the k input NEQs can be computed according to

$$\begin{aligned} (\hat{\boldsymbol{v}}^T \boldsymbol{P_{ll}} \hat{\boldsymbol{v}})_{c,k}^{(j)} &= \hat{\boldsymbol{x}}_\boldsymbol{c}^{(j)^T} \boldsymbol{N_k} \hat{\boldsymbol{x}}_\boldsymbol{c}^{(j)} - 2 \boldsymbol{y_k^T} \hat{\boldsymbol{x}}_\boldsymbol{c}^{(j)} + \boldsymbol{l_k^T P_{ll,k} l_k}, \\ r_{c,k}^{(j)} &= n + n_c - \frac{1}{\hat{\sigma}_k^{2(j)}} tr(\boldsymbol{N_k N_c^{(j)^{-1}}}). \end{aligned} \tag{2.111}$$

The updated variance factor results from

$$\hat{\sigma}_{0,k}^{2(j+1)} = \frac{(\hat{\boldsymbol{v}}^T \boldsymbol{P_{ll}} \hat{\boldsymbol{v}})_{c,k}^{(j)}}{r_{c,k}^{(j)}} \tag{2.112}$$

and the iteration starts again from Equation (2.110). Due to the fact that the iterative estimation of the variance factors is based on the individual NEQs, no iterative correction of the individual design matrices $\boldsymbol{A_k}$ is done. The a priori values of the first iteration are kept.

2.5 DGFI Orbit and Geodetic parameter estimation Software (DOGS)

The DOGS software, developed at DGFI since 1980 mainly by Dr. rer. nat. Michael Gerstl, provides the ability to process observations of different geodetic space techniques and to combine equation systems at different levels of the *Gauß-Markov* model. The program package is split up into the observation processing libraries

DOGS-OC Orbit Computation library of DOGS (see Section 2.5.1 and Gerstl, 1997),

DOGS-RI Radio Interferometry library of DOGS (not further discussed in this thesis)

and the combination library

DOGS-CS Combination and Solution library of DOGS (see Section 2.5.2 and Gerstl et al., 2001).

All libraries are programmed in *Fortran* 2003 standard. In the following two sections, the main properties of DOGS-OC and DOGS-CS are introduced.

2.5.1 Orbit Computation library of DOGS (DOGS-OC)

DGFI is developing and maintaining the software package DOGS-OC to process and analyze laser ranging observations to Retro-Reflector-Array (RRA) equipped satellites. This software is also used by the ILRS ACs located at DGFI. Figure 2.6 shows a simplified flow chart of the DOGS-OC program package. In general, it is possible to distinguish between four different execution modes (Gerstl, 1997):

MODUS = 0 Numerical integration of a satellite orbit and recording of the satellite positions and velocities together with selected disturbing accelerations along the integrated orbit.

MODUS = 1 Numerical integration of a satellite orbit and simulation of the observations of this satellite from given stations.

MODUS = 2 Numerical integration of a satellite orbit and setting up the normal equations for a set of model parameters using the given observations.

MODUS = 3 Numerical integration of a satellite orbit and fitting a set of model parameters to the given observations using an iterative least squares adjustment.

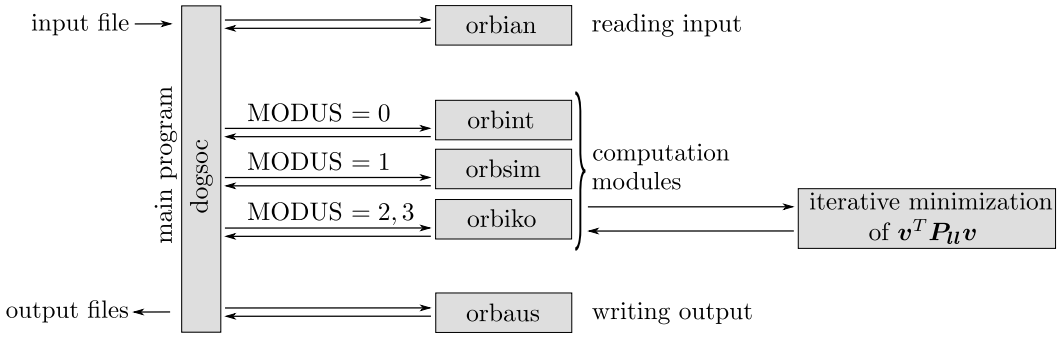

Figure 2.6: Schematic overview of DOGS-OC program package. The program is executed by starting dogsoc which calls the programs on the right from top to bottom. In the computation module "orbiko", an iterative minimization of the squared sum of the residuals $\boldsymbol{v}^T \boldsymbol{P}_{ll} \boldsymbol{v}$ is done (for details, see Section 2.1).

Within DOGS-OC, the functional model for processing laser ranging observations is set up as (P-C; Gerstl, 1997)

$$\begin{aligned} \rho + \epsilon = & ||\boldsymbol{r}_{\text{sat}}(t_M + \Delta t) - \boldsymbol{r}_{\text{sta}}(t_M + \Delta t)|| \\ & + \Delta\rho + c_{\text{trop}}(1 + \Delta r) + c_{\text{rel}} + c_{\text{sta}} + c_{\text{masc}} + c_{\text{mesc}} \end{aligned} \tag{2.113}$$

and comprises

ρ one-way range measurement (the vector of all ρ values is called $\boldsymbol{b}$ in Section 2.1),

ϵ measurement error (the vector of all ϵ values is called $\boldsymbol{v}$ in Section 2.1),

$\boldsymbol{r}_{\text{sat}}$ 3-dimensional position of the satellite in the GCRS [m],

t_M approximated epoch of reflection of the laser pulse at the satellite [s],

Δt time bias of measurement [s],

$\boldsymbol{r}_{\text{sta}}$ 3-dimensional position of the station in the ITRS [m],

$\Delta\rho$ range bias of measurement [m],

c_{trop} tropospheric range correction [m],

Δr bias of tropospheric refraction [-],

c_{rel} relativistic range correction [m],

c_{sta} station-dependent SLR correction [m],

c_{masc} satellite-specific center of mass correction (difference between reflector and center of mass of the satellite in measurement direction) [m],

c_{mesc} SLR array-dependent correction (e.g., phase center offset in measurement direction) [m].

In this modeling, two simplifications are assumed: (i) the two-way runtime is averaged and modeled as a one-way range measurement and (ii) the station position in the International Terrestrial Reference System (ITRS) is assumed to be constant during the runtime of the laser pulse (in the strict sense, the station rotates together with the Earth and Earth tides affect the station position during the pulse runtime). Besides the corrections of the range measurement, the station position $\boldsymbol{r}_{\text{sta}}(t_M + \Delta t)$ is corrected in advance for various effects at the epoch $t_M + \Delta t$. Displacements are conventionally corrected for solid Earth tides, ocean tides, diurnal and semidiurnal atmospheric pressure loading, rotational deformation due to polar motion and ocean pole tide loading (Petit and Luzum, 2010). Simultaneously, the position of the satellite $\boldsymbol{r}_{\text{sat}}(t)$ is affected by numerous gravitational and non-gravitational disturbing accelerations. The overall acceleration at the epoch t of a near-Earth satellite in the Geocentric Celestial Reference System (GCRS) is modeled in DOGS-OC as a sum of the direct gravitational acceleration $\boldsymbol{a}_{\text{DG}}(t)$ (direct effect on satellite), the indirect gravitational acceleration $\boldsymbol{a}_{\text{IG}}(t)$ (indirect effect on satellite via the Earth) and the non-gravitational acceleration $\boldsymbol{a}_{\text{NG}}(t)$

$$\begin{aligned}\ddot{\boldsymbol{r}}_{\text{sat}}(t) = \boldsymbol{a}(t) &= \boldsymbol{a}_{\text{DG}}(t) + \boldsymbol{a}_{\text{IG}}(t) + \boldsymbol{a}_{\text{NG}}(t) \\ &= \overbrace{\boldsymbol{a}_{\text{KEP}}(t) + \boldsymbol{a}_{\text{GE}}(t) + \boldsymbol{a}_{\text{GM}}(t) + \boldsymbol{a}_{\text{GP}}(t)} + \overbrace{\boldsymbol{a}_{\text{GT}}(t) + \boldsymbol{a}_{\text{GNT}}} + \boldsymbol{a}_{\text{NG}}(t).\end{aligned} \tag{2.114}$$

with

$\ddot{\boldsymbol{r}}_{\text{sat}}$ 3-dimensional total acceleration acting on a near-Earth satellite,

$\boldsymbol{a}_{\text{KEP}}$ 3-dimensional gravitational acceleration caused by the point-concentrated mass of the Earth (Stokes coefficient C_{00}),

$\boldsymbol{a}_{\text{GE}}$ 3-dimensional gravitational acceleration caused by the Earth (Stokes coefficients C_{nm}, S_{nm} with $n, m \in \mathbb{N}^+$ and $m \leq n$),

$\boldsymbol{a}_{\text{GM}}$ 3-dimensional gravitational acceleration caused by the Moon,

$\boldsymbol{a}_{\text{GP}}$ 3-dimensional gravitational acceleration caused by the Sun and other planets,

$\boldsymbol{a}_{\text{GT}}$ 3-dimensional gravitational acceleration caused by mass variations due to solid Earth and ocean tides,

$\boldsymbol{a}_{\text{GNT}}$ 3-dimensional gravitational acceleration caused by mass variations due to non-tidal loading effects (e.g., atmospheric, hydrological, oceanic).

In the context of this thesis, the DOGS-OC software has been further developed. Numerous improvements have been carried out for the indirect gravitational and the non-gravitational acceleration. In the following, the improvements are briefly discussed and the impact on the first-author publications is outlined.

The indirect gravitational acceleration consists of the acceleration $\boldsymbol{a}_{\mathrm{GT}}$, caused by solid Earth and ocean tides, and the acceleration $\boldsymbol{a}_{\mathrm{GNT}}$ which is caused by the gravitational effect due to non-tidal atmospheric, hydrological and oceanic crustal loading phenomena. Refined models for solid Earth and ocean tides and the ocean pole tide loading have been implemented in DOGS-OC version 5.3 according to the recommendations of the IERS Conventions 2010 (Petit and Luzum, 2010). Furthermore, the ocean tide modeling was improved in such a way that also secondary tidal waves are taken into account. The amplitudes of the secondary waves are linearly interpolated between the main wave amplitudes (provided via ocean tide models) under the assumption of a linear variation of the tidal admittance between closely spaced tidal frequencies. A detailed description of the programmed algorithm can be found in Petit and Luzum (2010). Especially the refined ocean tide modeling and the ocean pole tide modeling lead to significant improvements of the Stokes coefficients C_{21} and S_{21}. Hence, the accurate second-degree Stokes coefficients of P-III could be achieved.

According to Ciufolini (1987) and Lucchesi (2001; 2002), the non-gravitational acceleration $\boldsymbol{a}_{\mathrm{NG}}$ can be split up into

- radiation forces (direct solar radiation pressure, Earth albedo, satellite eclipses, Poynting-Robertson effect, Yarkovski-Rubincam effect (anisotropic thermal radiation), Yarkovski-Schach effect (infrared radiation)),
- drag-like forces (atmospheric drag, solar wind, interplanetary dust),
- other forces (e.g., Earth magnetic field, relativistic effect).

In order to compute the atmospheric drag, a refined model for the high atmosphere, JB2008 (Bowman et al., 2008), was implemented in the software. This improvement makes it possible to achieve a reliable orbit modeling for satellites at low altitudes (satellite height smaller than 2000 km; P-II, P-III, P-V) since for the precise orbit determination of these satellites, the high atmosphere has to be modeled (Sośnica, 2014).

The IERS Conventions 2010 recommend to model the relativistic acceleration of a near-Earth satellite by taking into account the *Schwarzschild* term, the gravitomagnetic effect (*Lense-Thirring* effect; Lense and Thirring, 1918) and the gravitoelectric effect (*de Sitter* effect; de Sitter, 1916). Up to version 5.2 of DOGS-OC, only the *Schwarzschild* term was considered. In the new version, all three types of the relativistic accelerations are implemented in the software. The effect of *Lense-Thirring* and *de Sitter* affect the satellite orbit and correlated geodetic parameters like LOD. In P-II, a secular effect of 0.0088 ms in LOD due to these accelerations was found.

The routines to import different non-tidal loading models and to compute the station displacement and satellite accelerations have been developed and integrated in the DOGS-OC version 5.3. Since these models are provided in various formats (0.5 degree to 2.5 degree grids) and temporal resolutions (three hours to one month), the models have been preprocessed by the Bundesamt für Kartographie und Geodäsie (BKG) in the framework of the Forschergruppe "Space-time reference systems for monitoring global change and for precise navigation in space" (FOR 1503; Nothnagel et al., 2010) of the Deutsche Forschungsgemeinschaft (DFG).

Currently, the treatment of non-spherical satellites is implemented in the software. This means, the new version has to take into account the satellite surface model (surface orientation and material properties), the orientation of the satellite (quaternions based on observations of star cameras), the orientation of solar panels, possible steering maneuvers and fuel consumption (variable center of mass).

2.5.2 Combination and Solution library of DOGS (DOGS-CS)

At DGFI, the program package used to combine observations or NEQs is called Combination and Solution library of DOGS (DOGS-CS). The software consists of several specialized routines which can be used to (i) apply operations on equation systems, (ii) combine equation systems and (iii) solve NEQ systems. In the following, a short description of the most important DOGS-CS routines is given.

i) Apply matrix operations with DOGS-CS

CS_TRAFO TRAnsFOrmation routine of DOGS-CS. This routine consists of various parameter transformations which use a regular transformation matrix $\boldsymbol{R}$. Examples for such transformations are given in Section 2.2.1.

CS_TRASI TRAnsformation with SIngluar transformation matrix routine of DOGS-CS. In contrast to CS-TRAFO, this routine consists of various transformations which use an irregular transformation matrix $\boldsymbol{R}$. Therefore, these transformations can be applied only at solutions. An example for such transformations is the differentiation of daily EOP or the interpolation between daily EOP.

CS_INPAR This routine can be used for the transformation of parameters with an introduction of new parameters into a NEQ system. The mathematical foundations and examples such as the introduction of station velocities, the introduction of a linear-trigonometric station motion model and the introduction of infinitesimal similarity transformation parameters are given in Section 2.2.2.

CS_REDUC With CS_REDUC, parameters of a NEQ or solution system can be reduced in order to keep the NEQs easy to handle (limited dimension of NEQs). The basics for this routine are summarized in Section 2.2.3.

CS_ELIM This routine is used to create elimination equations and apply them to NEQ systems according to Section 2.2.4. It can be used to fix parameters of an equation system to an arbitrarily defined value or to equalize two different parameters.

CS_COND This routine is used to create condition equations and apply them to an equation system (see Section 2.2.5). Examples for condition equations implemented in this routine are the NNT, NNR and NNS conditions (see also Angermann et al., 2004).

ii) Combine equation systems with DOGS-CS

CS_ADD CS_ADD is used to add two equation systems with arbitrary relative weights (see Section 2.3). If observation or condition equations are added to a NEQ, the additional NEQ system is set up in advance.

CS_WICHT This routine can be used to scale or re-weight a given equation system. An example for such an application is the re-weighting of the GNSS contribution w.r.t. the other geodetic space techniques in the computation of the DGFI Terrestrial Reference Frame (DTRF)2008 (for details, please see P-A).

iii) Solve NEQ systems with DOGS-CS

CS_INVERT This routine is used for the inversion of a NEQ and the solution of a linear equation system.

The advantage of the DOGS-CS program architecture is that computation procedures such as shown in Figure 2.1 can be built modular and therefore fit very well to any problem. Some examples for the use of DOGS-CS at DGFI are the computation of global TRF solutions like the DTRF2008 (Section 3.1.2), the computation of ERFs (Section 3.1.6a, 3.2.4a and P-I, P-IV and P-V) and the computation of multi-satellite SLR solutions (Section 3.2.4b, 3.3.5a and P-III, P-V). Furthermore, DOGS-CS is used at DGFI to combine SLR and GRACE NEQs (Section 3.3.5b and P-C). The examples given above emphasize the importance of DOGS-CS for the work presented in this thesis.

The DOGS-CS program package is also used by the official combination center of the IVS which is jointly operated by BKG and DGFI (Bachmann et al., 2014).

3 Fundamental geodetic parameters

This chapter provides general information about the fundamental geodetic parameter groups Terrestrial Reference Frame (TRF), EOP and Stokes coefficients which are associated with the three pillars of GGOS. They are addressed in the publications P-I to P-V and P-A to P-D. The theoretical basis (definition and realization) for each parameter group is recapitulated and the current state-of-the-art of the products is discussed and evaluated. Going into details, the sections discuss limitations of current products and present selected investigations on the combined solutions which are published in the first-author journal articles used for this dissertation in order to improve the products. In each section, the key role of SLR in the inter- and intra-technique combination is outlined. Figure 3.1 shows the first-author publications in relation to the geodetic parameters discussed in this chapter. The causal coherence of the first-author publications is emphasized in Figure 1.1.

Thereby, the main focus of P-I, P-IV and P-A is the optimal estimation of station coordinates and velocities through a combination of GNSS, SLR and VLBI (and DORIS in case of P-A). An optimal TRF determination involves the correct realization of the geodetic datum (origin, orientation, scale). A major result of P-I was the quantification of the annual variation of the terrestrial pole coordinates x_p and y_p which is caused by the neglect of center of network variations in the multi-year reference frame (MRF). In P-IV, the length of the combination interval is varied and the stability of different datum realizations is evaluated.

Publication P-II investigates the interactions of secular perturbations of the orbit and LOD. The study shows that systematics in the Stokes coefficient C_{20} significantly affect the LOD estimates. This impact is reduced, when observations to more than one satellite are combined.

The paper P-III studies the estimation of second-degree Stokes coefficients when observations of up to ten satellites are combined. Thereby, the impact of each satellite on the decorrelation of highly correlated parameters is investigated.

Finally, P-V uses this multi-satellite SLR solution to estimate all three parameter groups in one common adjustment.

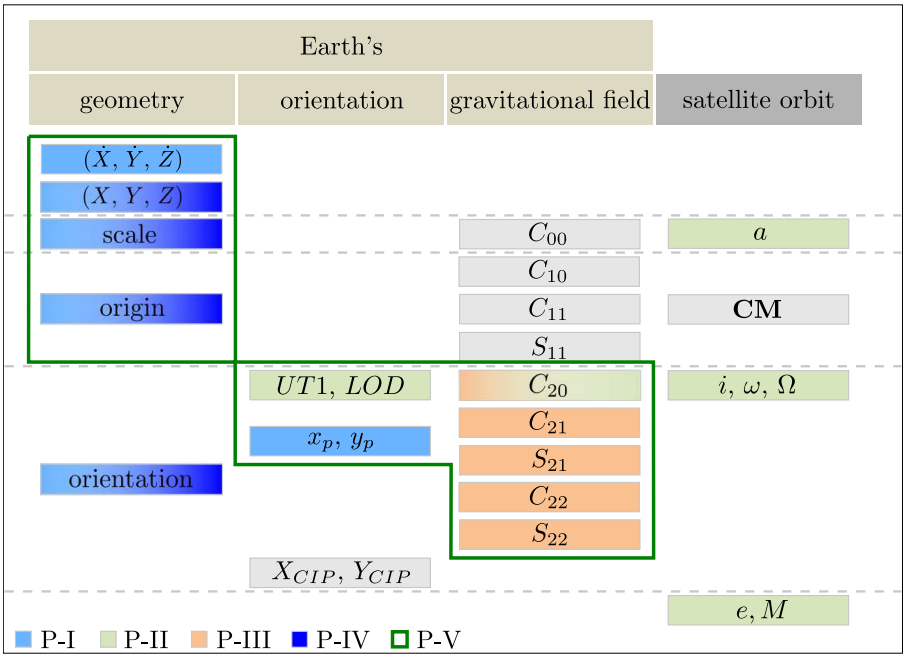

Figure 3.1: Overview of first-author publications incorporated in this cumulative dissertation. The content of the publications is related to the discussed parameters.

3.1 The Terrestrial Reference Frame (TRF)

This section gives a short overview of the state-of-the-art research and products of global TRFs and identifies their current limitations. Furthermore, strategies to overcome these limitations based on the publications P-I, P-IV and P-V are presented.

A Geocentric Terrestrial Reference System (GTRS) is defined to be a trihedron, whose basic vectors span a 3-dimensional, orthogonal and right-handed Euclidean vector space (Petit and Luzum, 2010). The system contains geocentric space-time coordinates within the framework of Special and General Relativity. It co-rotates with the Earth and is related to the GCRS through spatial rotations using the Earth Orientation Parameters (EOP) (IUGG Resolution 2, 2007).

3.1.1 Definition of the ITRS

Within the previously mentioned IUGG Resolution, the ITRS is defined as a specific GTRS with an orientation which was maintained by the Bureau International de l'Heure (BIH). This means, the ITRS

origin coincides with the geocenter which is the $\boldsymbol{CM}$ of the Earth including oceans and atmosphere at any epoch,

orientation is equatorial and equal to the orientation initially given by the BIH at the epoch 1984.0,

scale is consistent with the Temps Coordonné Geocentrique (engl.: Geocentric Coordinate Time) (TCG) time coordinate for a geocentric local frame. The unit of length is the meter (SI).

The time evolution of the orientation of this frame is ensured by using a No-Net-Rotation (NNR) condition w.r.t. horizontal tectonic motions over the whole Earth. The ITRS is defined, realized and promoted by the IERS (Petit and Luzum, 2010).

3.1.2 The realization of the ITRS, the ITRF

The ITRS is realized through 3-dimensional coordinates and velocities of points fixed to the Earth's crust (Kovalevsky and Mueller, 1989). These points can be monument points such as markers or reference points such as the intersection of axes of an SLR telescope, a VLBI antenna reference point or a DORIS/GNSS antenna reference point. They undergo changes due to various geophysical, instrumental and anthropogenic phenomena. The realization of the ITRS is called the International Terrestrial Reference Frame (ITRF) and is computed usually every three to five years by the ITRS Combination Centers. (and finally released by the ITRS Center). The most recent realization of the ITRS is the ITRF2008.

For the ITRF computation, input data of the four geodetic techniques GNSS, SLR, VLBI and DORIS are provided by the IERS Technique Centers (TCs). The datum of the ITRF2008 is realized as follows (see also Table 3.1):

origin The origin is realized solely through SLR.

orientation No rotation offsets neither rates are allowed between ITRF2008 and ITRF2005 at epoch 2005.0. These conditions are realized through a NNR condition applied to a selected subnet of stations.

scale The scale is realized as a weighted mean scale of VLBI and SLR.

For the ITRF2008, two ITRS CCs, namely the IGN and DGFI, computed two different and independent solutions using different software packages. The two solutions are named

ITRF2008 (Altamimi et al., 2011), which is the official IERS product and available at `ftp://itrf.ign.fr/pub/itrf/itrf2008/` and the

DTRF2008 DTRF (P-A), which is available via `doi.pangaea.de/10.1594/PANGAEA.834714`.

Table 3.1 summarizes the contributions of the four geodetic space techniques to the fundamental geodetic parameters estimated in the DTRF2008. Furthermore, it is shown which technique was used for the realization of the geodetic datum.

technique	station coordinates	terrestrial pole coordinates (x_p, y_p)		UT1-UTC		nutation offsets (ΔX_{CIP}, ΔY_{CIP})	origin	scale	orientation
		offset	rate	UT1-UTC	LOD				
GNSS	✓	✓	✓	✗	✓	✗	✗	✗	✓
SLR	✓	✓	✗	✗	✓	✗	✓	✓	✗
VLBI	✓	✓	✓	✓	✓	✓	✗	✓	✗
DORIS	✓	✓	✗	✗	✗	✗	✗	✗	✗

Table 3.1: Usage of geodetic space techniques to determine fundamental geodetic parameters and to realize the DTRF2008 datum (P-A).

3.1.3 Parametrization of station coordinates in the ITRF

The instantaneous station position $\boldsymbol{X}(t_i)$ which is fixed to the Earth's crust is defined in the IERS Conventions 2010 (Petit and Luzum, 2010) as the sum of a regularized station position $\boldsymbol{X_R}(t_i)$ and n correction terms $\boldsymbol{\Delta X_n}(t_i)$ which are described by n conventional geophysical models provided in the IERS Conventions

$$\boldsymbol{X}(t_i) = \boldsymbol{X_R}(t_i) + \sum_n \boldsymbol{\Delta X_n}(t_i). \tag{3.1}$$

Examples for conventional models are models for solid Earth tides (including the time-independent part), ocean tides, atmospheric tidal pressure loading, rotational deformation due to polar motion and ocean pole tide loading. For further descriptions, see (P-I) and Petit and Luzum (2010). The reason for this reduction is to obtain station positions with a time variation as close as possible to a linear variation. Since these models cannot account for all known or unknown geophysical, technical or anthropogenic phenomena and due to model inconsistencies, the remaining station motion is not purely linear (see red curve in Figure 3.2). However, the current mathematical model for the regularized station position comprises only a mean position $\boldsymbol{X}_{\mathrm{ITRF}}$ (t_0 is the reference epoch) and a constant station velocity $\dot{\boldsymbol{X}}_{\mathrm{ITRF}}$ (blue line in Figure 3.2). This means, a station position at an epoch t_i can be extrapolated using the ITRF2008 coordinates (reference epoch t_0 of ITRF2008 is 2005.0) by

$$\boldsymbol{X_R}(t_i) = \boldsymbol{X}_{\mathrm{ITRF}}(t_0) + (t_i - t_0)\dot{\boldsymbol{X}}_{\mathrm{ITRF}}(t_0). \tag{3.2}$$

The ability to extrapolate a station position over multiple years leads to the nomenclature multi-year reference frame (MRF) which is used for the conventional TRF realization in the following.

In the case of an abrupt change of the station position, e.g., due to a change of the GNSS antenna, a change in the VLBI or SLR antenna system or, e.g., due to an earthquake, the station position cannot be extrapolated linearly beyond this epoch using the position and velocity adjusted before the event. An example for an abrupt change due to the Chile earthquake in 2010 is shown in Figure 1 of P-IV. To incorporate the abrupt change in the station motion model, discontinuities are introduced at the epochs of such events. Afterwards, a new station position and a new velocity are estimated.

3.1.4 Removable discrepancies between ITRS definition and realization

Between the ITRS definition and realization, there exist two discrepancies which can be removed with the following formulas without causing any inconsistency.

a) Relativistic scale

The ITRS scale is specified to be consistent with TCG. Since all IERS ACs use a scale consistent to Temps Terrestre (engl.: Terrestrial Time) (TT) which is related to the Earth's crust, also the ITRF scale is TT. This means, in order to achieve a station position consistent with TCG, the following scaling has to be applied (IAU Resolution B1.9, 2006)

$$\boldsymbol{X_{R_{TCG}}}(t_i) = (1 - L_G)\,\boldsymbol{X_R}(t_i) \qquad \text{with} \qquad L_G = 6.969290134 \cdot 10^{-10}. \tag{3.3}$$

The scale difference has an amplitude of about 4.5 mm in the height component on the Earth's crust.

b) Treatment of permanent tide

In the IAG Resolution 16 (1983), it is recommended to use "mean-tide" values (only time-dependent tidal displacements are subtracted from the theoretical station position) for quantities associated with station displacements (Petit and Luzum, 2010). Nevertheless, the geodetic community has not implemented this recommendation in their data processing algorithms (Mäkinen and Ihde, 2008). The technique-specific ACs use a conventional model to account for the time-dependent and the time-independent part of the tidal displacement. The station coordinates are then related to the "conventional tide-free" crust. To adopt a different model than the conventional one, the ITRF station coordinates have to be transformed with the following formula

$$\boldsymbol{X}_{\boldsymbol{R}_{\text{diff. model}}}(t_i) = \boldsymbol{X}_{\boldsymbol{R}}(t_i) - \boldsymbol{\Delta X}_{\text{conv. model}}(t_i) + \boldsymbol{\Delta X}_{\text{new model}}(t_i). \tag{3.4}$$

In the height component, the permanent tide reaches a magnitude of -12.0 cm at the poles and about $+6.0$ cm at the equator (Petit and Luzum, 2010). This inconsistency of the definition and realization of the ITRS must be taken into account when using the ITRF in relation with other products, e.g., global gravitational field models or in the integrated estimation of station coordinates and Stokes coefficients (see Section 3.4).

3.1.5 Limitations of current ITRF realizations

The deficiencies of current ITRF realizations can be split up into the following five groups: origin, orientation, scale, station positions and velocities, and other limitations:

a) Origin

The ITRS is defined to be geocentric. Its realization, the ITRF is a so-called "*crust-fixed*" TRF (Petit and Luzum, 2010) which means that its station coordinates are realized as regularized (linear) coordinates fixed to the Earth's crust. Due to the neglect of non-linear station motions (P-I), the obtained coordinates are only geocentric in a sense of a mean. In order to access coordinates related to the instantaneous $\boldsymbol{CM}$, the neglected translations common to all stations have to be corrected with

$$\boldsymbol{X}_{\boldsymbol{R}_{\text{GC}}}(t_i) = \boldsymbol{X}_{\boldsymbol{R}}(t_i) - \boldsymbol{d}^{\boldsymbol{c}}_{\boldsymbol{t}}(t_i) \qquad \text{with the definition} \qquad \boldsymbol{CM} \equiv \boldsymbol{0} \ \text{ in the } \boldsymbol{CM}\text{-frame.} \tag{3.5}$$

The translations common to all stations $\boldsymbol{d}^{\boldsymbol{c}}_{\boldsymbol{t}}(t_i)$ are explained in detail in P-I. In the geodetic literature, $\boldsymbol{d}^{\boldsymbol{c}}_{\boldsymbol{t}}(t_i)$ is called "*geocenter motion*". It has to be emphasized here that the sign of the correction is not unique in the geodetic literature. The sign depends on how the vector $\boldsymbol{d}^{\boldsymbol{c}}_{\boldsymbol{t}}(t)$ is defined: pointing from the $\boldsymbol{CM}$ away or towards the $\boldsymbol{CM}$. Furthermore, in the most recent IERS Conventions, there is no recommended model to account for $\boldsymbol{d}^{\boldsymbol{c}}_{\boldsymbol{t}}(t)$.

Notice on "*geocenter motion*"

- The $\boldsymbol{CM}$ of the Earth is the barycenter of the Earth (solid Earth plus its non-rigid envelope; Blewitt, 2003; Dong et al., 2003; Tregoning and van Dam, 2005; Wu et al., 2012).
- The coordinates of the $\boldsymbol{CM}$ are always $\begin{pmatrix} 0 & 0 & 0 \end{pmatrix}^T$ in the $\boldsymbol{CM}$-frame.
- Changes in the system Earth which cause mass redistributions force the $\boldsymbol{CM}(t)$ to vary over time w.r.t. a "*crust-fixed*" frame
- Satellites are sensitive to the $\boldsymbol{CM}$ due to orbit dynamics at any time. Therefore, it is a matter of fact that they refer to the instantaneous $\boldsymbol{CM}$.
- Station positions are not sensitive to the $\boldsymbol{CM}$ since they undergo only changes due to loading effects. Mass redistributions which cause no site displacements are invisible for them.
- In the case of satellite techniques, the $\boldsymbol{CM}(t)$-sensitive satellites are observed by the $\boldsymbol{CM}(t)$-insensitive stations. Due to the connection via the observations, the station positions rely on the $\boldsymbol{CM}(t)$. However, observation and/or instrumental errors affect the measured range.

In principle, all satellite techniques are sensitive to the $\boldsymbol{CM}$ and can contribute to the ITRF origin. Nevertheless, the GNSS origin is not used in the ITRF datum realization. The reason for this is twofold: on the one hand, the GNSS geocenter coordinates are affected by orbit modeling deficiencies and the high altitude of the GNSS satellites. On the other hand, the GNSS origin is affected by the simultaneous estimation of epoch-wise clock offsets and tropospheric parameters (Rebischung, 2014). Proposed strategies to obtain a reliable GNSS origin are a refined modeling of the satellite clock offsets or the inclusion of GNSS Low Earth Orbiter (LEO) data (Rebischung, 2014).

In the case of DORIS, the modeling of, e.g., the solar radiation pressure is still a critical issue. In addition, the estimation of once-per-revolution cross-track accelerations is not uniquely performed by the IDS ACs (Willis et al., 2015). These inhomogeneities might cause systematic errors in the DORIS origin and therefore, the role of DORIS for the realization of the ITRF origin will be evaluated by the IERS CCs within the computation of the next release of the ITRF.

The most valuable satellite technique to realize the geocentric ITRS definition is SLR. The altitude of the SLR satellites used for the ITRF computation is about 6000 km for LAser GEOdynamics Satellite (LAGEOS) 1/2 and about 20000 km for Etalon 1/2, respectively. In addition, their spherical shapes and their cross-section-to-mass ratios allow a very accurate computation of the non-gravitational perturbation accelerations. If the station coordinates are estimated together with the satellite orbits and if, in addition, the first degree Stokes coefficients are fixed to zero (P-I), the obtained station coordinates are geocentric. SLR is sensitive to the $\boldsymbol{CM}(t)$ at any epoch. Therefore, for short time intervals (e.g., one day until one week), the $\boldsymbol{CM}$ coordinates are accessible, but not necessarily very accurate. However, in conventional ITRF solutions, the geocentric station coordinates are not accessible since the linear station positions are only geocentric in a mean sense. Furthermore, the network of SLR stations is not homogeneous over time. This variation causes a scatter of the "observed" $\boldsymbol{CM}(t)$ of about 1.5 mm (SLR network effect; Collilieux et al., 2009).

b) Orientation

The orientation is currently realized by a pure mathematical constraint which is based on a selected station network. This selection is not uniquely defined and therefore depends strongly on each individual ITRS CC. As a consequence, although the ITRF2008 and the DTRF2008 are aligned to the ITRF2005 (Altamimi et al., 2007), the orientation and the linear time evolution of the orientation are not consistent. After applying the NNR conditions, the DTRF2008 has a residual horizontal rotation of 0.06 ms/year (P-A) w.r.t. the Actual Plate KInematic and crustal deformation Model (APKIM; Drewes , 2009). APKIM is based on velocities of geodetic sites and takes 17 rigid plates and various deformation zones into account. In contrast to this, the ITRF2005 was aligned to the ITRF2000 (Altamimi et al., 2002) which in turn is aligned to the geophysical plate kinematic model NNR NUVEL-1A (mean plate motion modeled over millions of years and only 12 rigid plates are considered; Argus and Gordon, 1991). A more recent version of a plate motion model is NNR-MORVEL56 (56 plates included; Argus et al., 2011). Furthermore, translations common to all stations propagate into the orientation. This fact is caused by the correlations between translation and orientation parameters due to the inhomogeneously distributed station network (P-I).

c) Scale

The ITRF scale is realized as a weighted mean scale of VLBI and SLR. In the DTRF2008, both individual scales differ by about 0.55 to 0.9 parts-per-billion (P-A). In a strict sense, the scale difference is not a limitation since it fulfills the requirements of the ITRS definition. However, the scale difference restricts the accuracy potential of the current ITRF.

The scale information of GNSS and DORIS is not used in the DTRF2008 for the determination of the geodetic datum due to instrumental and computational aspects. Rebischung (2014) stated that the GNSS scale is highly correlated with satellite z-Phase Center Offsets (z-PCOs), zenith wet delays, station heights and satellite clock offsets. Strategies to reduce these correlations are given by Rebischung (2014) who proposed to include GNSS LEO observations in the ITRF input data or to estimate satellite Phase Center Offset (PCO)s relative to one fixed PCO for which pre-launch antenna calibrations are publicly available.

Willis et al. (2015) report inhomogeneities in the DORIS data processing which may cause systematic errors in the DORIS scale. As it is the case for the DORIS origin, the role of the DORIS scale will be evaluated by the CCs during the combination.

d) Station positions and velocities

Limitations of included station positions and velocities are

- the inaccessibility of the instantaneous station position due to the linear station motion model. Residual (not modeled or wrongly modeled) geophysical, technical and anthropogenic non-linear (periodic, episodic, abrupt) station motions are completely neglected in the current conventional mathematical model for the regularized station positions (see Figure 3.2). Strategies to overcome this lack of modeling (P-I and P-IV) are explained in Section 3.1.6.
- the exclusion of stations with observation intervals shorter than 2.5 years. This threshold is used since Blewitt and Lavallée (2002) showed that the estimated station velocity is affected significantly by annual signals when using a data span shorter than 2.5 years. This fact makes the ITRF partly "out-of-date" right in the moment of its publication.
- the approximation of post-seismic relaxations (exponential/logarithmic shape) through intervals with piecewise linear (pwl) segments. If an interval is shorter than 2.5 years (which is usually the case such approximations), the segment is usually not included in the ITRF (sometimes, in order to achieve more continuity for a station, shorter segments are still included).

Figure 3.2 shows schematically the regularized station position $\boldsymbol{X_R}(t)$ after all conventional models have been applied (red curve) and the conventionally parametrized (secular) ITRF position $\boldsymbol{X}_{\mathrm{ITRF}}(t)$. Due to non-modeled effects or inconsistencies in the conventional models, $\boldsymbol{X_R}(t)$ does not vary just linearly. In P-I, examples of such non-periodic effects are summarized such as: (i) post-seismic relaxations (logarithmic-shape) which might cause surface motions of 15 to 20 mm per year even 45 years after the earthquake (Freymueller, 2010) and (ii) neglected seasonal variations which can reach amplitudes of 50 to 75 mm (e.g., GPS station in Manaus; Bevis et al., 2005). Therefore, the conventional linear approximation of $\boldsymbol{X_R}(t)$ causes errors. The difference between both positions at an epoch t_i can be written as

$$\epsilon_1(t_i) = \boldsymbol{X_R}(t_i) - \boldsymbol{X}_{\mathrm{ITRF}}(t_i). \tag{3.6}$$

The difference $\epsilon_1(t_i)$ can be split up into common motions of all stations (translations, rotations and scale changes) and individual station motions such as local crustal dynamics due to groundwater withdrawal (Bawden et al., 2001). The common motions affect the TRF datum whereas the individual motions only partly bias the TRF datum. One strategy to approximate the non-linear station motions is the frequent estimation of station positions $\tilde{\boldsymbol{X}}(t_i)$ in so-called Epoch Reference Frames (ERFs). More details on ERFs are presented in Section 3.1.6 and P-I, P-IV.

e) Other limitations

Other limitations of current ITRS realizations are

- the latency of ITRS realizations of three to five years.
- the non-availability of the ITRF coordinates after a large earthquake. Such events may affect large areas.
- the inhomogeneous global distribution of (i) the ground station networks (see Figure 16 in P-A), (ii) the co-location sites (see Figure 13 in P-A) and (iii) the measured terrestrial difference vectors between technique-related reference points called Local Ties (LT). For the ITRF2008 processing, there have been only three co-location sites with LT for all four geodetic techniques.
- In addition to the global distribution, also the quality of the LT is inhomogeneous. The discrepancies between the single-technique solutions and the measured LT can reach magnitudes of several centimeters.
- the constraints in some input data that are not reported in the SINEX files (see Section 2.2.6 and P-A).

3.1.6 Strategies to resolve the ITRF limitations

In this section, selected strategies to overcome current limitations of ITRF realizations are presented. The Epoch Reference Frame (ERF) computation is discussed in detail in Section 3.1.6a) and P-I, P-IV, whereas the extended station parametrization and the refined geophysical modeling are only briefly addressed. It has to be mentioned here that the numbering of Section 3.1.5 is independent from the numbering within this section.

a) Epoch Reference Frames (ERFs)

The main strategy addressed in this thesis to overcome the lack of modeling of conventional MRFs is the frequent estimation of station position coordinates based on an epoch-wise combination of NEQs of different geodetic space techniques (Epoch Reference Frames (ERFs); P-I). The presented epoch-wise solutions contain instantaneous geocentric station coordinates and EOP. The time interval of the estimated ERF solutions can be varied (P-IV). Figure 3.2 shows, in addition to the residual regularized and conventionally extrapolated station positions, the frequently estimated station positions $\tilde{\boldsymbol{X}}(t_i)$ (white boxes). It is obvious that their approximation error $\epsilon_2(t_i)$ is, in general, much smaller than $\epsilon_1(t_i)$.

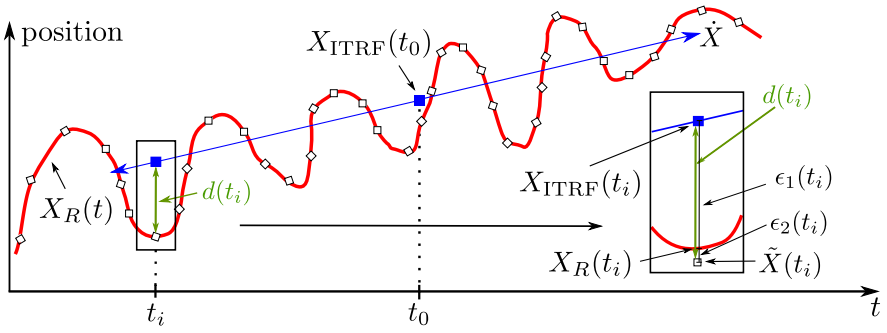

Figure 3.2: Approximation of the regularized station position through the conventional ITRS realization and the ERF realization (taken from P-I).

At DGFI, MRFs such as global TRFs (e.g., DTRF2008) are computed in the same way as ERFs using a combination method based on the *Gauß-Markov* model at NEQ level (see Chapter 2). In contrast to this approach, the ITRF2008 computation at IGN is based on the *Gauß-Markov* model at solution level (see Chapter 2 and Altamimi et al., 2011). In P-I, the procedure to compute ERFs is presented for the first time in detail and compared to the procedure for the computation of a conventional MRF. Both TRF realizations are based on identical input data which allows to study the impact of the epoch-wise estimation of station coordinates on (i) the geodetic datum of the obtained ERFs, (ii) the individual and common motions of all stations and (iii) the impact on commonly adjusted parameters such as the EOP. The investigations showed that

- individual non-linear station motions bias other parameters (e.g., EOP) in the secular approach.
- the non-linear station motions can be separated into common and individual station motions.
- the sparser the global station network is, the more correlated are the network translation and network rotation parameters.
- the geocentric NNR condition is affected by neglected non-linear variations in the a priori coordinates of the ERFs. In the MRFs, common non-linear variations are neglected and partly forced into the terrestrial pole coordinates. The signal can be found, if the pole coordinates of the MRF and the ERFs are compared. With this method, annual amplitudes of 23.6 μas and 39.8 μas were found for x_p and y_p of the combined solution (GNSS, SLR and VLBI). In case of the SLR-only solution, much larger (non-annual) amplitudes of 77.4 μas have been found.
- in the conventional approach, all existing LT can be used for the combination whereas for the ERF computation, only the LT at the co-location sites which observe during the particular week can be used. This causes instabilities regarding the integration of the different techniques and the datum definition for the ERFs.

One possibility to strengthen the combination of the different techniques is the introduction of computed LT. With more LT available in a week, the datum transfer from one technique-specific subnet to the other would improve. Another possibility to increase the datum stability of ERFs is the extension of the combination interval. This investigation is discussed in P-IV. There, three different combination intervals (weekly, two-weekly and four-weekly) have been tested and evaluated w.r.t. their ability to monitor non-linear station motions and to stabilize the ERF datum. The study shows that

- the larger the sampling interval for the ERFs is, the better is the network geometry (global coverage) and therefore, the more LT can be introduced. These improvements allow to realize a more stable geodetic datum and a better integration of the different space techniques.
- the shorter the sampling interval for the ERFs is, the better can the high-frequency motions be sampled (abrupt signals or periodic signals with at least twice the sampling interval can be monitored).

As a conclusion, we can state that an optimal TRF type or ERF sampling interval depends on the application the TRF is used for (see Table 3 of P-IV).

Another possibility to increase the datum stability of ERFs is the inclusion of observations to more satellites tracked by SLR. P-V shows that

- if only LAGEOS 1/2 observation are considered for an SLR-only solution, the origin and scale vary between 0.5 mm and 1.2 mm.
- if, in addition, observations to the LAser RElativity Satellite (LARES) are included, the variation of the datum parameters decrease by between 14 % and 22 %.
- if, in total, observations to 10 satellites are combined, the scatter in the x-coordinate of the origin and the scale increases. This fact might be caused by the perturbed orbits of some LEOs due to, e.g., not accurately modeled non-gravitational perturbations.
- The more satellites included in the combination, the better is the station coordinate repeatability, especially in the horizontal components. The RMS of the height component does not benefit significantly from the combination of 10 satellites since the annual signal dominates the height repeatability. Furthermore, the poor observation geometry is a limiting factor since only satellites in the hemisphere above the station can be observed. (see also Sośnica et al., 2014).

The characteristics of both TRF types are summarized below (see also Table 9 and 10 of P-I) and possible applications for both TRF types are given in Table 3 of P-IV.

ERFs describe instantaneous geocentric coordinates with a very short latency. Hence, ERFs are important to evaluate geophysical models. This fact makes them interesting especially after large earthquakes, when the secular station position is not valid any longer. However, ERFs have a less stable datum than the MRFs and can provide station positions only for the past.

MRFs are important for long-term studies. They can also be used for coordinate extrapolations which is very important for Precise Orbit Determination (POD) since station positions and EOP are kept fixed. Therefore, the station position should be described as accurately as possible (e.g. using the linear-trigonometric station motion model) in order to simply extrapolate into the future.

In summary, the investigations of P-I and P-IV show that ERFs can support and validate the MRFs.

b) Extended parametrization of station motions

In order to describe the time-varying station positions more accurately, an extension of the current mathematical model could be the additional estimation of trigonometric functions. This extended (linear-trigonometric) parametrization reads according to Equation (2.59)

$$\boldsymbol{X}_{\boldsymbol{R}_{\text{ext}}}(t_i) = \boldsymbol{X}_{\text{ITRF}}(t_0) + (t_i - t_0)\dot{\boldsymbol{X}}_{\text{ITRF}}(t_0) + \boldsymbol{c}_{\text{ITRF}}(t_0)\cos\left((t_i - t_0)\omega\right) + \boldsymbol{s}_{\text{ITRF}}(t_0)\sin\left((t_i - t_0)\omega\right). \quad (3.7)$$

The advantage of this extended parametrization is, that the non-linear residuals of $\boldsymbol{X}_{\boldsymbol{R}}(t)$ can be approximated much more accurately than when using only a linear parametrization. This extended parametrization is currently investigated in a joint project of DGFI and BKG within the framework of the DFG research unit Forschergruppe "Space-time reference systems for monitoring global change and for precise navigation in space" (FOR 1503; Nothnagel et al., 2010). In order to realize the geodetic datum of such an extended MRF, the NNR condition has to be modified to prevent common periodic motions of all stations from aliasing into the translation, orientation and scale. There are two main limitations of such an extension: (i) only strictly periodic signals with constant period and amplitudes can be approximated. Most of the geophysical and equipment related effects do not occur,

however, with a constant frequency and amplitude. To reduce this discrepancy, also semi-annual functions can be estimated in addition to the annual functions (Meisel et al., 2009). Furthermore, non-periodic signals such as post-seismic deformations can only be approximated accurately by, e.g., additional exponential or logarithmic functions. (ii) Spurious periodic variations which are estimated due to outliers (e.g., due to snow coverage during winter-time), might disturb the station coordinate estimates.

c) Refined geophysical modeling of non-tidal loading effects

A refined geophysical modeling for taking into account the non-tidal loading effects caused by, e.g., atmosphere, ocean and hydrology is currently not recommended in the IERS Conventions. The geodetic community accommodates the importance of a better understanding of non-tidal loading effects and installed the Joint Working Group (JWG) 1.2 of the IAG and the IERS which is named "*Modeling environmental loading effects for reference frame realizations*". Furthermore, a joint project of BKG and DGFI investigates the effect of different geophysical model combinations on geodetic parameters (station coordinates, EOP, Stokes coefficients). This project is funded within the DFG research unit FOR 1503 (Nothnagel et al., 2010). The obtained refined geophysical models for non-tidal loading effects can be used, e.g., for accounting for translations common to all stations $\boldsymbol{d}_i^c(t)$ in Equation (3.5).

3.2 The Earth Orientation Parameters (EOP)

In this section, a short introduction on the definition of the EOP is given and current official time series are presented. Selected limitations of the time series are addressed and strategies to resolve them based on the publications P-II and P-V are discussed. The results have been obtained within the DFG Forschergruppe "Earth Rotation and Global Dynamic Processes" (FOR584; Schuh et al., 2003).

3.2.1 Definition of the EOP

The transformation from the International Terrestrial Reference System (ITRS) to the Geocentric Celestial Reference System (GCRS) comprises the three rotation matrices

$$\left[\text{GCRS}\right] = \boldsymbol{Q}(t)\boldsymbol{R}(t)\boldsymbol{W}(t)\left[\text{ITRS}\right], \tag{3.8}$$

which describe the motion of the Celestial Intermediate Pole (CIP) in the celestial reference system $\boldsymbol{Q}(t)$, the rotation $\boldsymbol{R}(t)$ of the Earth around the axis associated with the pole and polar motion $\boldsymbol{W}(t)$, respectively (Petit and Luzum, 2010). Thereby, polar motion describes the motion of the CIP in the ITRS including all terms outside the retrograde diurnal band. The celestial motion of the CIP includes all terms with periods larger than 1.5 days in the GCRS. In principle, there exist two different procedures for this transformation (see Table 3.2), where the first one described below is the currently recommended transformation and the second one is the classical transformation.

The "Celestial Intermediate Origin (CIO)-based transformation" was introduced to ensure a Non Rotating Origin (NRO) in the GCRS and ITRS. This transformation has the advantage that the Earth Rotation Angle (ERA) is insensitive at the milliarcsecond level to the International Astronomical Union (IAU) precession-nutation model (Mathews et al., 2002) and to the observed celestial pole offsets.

The second procedure is called the "Equinox-based transformation" which composes the classical nutation-precession matrices using the nutation angles $\Delta\psi$ and $\Delta\epsilon$ in longitude and obliquity referred to the ecliptic of date and the mean obliquity of date. This procedure uses the Greenwich Apparent Sideral Time (GAST) angle Θ to rotate from the Terrestrial Intermediate Reference System (TIRS) into the "True equinox and equator of date" system. The angle depends on the precession-nutation model and the observed celestial pole offsets which is in contrast to the desirability of describing the rotation of the Earth independently from its orbital motion (IAU Resolution B1.8, 2006). The "Equinox-based transformation" is shown for completeness in Table 3.2 but is not further discussed in this thesis. A detailed description of both transformations can be found in Capitaine (2002) and Petit and Luzum (2010). Göttl (2013) provides a descriptive explanation of both transformations. Kaplan (2005) describes how to transform the IERS values $(\Delta X_{\text{CIP}}, \Delta Y_{\text{CIP}})_{\text{IERS}}$ into the nutation angles $\Delta\psi$ and $\Delta\epsilon$.

Table 3.2: Transformation from the ITRS to the ICRS. The alignment of the ICRS and the GCRS orientation to the Fifth Fundamental Catalogue (FK5) is described in detail in Arias et al. (1995).

System		BCRS, ICRS	⟵	GCRS	⟵	CIRS, $*^2$	⟵	TIRS	⟵	ITRS	
Time		TDB, TCB		TCG		TCG		TCG		TCG	
CIO-based transformation	trans.		$*^1$		$Q(t)$		$R_3(-ERA)$		$W(t)$		
	x-axis	FK5		FK5		CIO		TIO		BIH orientation 1984.0 (Greenwich)	
	z-axis	FK5		FK5		CIP		CIP		mean Earth rotation axis	
Equinox-based transformation	trans.		$*^1$		$B(t)P(t)N(t)$		$R_3(GAST)$		$W(t)$		
	x-axis	FK5		FK5		Υ		TIO		BIH orientation 1984.0 (Greenwich)	
	z-axis	FK5		FK5		CIP		CIP		mean Earth rotation axis	

$*^1$ This transformation comprises a translation from the Geocenter to the Barycenter and a scaling due to a change of the time system $\frac{\mathrm{TCG}}{\mathrm{TCB}} = 1 - L_C$ with $L_C = 1.48082686741 \cdot 10^{-8} \pm 2 \cdot 10^{-17}$ (IAU Resolution B1.5, 2006).
$*^2$ In the equinox-based transformation, this system is called "True equinox and equator of date" system.

The three rotation matrices of Equation (3.8) for the "CIO-based transformation" can be written as

$$\begin{aligned} \boldsymbol{W}(t) &= \boldsymbol{R_3}(-s')\boldsymbol{R_2}(x_p)\boldsymbol{R_1}(y_p), \\ \boldsymbol{R}(t) &= \boldsymbol{R_3}(-\mathrm{ERA}), \\ \boldsymbol{Q}(t) &= \boldsymbol{R_3}(-E)\boldsymbol{R_2}(-d)\boldsymbol{R_3}(E)\boldsymbol{R_3}(s) \\ &= \begin{bmatrix} 1 - aX_{\mathrm{CIP}}^2 & -aX_{\mathrm{CIP}}Y_{\mathrm{CIP}} & X_{\mathrm{CIP}} \\ -aX_{\mathrm{CIP}}Y_{\mathrm{CIP}} & 1 - aY_{\mathrm{CIP}}^2 & Y_{\mathrm{CIP}} \\ -X_{\mathrm{CIP}} & -Y_{\mathrm{CIP}} & 1 - a(X_{\mathrm{CIP}}^2 + Y_{\mathrm{CIP}}^2) \end{bmatrix} \boldsymbol{R_3}(s), \end{aligned} \tag{3.9}$$

using $a = \frac{1}{2} + \frac{1}{8}(X_{\mathrm{CIP}}^2 + Y_{\mathrm{CIP}}^2)$ and

$$ERA(t) = 2\pi(\mathrm{UT1} + 0.7790572732640 + 0.00273781191135448\,t). \tag{3.10}$$

The time t is the Julian UT1 date - 2451545.0 in day fractions. The "CIO-locator" s and the "Terrestrial Intermediate Origin (TIO)-locator" s' can be modeled using the formulas described in Petit and Luzum (2010). Thereby, s provides the position of the CIO on the equator of the CIP. The main constituents of s' are caused by the Chandlerian and annual Earth rotation wobbles.

3.2.2 EOP products

The EOP in Equation (3.9) and (3.10) comprise

$$\begin{aligned} (x_p, y_p) &= & & & (x,y)_{\mathrm{IERS}} &+ (\Delta x, \Delta y)_{\text{ocean tides}} &+ (\Delta x, \Delta y)_{\text{libration}}, \\ \mathrm{UT1} &= & \mathrm{UTC} &+ (\mathrm{UT1} - \mathrm{UTC})_{\mathrm{IERS}} &+ \Delta\mathrm{UT1}_{\text{ocean tides}} &+ \Delta\mathrm{UT1}_{\text{libration}}, \\ \mathrm{LOD} &= & & & \mathrm{LOD}_{\mathrm{IERS}} &+ \Delta\mathrm{LOD}_{\text{ocean tides}} &+ \Delta\mathrm{LOD}_{\text{libration}}, \\ (X_{\mathrm{CIP}}, Y_{\mathrm{CIP}}) &= & (X_{\mathrm{CIP}}, Y_{\mathrm{CIP}})_{\mathrm{IAU}} &+ (\Delta X_{\mathrm{CIP}}, \Delta Y_{\mathrm{CIP}})_{\mathrm{IERS}} & & \end{aligned} \tag{3.11}$$

in which the quantities with the index IERS are provided at daily 0h Universal Time Coordinated (UTC) epochs in the IERS 08 C04 time series (see Figure 3.3; Bizouard and Gambis, 2011; Gambis et al., 2013). All IERS

quantities except $(\text{UT1-UTC})_{\text{IERS}}$ and LOD_{IERS} can be interpolated to any epoch using a linear interpolation although the interpolation error is at the limit looking at today's accuracy of the geodetic space techniques. Besides the linear interpolation of $(\text{UT1-UTC})_{\text{IERS}}$ and LOD_{IERS}, zonal terms have to be considered (see Section 2.2.1). The other quantities (without the index IERS) are based on conventional models which are provided in the IERS Conventions (Petit and Luzum, 2010). Errors in these quantities are caused by possible model errors. As an example, the modeling of $(X_{\text{CIP}}, Y_{\text{CIP}})_{\text{IAU}}$ is based on the IAU 2000/2006 precession-/nutation model (Mathews et al., 2002; Capitaine et al., 2003) which has an accuracy of about 10 μas for most of its terms (Petit and Luzum, 2010). Besides, this model does not include a Free Core Nutation (FCN) model since this free retrograde diurnal motion of the Earth's rotation axis w.r.t. the Earth comprises a time-varying excitation and damping. Due to the neglect of the FCN, the accuracy of the CIP direction in the GCRS of the IAU 2000/2006 precession-/nutation model is limited to about 0.3 mas (Petit and Luzum, 2010). The so-called Length Of Day (LOD) is related to UT1 through

$$\frac{d}{dt}(\Delta\text{UT1}) = -\frac{\Delta\text{LOD}}{86400\,s} \quad \text{with} \quad \Delta\text{LOD} = \text{LOD} - 86400\,s \quad \text{and} \quad \Delta\text{UT1} = \text{UT1} - \text{UTC}. \tag{3.12}$$

If time is measured in days of 86400 s, the excess Length Of Day (ΔLOD) describes the difference between LOD and 86400 s (Seitz F. and Schuh, 2010). Since UTC contains leap seconds, the first derivative is not unique at these epochs. To compute an unique derivative, the continuous time scale Temps Atomique International (engl.: International Atomic Time) (TAI) can be used instead of UTC. The relationship between both time scales is given by UTC = TAI $- N$ with N being the number of leap seconds introduced since 1972 (currently 35 s). The leap seconds are announced and published by the IERS in the Bulletin C[6]. Besides the IERS EOP, also other time series of combined EOP are publicly available. One example for such a time series are the SPACE2011, COMB2011 and POLE2011 time series (Ratcliff and Gross, 2013) of the Jet Propulsion Laboratory (JPL).

INTERNATIONAL EARTH ROTATION AND REFERENCE SYSTEMS SERVICE
EARTH ORIENTATION PARAMETERS
EOP (IERS) 08 C04

FORMAT(3(I4),I7,2(F11.6),2(F12.7),2(F11.6),2(F11.6),2(F11.7),2F12.6)

Date			MJD	x	y	UT1-UTC	LOD	dX	dY	x Err	y Err	UT1-UTC Err	LOD Err	dX Err	dY Err
			(0h UTC)	"	"	s	s	"	"	"	"	s	s	"	"
1962	1	1	37665	-0.012700	0.213000	0.0326338	0.0017230	0.000000	0.000000	0.030000	0.030000	0.0020000	0.0014000	0.004774	0.002000
1962	1	2	37666	-0.015900	0.214100	0.0320547	0.0016690	0.000000	0.000000	0.030000	0.030000	0.0020000	0.0014000	0.004774	0.002000
1962	1	3	37667	-0.019000	0.215200	0.0315526	0.0015820	0.000000	0.000000	0.030000	0.030000	0.0020000	0.0014000	0.004774	0.002000
1962	1	4	37668	-0.021999	0.216301	0.0311435	0.0014960	0.000000	0.000000	0.030000	0.030000	0.0020000	0.0014000	0.004774	0.002000
1962	1	5	37669	-0.024799	0.217301	0.0308154	0.0014160	0.000000	0.000000	0.030000	0.030000	0.0020000	0.0014000	0.004774	0.002000
1962	1	6	37670	-0.027599	0.218301	0.0305353	0.0013820	0.000000	0.000000	0.030000	0.030000	0.0020000	0.0014000	0.004774	0.002000
1962	1	7	37671	-0.030199	0.219301	0.0302682	0.0014130	0.000000	0.000000	0.030000	0.030000	0.0020000	0.0014000	0.004774	0.002000
1962	1	8	37672	-0.032798	0.220202	0.0299280	0.0015050	0.000000	0.000000	0.030000	0.030000	0.0020000	0.0014000	0.004774	0.002000
1962	1	9	37673	-0.035198	0.221102	0.0294869	0.0016280	0.000000	0.000000	0.030000	0.030000	0.0020000	0.0014000	0.004774	0.002000
1962	1	10	37674	-0.037498	0.222002	0.0289268	0.0017380	0.000000	0.000000	0.030000	0.030000	0.0020000	0.0014000	0.004774	0.002000
1962	1	11	37675	-0.039697	0.222803	0.0282797	0.0017940	0.000000	0.000000	0.030000	0.030000	0.0020000	0.0014000	0.004774	0.002000
1962	1	12	37676	-0.041797	0.223703	0.0276136	0.0017740	0.000000	0.000000	0.030000	0.030000	0.0020000	0.0014000	0.004774	0.002000
1962	1	13	37677	-0.043797	0.224503	0.0270075	0.0016670	0.000000	0.000000	0.030000	0.030000	0.0020000	0.0014000	0.004774	0.002000
1962	1	14	37678	-0.045697	0.225203	0.0265403	0.0015100	0.000000	0.000000	0.030000	0.030000	0.0020000	0.0014000	0.004774	0.002000
1962	1	15	37679	-0.047496	0.226004	0.0262572	0.0013120	0.000000	0.000000	0.030000	0.030000	0.0020000	0.0014000	0.004774	0.002000
1962	1	16	37680	-0.049196	0.226704	0.0261751	0.0011120	0.000000	0.000000	0.030000	0.030000	0.0020000	0.0014000	0.004774	0.002000
1962	1	17	37681	-0.050796	0.227404	0.0262740	0.0009360	0.000000	0.000000	0.030000	0.030000	0.0020000	0.0014000	0.004774	0.002000
1962	1	18	37682	-0.052295	0.228005	0.0265299	0.0008110	0.000000	0.000000	0.030000	0.030000	0.0020000	0.0014000	0.004774	0.002000
1962	1	19	37683	-0.053595	0.228705	0.0268868	0.0007330	0.000000	0.000000	0.030000	0.030000	0.0020000	0.0014000	0.004774	0.002000
1962	1	20	37684	-0.054895	0.229305	0.0273077	0.0006810	0.000000	0.000000	0.030000	0.030000	0.0020000	0.0014000	0.004774	0.002000
1962	1	21	37685	-0.055995	0.229905	0.0277506	0.0006780	0.000000	0.000000	0.030000	0.030000	0.0020000	0.0014000	0.004774	0.002000
1962	1	22	37686	-0.057094	0.230506	0.0281834	0.0007210	0.000000	0.000000	0.030000	0.030000	0.0020000	0.0014000	0.004774	0.002000
1962	1	23	37687	-0.057994	0.231006	0.0285533	0.0007900	0.000000	0.000000	0.030000	0.030000	0.0020000	0.0014000	0.004774	0.002000
1962	1	24	37688	-0.058794	0.231606	0.0288522	0.0008620	0.000000	0.000000	0.030000	0.030000	0.0020000	0.0014000	0.004774	0.002000
1962	1	25	37689	-0.059594	0.232106	0.0290721	0.0009440	0.000000	0.000000	0.030000	0.030000	0.0020000	0.0014000	0.004774	0.002000
1962	1	26	37690	-0.060193	0.232607	0.0292210	0.0010040	0.000000	0.000000	0.030000	0.030000	0.0020000	0.0014000	0.004774	0.002000
1962	1	27	37691	-0.060693	0.233207	0.0293239	0.0010370	0.000000	0.000000	0.030000	0.030000	0.0020000	0.0014000	0.004774	0.002000

Figure 3.3: Screenshot of the official IERS 08 C04 data file (available at `http://hpiers.obspm.fr/eop-pc/`).

3.2.3 Limitations of current EOP realizations

a) Alignment to the ITRF and the International Celestial Reference Frame (ICRF)

The IERS EOP time series is based on the combination of input data of different technique-dependent ACs. The input data are often referred to different terrestrial and celestial frames (Bizouard and Gambis, 2011). To align the EOP (celestial and terrestrial pole coordinates, UT1) to the most recent realization of the ITRF and ICRF, a linear model (offset and drift) is estimated and subtracted from the input data. The obtained EOP time series are then considered to be consistent to the current ITRF and ICRF. Until now, it has not clearly been demonstrated by the authors of the IERS 08 C04 time series that their approach can be considered as fully rigorous.

[6] `http://www.iers.org/IERS/EN/DataProducts/EarthOrientationData/eop.html`, (2014-07-31)

b) Systematics in the terrestrial pole coordinates of conventional MRFs

Due to an inhomogeneous station distribution, translations common to all stations are correlated with common rotations. As described in Section 3.1.6a) and P-I, the neglected non-linear translations affect the orientation of any conventional global MRF. This means, that the pole coordinates as complementary parameters to the TRF orientation are equally affected by the annual variations suppressed in the linear station motion model.

c) Systematics in satellite-technique LOD estimates

The relationship between the rotation of the Earth around its pole and the precession of the orbital plane of any satellite is investigated in P-II and can be written as

$$\frac{d}{dt}(\Delta\mathrm{UT1}) = -\frac{\Delta\mathrm{LOD}}{86400\,s} = -\left(\dot{\Omega} + \cos(i)\cdot\dot{u}_0\right)\rho^{-1}. \tag{3.13}$$

Thereby, ρ is the ratio between UT and sidereal time (rate of advance of ERA: $\rho = 1.273781191135448$ rev/UT1 day; Petit and Luzum, 2010). This means that LOD estimates derived from satellite observations are corrupted by the precession of their orbital plane and by the $\cos(i)$-mapped along-track motion of the satellites. These parameters are themselves highly correlated with the even zonal Stokes coefficients.

In contrast to the alignment of the terrestrial and celestial pole coordinates, the $\mathrm{LOD}_{\mathrm{GNSS}}$ values are made consistent with the $\mathrm{LOD}_{\mathrm{VLBI}}$ values by filtering and removing all spurious drifts above 20 days (Bizouard and Gambis, 2011). Nearly 99 % of the total signal have a period below 19 days (Bizouard and Gambis, 2009). The $\mathrm{LOD}_{\mathrm{SLR}}$ values are not used for the LOD combination. A detailed theoretical discussion and additional numerical examples are presented in P-II and P-V.

If, instead of LOD, UT1-UTC values parametrized as piece-wise linear (pwl) polygons, the absolute offset of these polygons cannot be determined with satellite techniques (P-I). To remove this singularity, at least one value of the polygon has to be fixed to its a priori value (see Section 2.2.4).

3.2.4 Strategies to resolve the EOP limitations

The strategies to resolve the EOP limitations addressed in this thesis follow two different approaches. The first approach is based on the combination of different geodetic space techniques and a simultaneous frequent estimation of commonly adjusted parameters (station coordinates), whereas the second approach is based on the combination of multiple SLR-tracked satellites.

a) Epoch Reference Frames (ERFs)

The estimation of ERFs is presented in detail in P-I, P-IV and Section 3.1.6. The results show that the frequent estimation of station positions do not force the common non-linear rotations of the station network to propagate into the terrestrial pole coordinates. Hence, the ERF pole coordinates are only affected by the datum instability and can be considered as "reduced biased" (Figure 1.1).

In order to avoid the artificial removal of the UT1-UTC polygon singularity, the satellite techniques can be combined with VLBI. This is the only space technique which is sensitive to the full set of EOP.

b) Combination of satellites with different orbit characteristics

In P-II, the correlations of the orbit parameter rates with C_{20} using the first order Gaussian perturbation equations are worked out (please note that the Stokes coefficients C_{nm}, S_{nm} are explained in detail in Section 3.3). Thereby, only secular perturbations during one week are discussed since only weekly C_{20} values are estimated.

The major results and findings of P-II and P-III are summarized below:

- Secular perturbations in the orbital elements Ω, ω and M are caused by the even zonal Stokes coefficients (especially C_{20}). Hence, the estimated ΔLOD values are affected as they describe the same rotations. In the single-satellite solutions, the impact of the fixed a priori gravitational field is significant. If a maximum difference of $8 \cdot 10^{-10}$ is assumed for the C_{20} values (Figure 6 in P-II), the effect for a satellite at 500 km altitude and $i = 0°$ (maximum effect) is about 1.0 $\frac{ms}{d}$.

- Estimated offsets in the semi-major axis a cause a change of the mean motion n of the satellite. This mean motion compensates the along-track perturbation caused by C_{20}.
- To decorrelate $\dot{\Omega}$ and LOD, the combination of satellites with different inclinations are necessary. In P-II, the combination of LAGEOS 1 and 2 leads to a significant decorrelation. In P-II, various satellite constellations are tested if they are able to decorrelate $\dot{\Omega}$ and C_{20}. It can be concluded, that LAGEOS 1 and 2, Ajisai, Stella, Starlette and LARES have a significant impact on the decorrelation whereas the impact of Etalon 1 and 2, Ball Lense In The Space (BLITS) and Larets vanishes.
- In comparison to the single-satellite solutions, the reduced correlations allow it to estimate improved LOD values in an SLR-only multi-satellite solution.

Within the SLR-only solutions, the orbit modeling refinements described below are considered to be correct. In the obtained solutions, the LOD information is stored in the pwl UT1-UTC polygons. The mid-arc value of these polygons is fixed to its corresponding a priori value in order to remove the rank deficiency (see Figure 4 in P-V). The outcome of the studies is, that

- the LAGEOS 1 LOD values are significantly and systematically affected by deviations of up to ±20 ms. Hence, if LOD and C_{20} are estimated together using only one satellite, no reliable results can be obtained.
- the deviations of the LAGEOS 1/2 LOD values are about 10 times smaller than the LAGEOS 1 LOD values.
- the deviations of the combined LAGEOS 1/2 and LARES LOD values are about ±0.3 ms.
- nearly no systematic deviations occur in the ten satellite LOD values.

The terrestrial pole coordinates also benefit significantly from the inclusion of more satellites in the SLR-only solution. Their weighted Root Mean Square (WRMS) w.r.t. the IERS 08 C04 time series is reduced by about 60 % in the x-coordinate and about 67% in the y-coordinate. The results of P-V confirm the most recent plans of the ILRS Analysis Working Group (AWG) to include LARES in its official TRF-EOP-products.

c) Refined orbit modeling

In addition to the interaction of the satellite orbit and C_{20}, other secular perturbations of the orbital precession are discussed in P-II:

- Periodic empirical accelerations estimated perpendicular to the orbital plane (once-per-revolution sine-term in cross-track direction) cause only very small secular rotations if the parameter is constrained (Equation (7) in P-II). If a typical maximum value of $1 \cdot 10^{-12}\ \frac{m}{s^2}$ is used (Combrinck, 2010), the maximum effect of $0.1\ \frac{\mu s}{d}$ for $i = 90°$ is obtained. If the empirical accelerations are not constrained, no reliable estimates can be achieved.
- If relativistic accelerations for satellites due to *Lense-Thirring* (Lense and Thirring, 1918) or *deSitter* (de Sitter, 1916) are neglected, secular nodal rotations of 0.0088 ms are caused for satellites at LAGEOS altitude.

Besides the multi-satellite combination in the case of SLR, P-B presents a strategy to reduce the LOD error in GNSS solutions by an improved modeling of the solar radiation pressure. This improvement is achieved by the use of an adjustable box-wing model (Rodriguez-Solano et al., 2012).

3.3 The Earth's gravitational field (Stokes) coefficients

The third parameter group addressed in this thesis are the Stokes coefficients. In the following section, the definition of the Stokes coefficients is presented. Furthermore, the geometrical and physical interpretation of the low-degree coefficients is shown since this knowledge is fundamental for the understanding of the correlations between the different parameter groups. Finally, strategies for a reliable estimation of low-degree Stokes coefficients based on the publications P-III and P-V are presented.

The gravitational potential $\boldsymbol{V}$ expanded into spherical harmonics of degree n and order m can be written as (Heiskanen and Moritz, 1967)

$$V = \frac{GM}{r}\left(1 + \sum_{n=1}^{\infty}\left(\frac{a}{r}\right)^n \sum_{m=0}^{l}\left(C_{nm}\cdot\cos m\lambda + S_{nm}\cdot\sin m\lambda\right) P_{nm}(\cos\vartheta)\right). \tag{3.14}$$

Therein, GM is the gravitational constant multiplied with the Earth's mass M, $(\vartheta,\lambda,r)^T$ are the geocentric spherical coordinates of a satellite in the ITRS, a is the equatorial semi-major axis of the Earth and P_{nm} are the associated Legendre functions. Equation (3.14) provides a special solution of Laplace's second-degree differential equation $\Delta V = 0$ for the Earth's exterior gravitational field. The harmonic coefficients (Stokes' coefficients/constants) of degree n and order m are given by

$$\begin{aligned} C_{n0} &= \frac{1}{M}\iiint_{\text{Earth}}\left(\frac{a}{r}\right)^n P_n(\cos\vartheta)\,dM \qquad \text{and} \\ \begin{Bmatrix} C_{nm} \\ S_{nm} \end{Bmatrix} &= \frac{2}{M}\frac{(n-m)!}{(n+m)!}\iiint_{\text{Earth}}\left(\frac{a}{r}\right)^n P_{nm}(\cos\vartheta)\begin{Bmatrix}\cos m\lambda \\ \sin m\lambda\end{Bmatrix} dM \qquad \text{for} \qquad m \neq 0. \end{aligned} \tag{3.15}$$

From Equation (3.14), it is obvious that for zero order the coefficients S_{n0} disappear. The factor $\left(\frac{a}{r}\right)^n$ causes a decreasing sensitivity of a test mass on the Earth's gravitational field with higher altitude (upward continuation). The relation between the normalized Stokes coefficients ($\overline{C}_{nm}$, $\overline{S}_{nm}$) and associated Legendre functions ($\overline{P}_{nm}$) and the corresponding unnormalized quantities (C_{nm}, S_{nm} and P_{nm}) is

$$C_{nm} = N_{nm}\overline{C}_{nm}, \qquad S_{nm} = N_{nm}\overline{S}_{nm} \quad \text{and} \quad P_{nm} = N_{nm}\overline{P}_{nm} \tag{3.16}$$

with

$$N_{nm} = \sqrt{(2-\delta_{0m})(2n+1)\frac{(n-m)!}{(n+m)!}}, \qquad \delta_{0m} = \begin{cases} 1 & \text{if } m = 0 \\ 0 & \text{if } m \neq 0 \end{cases}. \tag{3.17}$$

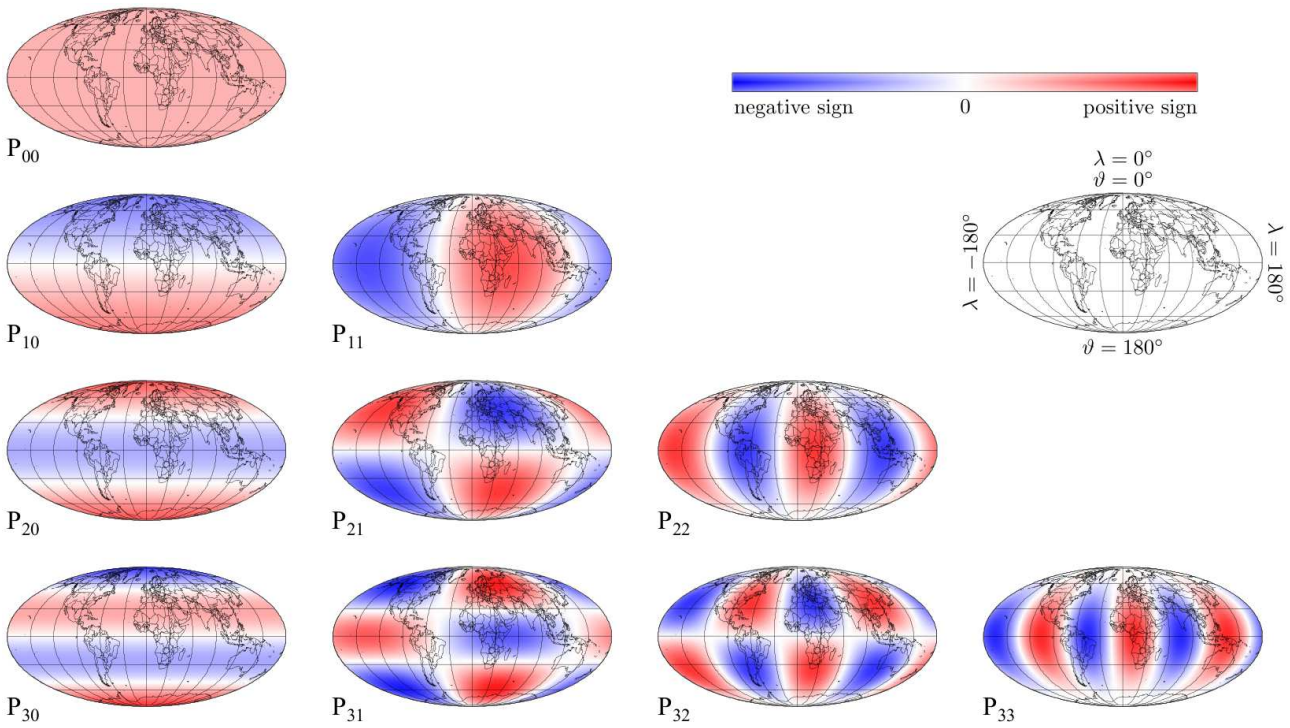

Figure 3.4: Laplace's fully normalized surface spherical harmonic functions of degree $0 \le n \le 3$ and order $0 \le m \le n$.

3.3.1 Geometric interpretation of the spherical harmonic functions

Figure 3.4 shows Laplace's fully normalized surface spherical harmonic functions $\overline{P}_{nm}(\cos\vartheta)\cos m\lambda$ with $\overline{P}_{nm}$ being the fully normalized associated Legendre functions of degree $0 \leq n \leq 3$ and order $0 \leq m \leq n$. The shown amplitudes and signs depend on the normalization formula used (e.g., Equation (3.17)). The zero points of these functions divide the surface of the Earth into regions with alternating signs, bounded by meridians and parallels (Torge, 2001). If the order m is equal to zero, the Legendre polynomials $P_n(\cos\vartheta)$ are independent of the geographical longitude λ and the Earth is divided by parallels into $n+1$ regions with positive and negative signs in the interval $0 \leq \vartheta \leq \pi$. Because of the parallel division, the spherical harmonic functions, realized through Legendre polynomials with order $m = 0$, are called "zonal" harmonics. If the degree is even, the Earth is divided symmetrically w.r.t. the equator. For odd degrees, the division is asymmetric. For the order $m \neq 0$ and $m \neq n$, the $P_{nm}(\cos\vartheta)$ have $n - m$ zero points in the interval $0 \leq \vartheta \leq \pi$. Due to the longitude dependency, $2m$ zero points are caused in the interval $0 \leq \lambda \leq 2\pi$. These harmonic functions are called "tesseral" harmonics. The last group of harmonic functions with $m = n$ are called "sectoral" harmonics since the latitude dependency vanishes. The amplitudes of the spherical harmonics are given by the Stokes coefficients (see Equation (3.14)).

3.3.2 Physical interpretation of the Stokes coefficients

The physical interpretation of the Stokes coefficients can be done using Equation (3.14). For $n = m = 0$, Equation (3.14) yields

$$V_0 = \frac{GM_\oplus}{r} \tag{3.18}$$

which describes a radially layered spherical Earth (Torge, 2001). If $C_{00} \neq 1$, Equation (3.18) is scaled by C_{00}, which corresponds to a change of the global scale. According to Equation (3.15) and by transforming the spherical coordinates into Cartesian coordinates (Torge, 2001; Hofmann-Wellenhof and Moritz, 2006), the first-degree coefficients can be written as

$$C_{10} = \frac{1}{aM}\iiint_{\text{Earth}} Z\,dM, \qquad C_{11} = \frac{1}{aM}\iiint_{\text{Earth}} X\,dM \quad \text{and} \quad S_{11} = \frac{1}{aM}\iiint_{\text{Earth}} Y\,dM. \tag{3.19}$$

The three integrals divided by the Earth mass M give the coordinates $\begin{pmatrix} X & Y & Z \end{pmatrix}^T$ of the $\boldsymbol{CM}$. Since the coordinate system should be centered in the $\boldsymbol{CM}$, the first-degree Stokes coefficients have to be fixed to zero ($C_{10} = C_{11} = S_{11} = 0$). This condition ensures that an estimated satellite orbit is geocentric (P-I). If the first-degree terms are estimated, neither the resulting satellite orbit nor the adjusted station coordinates are geocentric any longer. This is also not the case if the origin is realized through an NNT condition (P-I and Section 3.1.5). The same procedure as applied for Equation (3.19) yields to the second-degree coefficients

$$\begin{aligned}
C_{20} &= \frac{1}{a^2M}\iiint_{\text{Earth}} \left(Z^2 - \frac{X^2+Y^2}{2}\right) dM, \\
C_{21} &= \frac{1}{a^2M}\iiint_{\text{Earth}} XZ\,dM, \qquad & S_{21} &= \frac{1}{a^2M}\iiint_{\text{Earth}} YZ\,dM, \\
C_{22} &= \frac{1}{4a^2M}\iiint_{\text{Earth}} \left(X^2 - Y^2\right) dM \quad \text{and} & S_{22} &= \frac{1}{2a^2M}\iiint_{\text{Earth}} XY\,dM.
\end{aligned} \tag{3.20}$$

According to Torge (2001) and Hofmann-Wellenhof and Moritz (2006), the above expressions are functionals of the moments of inertia

$$A = \iiint \left(Y^2 + Z^2\right) dM, \qquad B = \iiint \left(X^2 + Z^2\right) dM, \qquad C = \iiint \left(X^2 + Y^2\right) dM \tag{3.21}$$

and the products of inertia

$$D = \iiint YZdM, \qquad E = \iiint XZdM \quad \text{and} \quad F = \iiint XYdM. \tag{3.22}$$

If the Z-axis is equal to the principal axis of maximum inertia (no polar motion), the products of inertia D and E become zero which results in zero C_{21} and zero S_{21} coefficients. The remaining product F would be zero if the conventionally defined x-axis (axis through Greenwich meridian; see Table 3.2) coincides with one of the equatorial principal axes (Torge, 2001).

The Stokes coefficient C_{20} is also known as the dynamical form factor of the Earth and describes its polar flattening. This coefficient is about three orders of magnitude larger than all other coefficients. C_{22} describes the asymmetry of the equatorial mass distribution w.r.t. the rotation axis and S_{22} quantifies the rotation of the equatorial principal axes w.r.t. the conventionally defined axes. The coefficient C_{30} can be interpreted as the difference of the Earth flattening for the northern and the southern hemisphere.

Notice on the realization of a "*physical TRF orientation*"

- C_{21} and S_{21} describe the deviations of the Earth's mean rotation axis (CIP) w.r.t. the principal axis of maximum inertia. If C_{21} and S_{21} are fixed to zero, both axes coincide. The coefficients should not be mixed up with the terrestrial pole coordinates x_p and y_p which describe the deviation of the ITRS z-axis w.r.t. the CIP.
- S_{22} describes the rotation of the conventional coordinate system relative to the equatorial principal axes of inertia.
- Since the tensor of inertia $\boldsymbol{I}$ is uniquely defined through six independent components and only five second-degree Stokes coefficients refer to them (see Equations (3.20), (3.21) and (3.22)), an additional piece of information is required to determine $\boldsymbol{I}$ uniquely (Liu and Chao, 1991).
- The rotation angle of the equatorial principal axes of inertia w.r.t. the conventional equatorial axes according to Liu and Chao (1991) reads $\Lambda = \frac{1}{2} arg(C_{22} + iS_{22})$.

Hence, to physically orientate a TRF, C_{21}, S_{21} and Λ have to be fixed to zero. The problem thereby is, that the satellite (system) must be sensitive enough on variations of the second-degree Stokes coefficients. Otherwise, the realized reference system would still contain a degree of freedom w.r.t. the orientation. An example for such a satellite system is given in P-III. Therein, the significant sensitivity of a multi-satellite SLR system to the second-degree Stokes coefficients is discussed. Further investigations should study, if a "*physical TRF orientation*" can be determined through such a system. An example for such studies is the currently running project "Consistent dynamic satellite reference frames and terrestrial geodetic datum parameters (PN6)" of DGFI and the Forschungseinrichtung Satellitengeodäsie (FESG) of the Technische Universität München (TUM) within the DFG research unit FOR 1503 (Nothnagel et al., 2010).

3.3.3 Static and temporal global gravity field models

Current gravity field missions such as GRACE and GOCE have been developed to measure the Earth's gravitational field with high temporal resolution (Tapley et al., 2004) or its mean gravitational field with very high spatial resolution, respectively (ESA, 1999; Bouman et al., 2013). Various global gravity field models are provided through the International Center for Global Gravity Field Models (ICGEM) webpage[7]. Most recent static gravity field models combine observations of GRACE, GOCE and LAGEOS (e.g., GOCO01S; Pail et al., 2011). The maximum degree and order of such models vary from 230 to 360. An exception are the static EIGEN gravity field models which provide Stokes coefficients up to degree and order 1949 (Förste et al., 2012) by including terrestrial and other measurements.

In addition to the static global gravitational field models, the ICGEM webpage also provides temporal global models for dedicated time periods with weekly and monthly resolution. These models are primarily based on GRACE measurements.

[7] http://icgem.gfz-potsdam.de/ICGEM/

3.3.4 Limitations of temporal global gravity field models

Chen et al. (2005) stated that the GRACE mission lacks the ability to determine the long wavelengths of the Earth's gravitational field with very high accuracy. This means that the weekly/monthly gravitational fields contain C_{20} coefficients that are not well determined. The latest state-of-the-art is that Flechtner et al. (2013) recommended to replace the C_{20} coefficients in the GRACE monthly solutions by values obtained from SLR measurements (P-III, P-C). The commonly used SLR time series of monthly (and weekly) low-degree Stokes coefficients is computed by CSR (Cheng and Ries, 2012; 2013). These time series are based on consistent a priori models used for the ReLease (RL) 04 and RL05 monthly GRACE solutions and use observations to the 5 satellites LAGEOS 1/2, Stella, Starlette and Ajisai. It has to be emphasized here that the replacement of the coefficients in the GRACE solution is not a rigorous combination with a proper error propagation.

3.3.5 Strategies to improve the low-degree Stokes coefficients

The low-degree Stokes coefficients can be estimated accurately by a) combining multiple SLR-tracked satellites ond/or by b) rigorously combine SLR and GRACE measurements.

a) Combination of multiple SLR-tracked satellites

In order to validate the commonly used Center for Space Research (CSR) time series, a CSR-comparable time series is presented and evaluated in detail in P-III. Thereby, a special focus was on the detailed description of how the time series has been computed in order to simplify the interpretation of results for users. The main results of P-III are:

- Reliable second-degree Stokes coefficients have been achieved by combining observations of up to 10 different satellites. Thereby, the correlations of the Stokes coefficients themselves and of the Stokes coefficients and the orbital parameters are significantly reduced.
- Various satellite constellations have been compared w.r.t. their ability to decorrelate $\dot{\Omega}$ and C_{20}. Whereas both LAGEOS satellites, Ajisai, Stella, Starlette and LARES significantly contribute to a decorrelation, the impact of the Etalon satellites, BLITS and Larets nearly vanishes.
- The formal errors of the monthly DGFI Stokes coefficients are about four times smaller than the CSR RL04 and RL05 coefficients. This fact is caused by the different orbit modeling and the higher number of observations (due to a higher number of observed satellites) than in the CSR solution. In contrast to the monthly arc of the CSR solution, the DGFI solution contains four weekly arcs stacked to a monthly solution. Therefore, the number of parameters in the DGFI solution is much higher than in the CSR solution.
- The coefficients obtained show a much smaller variation in the standard deviation since the variation of the global network geometry is reduced by the inclusion of more than five satellites.

The external accuracy is validated by comparing the C_{21}-/S_{21}-derived mass-related equatorial excitation functions $\chi_{1,2}^{\text{mass}}$ of polar motion among themselves and w.r.t. external geophysical model combinations. A more detailed evaluation of the monthly DGFI C_{21} and S_{21} coefficients is published in P-D. This study presents a procedure to separate geophysical excitation mechanisms of Earth rotation. Thereby, the C_{21} and S_{21} time series of CSR and DGFI are compared on the basis of relative weighting factors in the adjustment process. The obtained relative weights for the CSR solution are smaller than those for the DGFI solution.

A geophysical application is also given in P-III. Since the fact, that Antarctic ice mass change estimates are dominated by the used time-varying C_{20} estimates, P-III studies the quantity of C_{20}-induced ice mass changes in Antarctica. Thereby, differences of 12.3 Gt per year are found in the long-term trends between the GRACE solutions with C_{20} from DGFI and CSR, respectively. This is about 13 % of the total ice mass loss in Antarctica (Shepherd et al., 2012).

In P-V, the sensitivity of different SLR-only satellite constellations w.r.t. the Stokes coefficients up to degree and order 20 is investigated. Therefore, a monthly gravitational field up to degree and order 20 has been computed for January 2007. If only LAGEOS 1 and 2 are combined, the NEQ matrix is singular and constraints have to be added. If 8 satellites are combined, the sensitivity is increased, no additional constraints are necessary and

reliable estimates can be obtained for all Stokes coefficients. Nevertheless, in this solution, the zonal Stokes coefficients between order 10 and 18 have a higher standard deviation than the other Stokes coefficients. The small standard deviations of the zonal coefficients between order 18 and 20 are explained by the fact, that the higher degree and order Stokes coefficients are fixed to its a priori values and therefore, they implicitly constrain these coefficients.

b) Rigorous combination of SLR and GRACE

In P-C, it is shown that the low even degree Stokes coefficients of SLR are correlated. These correlations are neglected, if the C_{20} values are simply replaced in the GRACE solutions. The results of P-C show that the rigorous combination of the NEQs of SLR and GRACE leads to a NEQ with smaller standard deviations of nearly all Stokes coefficients in the NEQ. Furthermore, the correlations in the rigorously combination NEQ are decreased.

3.4 Integrated estimation of TRF, EOP and Stokes coefficients

As one of the main goals of GGOS, the integrated estimation of TRF, EOP and Stokes coefficients is investigated in this thesis. In the previous three sections, each of the parameter groups was discussed and potential improvements have been revealed. This section now focuses on their integrated estimation which involves the need for separating parameters which are highly correlated (see Figure 3.5). Since SLR is a suitable observation technique which is able to provide contributions to all three "pillars" of GGOS with very high accuracy, this technique allows to study the interactions of the different parameter groups shown in Figure 3.5. Hence, SLR might serve as a case study for the realization of GGOS. In this thesis, a point of special interest is the performance of the multi-satellite SLR solution.

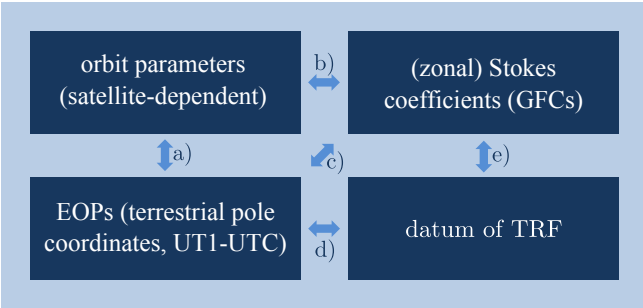

Figure 3.5: Interactions between the three "pillars" of GGOS and the satellite orbits (according to Figure 1 of P-V).

3.4.1 Limitations of the integrated estimation

Below, some critical aspects and existing interactions concerning the integrated estimation of TRF, EOP and Stokes coefficients are summarized. Furthermore, the link to the publications incorporated in this thesis is shown.

a) Correlation of orbit parameters and EOP

The rotation of the orbital plane of a satellite is equal to a rotation of the Earth around its z-axis, the "motion" of the stations projected to the equatorial plane, which is described by UT1-UTC and ΔLOD. The relationship between both parameter groups is given in Equation (3.13). The magnitude and direction of the rotation of the orbital plane depends on its inclination. If orbital planes with different inclinations are combined, the different orbital plane rotations can be distinguished from the common Earth rotation. Detailed studies on this topic can be found in Section 3.2.4, P-II and P-V.

Besides the ability of satellite techniques to determine LOD, they are also able to determine other rates of Earth orientation angles such as nutation rates $\Delta\dot{\epsilon}$ and $\Delta\dot{\psi}$ in obliquity and longitude. This fact was discussed by Rothacher et al. (1999) for the first time. They stated that offsets in (UT1 − UTC), $\Delta\epsilon$ and $\Delta\psi$ can be fully absorbed by rotations around Ω, i and u_0. However, their rates can be determined.

b) Correlation of orbit parameters and (zonal) Stokes coefficients

The correlation of orbit parameters and (zonal) Stokes coefficients is described by the Gaussian perturbation equations of first order (see, e.g., Kaula, 1966; Beutler, 2005a;b). The total differential of these equations is used in P-II in order to compute the secular rates of Ω, ω and M which are caused by offsets in the Stokes coefficient C_{20}. For the other three Keplerian elements a, e and i, no secular rates are caused. The perturbation equations of Ω and ω for higher degrees (C_{n0} with $n = 3, \ldots, 10$) can be found in Iorio (2002).

c) Correlation of EOP and (zonal) Stokes coefficients

Due to the two interactions described above, there is also an indirect relationship between the measured Earth rotation and an offset in the estimated C_{20} coefficient. In P-II, the correlations of the Keplerian elements, C_{20} and the daily estimated LOD values are studied and shown in the cases (a), (b) and (c) of Figure 4.

The Stokes coefficients C_{21} and S_{21} describe the offset of the principal axis of maximum inertia w.r.t. the mean rotation axis of the Earth. In contrast to this, the terrestrial pole coordinates x_p and y_p describe the offset of the realized ITRS z-axis w.r.t. the mean Earth rotation axis. If the orientation of the ITRS realization changes, the Stokes coefficients must compensate this rotation since they are determined in the ITRS realization. Due to this interaction, the Stokes coefficients C_{21}, S_{21} and the pole coordinates x_p, y_p are correlated (see case (e) in Figure 4 of P-II).

d) Correlation of EOP and TRF orientation

The terrestrial pole coordinates describe the motion of the CIP in the ITRS. Complementary to this rotation, the non-equatorial orientation of the TRF is also described through rotations around the x- and y-axis. If the station network of the geocentric NNR condition contains systematic variations or outliers, the TRF x-/y-orientation is biased. This bias is forced into the terrestrial pole coordinates (P-I).

e) Correlation of TRF datum and Stokes coefficients

The relationship between the TRF datum and the Stokes coefficients can be explained by the correlations summarized in the cases (c) and (d). As explained in Section 3.3.2, the degree-zero and degree-one coefficients correspond to the scale and the origin of the TRF, respectively. The coefficients C_{22} and S_{22} are related to the orientation of the conventional TRF w.r.t. the equatorial principal axes of inertia. It has to be mentioned here again that according to the IAG Resolution 16 (1983), the Stokes coefficients should be related to the "zero-tide" system and the TRF coordinates to the "mean-tide" system. In contrast to this definition, the ITRF is related nowadays to the "conventional tide-free" system (Petit and Luzum, 2010). However, this inconsistency can be corrected using Equation (3.4).

3.4.2 Strategies to improve/stabilize the integrated estimation

In this thesis, two possibilities are discussed which lead to a stabilized integrated estimation of station coordinates, EOP and Stokes coefficients. Within both approaches, the special role of SLR is addressed.

a) Epoch Reference Frames (ERFs)

In P-I, the weekly ERFs are derived from a combination of the geodetic space techniques GNSS, SLR and VLBI. The combination allows to use the strengths of each technique in order to remove singularities and to decorrelate parameters. A selected network of dense and homogeneously distributed GNSS stations is used for the realization of the orientation of the combined ERFs. In addition, this network allows to decorrelate common translations and rotations and to decrease the impact of the variable SLR origin on the orientation. This means, that the EOP as complementary parameters to the TRF orientation and the station coordinates are decorrelated (case (d) of Section 3.4.1). The scale of the ERFs is obtained from a combination of SLR and VLBI and therefore, technique-specific systematics are reduced. If the combination interval is extended (e.g., to four weeks), the

density of the station networks and hence the datum stability are increased (P-IV). In addition, the number of co-locations and LT is increased and allows a better connection of the technique-dependent station coordinates.

Since VLBI is the only technique to determine the full set of EOP, it is used in the ERF computation to remove the singularity of the UT1-UTC polygon of the satellite techniques.

b) SLR multi-satellite solution

The multi-satellite SLR solution can be used to significantly stabilize the SLR-only solution. If observations to satellites with different inclinations are combined (two perpendicular orbital planes with inclinations smaller and larger than 90 degree would allow a perfect decorrelation), various parameter groups decorrelate (case (a), (b) and (c) of Section 3.4.1). In P-II, the significant decrease of the correlation between LOD and C_{20} due to the combination of LAGEOS 1 and 2 is shown. P-III presents second-degree Stokes coefficients which are obtained from a ten-satellite SLR solution. The sensitivity of this solution for C_{2m} and S_{2m} is so high that it contributes to decorrelate the TRF and the Stokes coefficients (case (e) of Section 3.4.1). Furthermore, this solution can be used to study the possibilities to physically orientate the TRF (Section 3.3.2). Finally, P-V discusses a multi-satellite SLR solution, where satellite orbits, station coordinates, EOP and second-degree Stokes coefficients are estimated in one common adjustment. If up to ten satellites are used, all parameters can be determined more accurately.

4 Summary and Outlook

Summary

The integration of multiple sensor systems into one consistent Global Geodetic Observing System (GGOS) requires the understanding of the interactions and correlations of the different fundamental geodetic parameters. The rigorous combination of the diverse observations into one observing system has become an important research topic in the geodetic community due to current accuracy requirements. Nowadays, geodesy is faced to monitor the effects of global change and to provide reliable observations and interpretations for other scientific disciplines.

This thesis provides an extensive investigation on how the geodetic space technique SLR can contribute to the realization of GGOS. Going into details, the key role of SLR for the estimation of station coordinates, EOP and Stokes coefficients is studied. SLR is the unique geodetic space technique to provide the ability to study and quantify the correlations of the above mentioned parameters with high accuracy. In the first part, the mathematical foundations are presented in detail. The combination methodology is compared at the three levels of the *Gauß-Markov* model, namely the observation equation, NEQ and solution level, and the pros and cons of each level are described. In the second part, the theoretical and computational foundations of the state-of-the-art realizations of TRF, EOP and Stokes coefficients are worked out and their correlations are discussed. In addition to the interactions of fundamental geodetic parameters, the interactions of the satellite orbit with each parameter group are addressed. The contribution of SLR to GGOS is evaluated using two different approaches: (i) by combining SLR with the geodetic space techniques GNSS and VLBI (inter-technique combination) and (ii) by combining observations to multiple SLR-tracked satellites (intra-technique combination). The specific investigations documented in the first-author publications P-I to P-V are integrated as strategies for the improvement and stabilization of the fundamental geodetic parameters.

For the first time, the strategy to compute combined Epoch Reference Frames (ERFs) is documented in detail in this thesis and in P-I. In this new development, the station coordinates are estimated frequently (e.g., weekly) in contrast to the conventional linear station motion model realized in multi-year reference frames (MRFs). By studying the combined ERFs and the differences to a combined MRF, the following results have been achieved:

- The geodetic datum of the ERFs and the MRF is realized in such a way that the origin is derived from SLR only, whereas the scale is a weighted mean scale of SLR and VLBI. The orientation is realized through an NNR condition applied on a subnet of selected GNSS stations.
- Since the ERFs allow to approximate non-linear station motions with high accuracy, they provide instantaneous geocentric ($\boldsymbol{CM}$-related) station positions. In the conventional MRF, the station position refers only to a $\boldsymbol{CM}$ in a mean sense. This fact makes the ERFs a valuable tool to evaluate geophysical models.
- The geodetic datum of the ERFs is unstable. Due to the sparse weekly SLR station network, the common translations of all stations are correlated with the orientation of the ERFs. This correlation can be reduced, if SLR is combined with, e.g., GNSS which provides a very dense and homogeneously distributed global station network. Another effect of the sparse weekly station networks are the reduced number of LT available for the combination. This fact additionally causes instabilities of the geodetic ERF datum. In the MRF solutions, the networks are more dense and consequently the integration of the different space techniques and the datum definition is more stable.
- To increase the ERF datum stability, one possibility is to enlarge the computation interval (P-IV). If, e.g., a four-weekly interval is used, the datum stability increases but the ability to monitor short-term station motions decreases. Hence, the optimal combination interval depends on the application of the ERFs.
- In order to improve the datum stability without enlarging the computation interval, the number of SLR-tracked satellites can also be increased. The study published in P-V quantifies the effect of including up to six more satellites in addition to the standard ILRS TRF-determination satellite system (usually LAGEOS

1/2 and Etalon 1/2 are considered). The study shows that with a ten satellite solution, the stability of the origin (especially in the z-direction) can be increased by about 30 %. The station repeatability can be improved in the horizontal components by about 35 %.

- Besides the datum stability, the frequent computation of ERFs also reduces the latency of global inter-technique TRFs after large earthquakes since the conventional MRF is updated usually every three to five years. The latency of ERF solutions only depends on the availability of observations after an earthquake.

In summary, the computation of ERFs is a valuable strategy to account for non-linear station motions. Its main limitation is the unstable geodetic datum. However, due to the characteristics mentioned above, the ERFs provide an important supplement to conventional MRFs.

In addition to the TRF computation, SLR can also contribute to improve the realization of the EOP. The investigations of this thesis address the impact of non-linear station motions on the terrestrial pole coordinates and the systematic spurious effects in satellite-technique derived LOD values.

- Due to the correlation of common translations and rotations (network orientations), the neglected common non-linear station motions of the MRF systematically affect the commonly estimated terrestrial pole coordinates (complementary parameters to the network orientation). In the ERFs, this effect is reduced since they account for non-linear station motions. In P-I, the common translations are quantified and their effect on the terrestrial pole coordinates is shown by comparing the differences of the combined MRF and ERFs. The differences show systematic annual variations with amplitudes of up to 39.8 μas. Due to the use of identical input models for both TRF approaches, only the non-linear station motions can cause these systematics.
- In P-II, the interactions between the Earth's gravitational field and the orbital precession of a satellite are studied theoretically and numerical examples are presented. It is shown, that LOD is highly correlated with C_{20} if only one satellite is used. This correlation is caused by the fact that the Earth's flattening (described by the even low degree Stokes coefficients) forces the orbital plane of a satellite into a precession in the equatorial plane. Consequently, this motion cannot be separated from the Earth's rotation. Hence, if LOD and C_{20} are estimated together using only one satellite, no reliable results can be obtained. Furthermore, the satellite orbit is secularly affected by, e.g., relativistic effects such as *Lense-Thirring* and *deSitter* and estimated once-per-revolution empirical accelerations in cross-track direction.
- If the orbit modeling is done correctly and if observations to satellites with different inclinations (LAGEOS1/2 in P-II) are combined, the parameters decorrelate. Hence, the combined adjustment of EOP and Stokes coefficients can be realized and reliable results can be obtained.
- To further improve the estimates of LOD and C_{20}, P-III study various SLR-tracked satellite constellations in order to quantify the impact of each satellite on the decorrelation of $\dot{\Omega}$ and C_{20}. In a ten-satellite solution, only LAGEOS 1, 2, Ajisai, Stella, Starlette and LARES contribute significantly to this decorrelation. The other four satellites, namely Etalon 1, 2, BLITS and Larets do not contribute significantly. P-V investigates the usage of the multi-satellite SLR solution for the integrated estimation of TRF, EOP and Stokes coefficients. The scatter of the terrestrial pole coordinates could be decreased by up to 67 % w.r.t. a single-satellite solution. The systematic offsets of LOD w.r.t. the IERS08C04 time series are reduced by about 10 times compared to a LAGEOS 1/2 solution. The results of P-II, P-III and P-V show that the SLR multi-satellite solution allows to obtain reliable estimations of station coordinates, EOPs and Stokes coefficients in one common adjustment.

The major findings of the EOP part of this thesis are the understanding of the interaction of non-linear station motions and terrestrial pole coordinates and the understanding of the LOD correlations with the Earth's gravitational field.

For the Stokes coefficients, the following improvements could be achieved:

- If up to ten satellites are combined (P-III), the estimation of orbital elements, EOP and Stokes coefficients can be done very accurately. Furthermore, the inclusion of LEOs increases the sensitivity of the SLR solution on higher degree Stokes coefficients. All this leads to the ability to frequently estimate low degree Stokes coefficients over a long time span (in P-III about 13 years) with very high accuracy.
- In comparison with the Stokes coefficient time series provided by CSR, the variation of the time series of formal errors is significantly decreased since the observation geometry improves with incorporating more satellites into the solution.

- In comparison with geophysical models on the basis of equatorial excitation functions of polar motion, the ten-satellite solution performs equal to the CSR time series in the χ_2 component. In contrast to this, the χ_1 values derived from the ten-satellite solution agree better in amplitude and phase to three of four geophysical models.
- The second-degree Stokes coefficients provide a valuable basis for the long-term monitoring of effects of global change. As an example, P-III quantifies the impact of two different C_{20} time series (ten-satellite solution and CSR solution) on the Antarctic ice mass loss determination. It is found that the different time series cause a trend difference of 12.3 Gigatons per year which corresponds to about 13 % of the total ice mass loss in Antarctica.

The results for the Stokes coefficients emphasize the potential of the multi-satellite SLR solution. Since numerous correlations are decreased, also the TRF and EOP can be estimated together with the Stokes coefficients in one common adjustment.

In addition to the individual discussion of the fundamental geodetic parameters, also their integrated estimation based on a multi-satellite SLR solution is discussed (P-V). In this thesis, a special focus is on the correlations between the different parameters. The understanding of these interactions is essential for their integrated estimation. The obtained results from the case study of SLR can be transferred to other geodetic space techniques, in particular when a combination of geodetic and gravimetric observations is done.

Outlook

Curretnly, the main limitation for the ERFs is the datum instability. To improve the geodetic datum and the integration of the geodetic space techniques for the ERFs, different approaches are currently under investigation at DGFI. The most important one studies the effect of different LT handling strategies on the ERFs. Until now, the introduction and weighting of available LT is purely based on experiments performed for MRF computations. In addition, the benefit of so-called space ties (difference vector between two satellite instruments) should be evaluated. Furthermore, the relative weighting of the techniques can be improved by applying VCE. First results were already published by Bloßfeld and Seitz M. (2012). Another possibility to improve the ERF datum is to incorporate the multi-satellite SLR solution to the inter-technique combination with GNSS and VLBI. The improvement of the geodetic datum in the SLR-only solution was clearly shown in this thesis. This strategy is also adapted by the ILRS which plans to include observations to LARES (in addition to LAGEOS 1/2 and Etalon 1/2 observations) in its standard TRF and EOP solution. The inclusion of LARES make it necessary to enlarge the parameter spectrum to the low degree Stokes coefficients in the standard solution since this satellite is very sensitive to the Earth's gravitational field. The benefit of the inclusion of LARES for the TRF and EOP is demonstrated in P-V.

In the case of the MRFs, the main limitation currently is the handling of non-linear station motions. The DFG research unit Forschergruppe "Space-time reference systems for monitoring global change and for precise navigation in space" (FOR 1503) focuses on two different approaches to improve global TRF solutions: (i) the extended parametrization of the station motion in conventional MRF realizations and (ii) the refined geophysical modeling of site dependent loading effects. Both approaches can be supported by the estimation of ERFs since the estimated amplitudes of annual (and semi-annual) signals and the refined geophysical models have to be validated. Therefore, the ERFs can provide combined, global and geocentric station coordinate time series.

Nowadays, there are two main limitations for global TRF computations: (i) non-unified a priori models and (ii) an inhomogeneous and a sometimes sparse global station network in particular for VLBI and SLR. These limitations cannot be solved by refined processing strategies. They are well addressed in the IAG/GGOS community and go beyond the scope of this thesis. In order to overcome these shortcomings, the GGOS community installed two bureaus which should coordinate and support the way towards a unified observing system.

The GGOS Bureau for Products and Standards[8] (formerly the Bureau for Standards and Conventions; Hugentobler et al., 2012; Angermann et al., 2014) shall ensure the use of common standards and conventions for all geodetic techniques and satellite missions. The bureau is currently operated by DGFI and the Institut für Astronomische und Physikalische Geodäsie, Technische Universität München, Germany (IAPG) under the umbrella of the Forschungsgruppe Satellitengeodäsie (FGS).

[8] http://bsc-ggos.dgfi.badw.de/en.,(2014-08-12)

The second GGOS Bureau for Networks and Observations[9]) (formerly the Bureau for Networks and Communications) primarily focuses on the improvement of the global ground network of tracking stations of the four geodetic space techniques GNSS, SLR, VLBI and DORIS. Different countries and organizations realize strategies to achieve the GGOS goals of 1 mm accuracy and 0.1 mm/y stability for all parameters (Gross et al., 2009). Examples are the VLBI2010 project[10] of the IVS or the "Space Geodesy Project"[11] of the National Aeronautics and Space Administration (NASA). Both projects aim to meet the requirements of GGOS core sites (Donovan et al., 2011).

To further support the GGOS goals, several working groups have been installed. One example is the Working group for Performance simuLations and Architectural Trade-Offs (PLATO) in order to assess the impact of the ground station network size, distribution and LT quality and the data quality on the TRF accuracy and datum. Another working group called Working Group on Satellite and Space Missions should provide the framework to incorporate new missions into GGOS.

In summary, the geodetic community proceeds on its way towards the Global Geodetic Observing System. Nevertheless, it has to be mentioned here that the potential of the integration of geometric and gravimetric observations in order to estimate the fundamental geodetic parameters in one common adjustment is not yet fully exploited. The findings of this thesis can be seen as a case study using SLR to identify the parameter interactions and might support the combination of geometric and gravimetric observations in future.

[9] http://192.106.234.28/Components/BNC/BNChome.html, (2014-08-12)
[10] http://ivscc.gsfc.nasa.gov/about/wg/wg3/IVS_WG3_report_050916.pdf, (2014-08-12)
[11] http://space-geodesy.nasa.gov/, (2014-08-12)

5 Content of publications

This chapter provides for a short summary and a declaration of the individual contributions of the co-authors for each of the five first-author publications. For each of the four co-author publications, also a short summary and a declaration of the contribution of M. Bloßfeld is included in this chapter. An overview of all publications and the contributions of M. Bloßfeld in categorized percentage is compiled in Table 5.1.

paper	idea and conceptual design	implementation and realization	analysis and discussion	manuscript writing and figure compilation	total own contribution
first-author publications					
P-I	70 %	90 %	80 %	70 %	**77.5** %
P-II	90 %	80 %	70 %	90 %	**82.5** %
P-III	80 %	60 %	80 %	70 %	**72.5** %
P-IV	100 %	100 %	80 %	80 %	**90.0** %
P-V	100 %	70 %	80 %	90 %	**85.0** %
co-author publications					
P-A	0 %	10 %	20 %	10 %	**10.0** %
P-B	0 %	10 %	20 %	10 %	**10.0** %
P-C	30 %	10 %	20 %	30 %	**22.5** %
P-D	10 %	20 %	10 %	0 %	**10.0** %

Table 5.1: Contributions of M. Bloßfeld to the papers P-I to P-V and P-A to P-D in categorized percentage. All given percentage are pragmatic and rounded values. For a detailed description of the contributions of M. Blossfeld, please see the sections below.

5.1 P-I: Non-linear station motions in epoch and multi-year reference frames

Bloßfeld M., Seitz M., Angermann D. (2014) Non-linear station motions in epoch and multi-year reference frames. In: J Geodesy 88(1), pp: 45-63, DOI: 10.1007/s00190-013-0668-6

Copyright

Summary of publication I

In this paper, an alternative approach to the conventional ITRS realization is introduced. For the first time, the methodology to compute epoch-wise (weekly) estimated TRFs called Epoch Reference Frames (ERFs) from a combination of the geodetic space techniques GNSS, SLR and VLBI is presented. The procedures to obtain an MRF and an ERF are directly compared to each other and the differences are discussed in detail. In this new approach, the station positions are estimated weekly and thus all non-linear station motions are sampled frequently. Differences between the conventional (linear) approach (multi-year reference frame (MRF)) and the new approach (ERF), mainly caused by neglected atmospheric, oceanic and hydrological site-dependent loading effects, comprise common motions of all stations and individually performed station motions.

A major topic of this publication is the investigation of the datum stability of both TRF types. Therefore, all computed solutions are compared to the DTRF2008 using a seven and 14-parameter similarity transformation,

respectively. Whereas the (single-technique and combined) MRFs have a very stable geodetic datum (all transformation parameters and rates below a few millimeter), the datum of the ERF solutions is more unstable (variations at the centimeter level). This fact is caused by the varying weekly ground station networks and the consequently variable availability of LT. In the MRF, the common translations are neglected by the linear station motion model.

Due to correlations of the similarity transformation parameters, the translations are forced into the terrestrial pole coordinates (complementary parameters to the network orientation). In contrast to the MRF, this variation is not forced into the pole coordinates when ERFs are computed. As a consequence, the differences between both pole coordinate time series show systematics with non-annual periods and amplitudes of up to 77.3 μas in the SLR-only solution and systematics with an annual period and an amplitude of up to 39.8 μas in the combined solution, respectively. The amplitudes in the SLR-only differences are larger since the combined solutions have a more dense and more homogeneously distributed station network and consequently the correlations between common translations and rotations are smaller. In addition to the common motions, also the individual station motions affect other commonly adjusted parameters.

In the case of the station coordinates, there are two major findings achieved by this paper: (i) the station coordinates of the MRF are geocentric coordinates only in a mean sense whereas (ii) the ERF coordinates are instantaneous geocentric coordinates. To be able to discuss this finding, a detailed review on currently used definitions of $\boldsymbol{CM}$, $\boldsymbol{CF}$ and other important points is documented in the paper.

At the end of this paper, a short outlook on strategies to improve the ERF datum stability is given. One possibility is the improvement of the global ground station network and the simultaneous improvement of the quality and global coverage of LT. Since the availability of improved networks will take some time, other strategies have to be considered such as the extension of the sampling interval from one week to four weeks or the incorporation of other geodetic space techniques (e.g, DORIS).

If a stable datum and unbiased EOP can be achieved, the ERFs will be valuable for (i) the supporting of secular ITRF realizations to ensure accurate station positions with high timeliness, (ii) monitoring non-linear station motions (geophysical and anthropogenic phenomena), (iii) the determination of EOP since the strengths of all techniques are used and the EOP are unbiased, (iv) geophysicists who need coordinate time series in a $\boldsymbol{CM}$ frame to interpret geophysical phenomena and validate their models.

Declaration of individual contribution

The idea of computing ERFs is already documented in the thesis of M. Seitz (Seitz M., 2009). The development of the computation strategy as well as the development of the software package which uses the DOGS-CS routines was done by M. Bloßfeld. The reprocessing of the complete SLR input data and the processing of the various MRF and ERF solutions was also done by M. Bloßfeld. The reprocessing of the GNSS input data was done by P. Steigenberger in the framework of the GGOS-D project. In the same project, the VLBI data was computed by S. Böckmann. The conception of the paper, the creation of figures and the writing of the first manuscript version was done by M. Bloßfeld. The co-authors contribute to the publication through various discussions of the results and very constructive iterations of the manuscript. Finally, the three anonymous reviewers and the associated editor (J. Freymueller) improved the publication through comments on content and linguistic issues.

5.2 P-II: Systematic effects in LOD from SLR observations

Bloßfeld M., Gerstl M., Hugentobler U., Angermann D., Müller H. (2014) Systematic effects in LOD from SLR observations. In: Adv Space Res 54, pp: 1049–1063, DOI: 10.1016/j.asr.2014.06.009

Copyright

Summary of publication II

In this paper, the reasons for the spurious systematic effects in SLR-derived Length Of Day (LOD) values are investigated. The theoretical relationship between the orbital elements, EOP and second-degree Stokes coefficients is worked out using first-order Gaussian perturbation equations. It is shown that the flattening of the

Earth, described by even low-degree Stokes coefficients, forces the orbital plane of a satellite into a precession motion in the equatorial plane. This motion cannot be separated from the Earth's rotation which is described by LOD. Therefore, C_{20} and LOD are highly correlated. Besides this correlation, also the orbit modeling causes a secular effect in LOD. If the relativistic accelerations due to the *Lense-Thirring* and *deSitter* effect are neglected, a constant offset in LOD is caused. Furthermore, the estimation of empirical once-per-revolution accelerations in cross-track direction, originally introduced to absorb non-modeled effects in the orbit, can cause secular effects in the satellite's nodal precession and consequently in LOD.

In order to quantify the different effects in LOD, different test cases w.r.t. altitude, inclination, a priori values of C_{20} and a priori empirical accelerations have been evaluated. Secular rotations of up to 1.0 ms for an error of $8.0 \cdot 10^{-10}$ in the a priori C_{20} model are caused for satellites at 500 km altitude and zero-degree inclination (maximum effect). Periodic empirical accelerations estimated perpendicular to the orbital plane (sine-term $s(W')$ constrained) cause only very small secular rotations. This impact increases if the accelerations are not constrained. If relativistic accelerations of near-Earth satellites are neglected, secular rotations of 0.0088 ms are caused for satellites at LAGEOS altitude. One way to reduce the high correlations is to combine observations to different satellites with different inclinations.

The theoretical effects, derived in the first part of this paper, have been verified in the second part. For quantification, several test computations have been computed using in total 31 years of SLR data of the satellites LAGEOS 1 and 2 between 1983.0 and 2014.0. The first four solutions contain four different a priori gravity field models (GGM02S, GGM02C, EIGEN-6S, EIGEN-6C2). Especially when only LAGEOS 1 is available (1983.0 until 1993.0), systematics such as periodical variations or long-term drifts of up to 0.02 ms can be found in the ΔLOD values. These systematics are the reason for the exclusion of the SLR ΔLOD in the DTRF2008 computation (P-A). A possibility to reduce the systematics would be to combine LAGEOS 1 and Starlette observations (also available since 1982.0). Thereby, the modeling of the atmospheric drag is problematic due to the lack of accurate high atmosphere models (altitude of Starlette is about 957 km) in the early years. The investigations of this paper point out very clearly that it is important to use the same a priori gravity field model to compute the SLR ΔLOD values. For the ITRF2013 reprocessing, the ILRS requests its ACs to use one common model for the reprocessing.

Another topic, addressed in this paper, is the combined estimation of different parameter groups. To test the parameter correlations, we computed two more test solutions. In one solution, the gravity field coefficients of degree and order two are estimated. The correlations of ΔLOD and Ω cause large errors in the ΔLOD values (no reliable results) derived solely from LAGEOS 1 observations. If the observations to both LAGEOS satellites are combined, the spurious signals in ΔLOD are reduced. The major part of the ΔLOD errors can be explained with the nodal precession due to an offset in C_{20}. Changes in a, e and i which could also affect $\dot{\Omega}$, $\dot{\omega}$ and $\dot{M}$, are not considered here since only Gaussian perturbation equations of first order are used. The secular precession of ω and M is compensated through variations in the semi-major axis a, which induce changes in the mean angular velocity n of the satellite. In addition, the along-track motion might be compensated by estimated along-track empirical accelerations. If the $s(W')$ once-per-revolution acceleration is estimated, the single-satellite solution only slightly improves. If the cross-track accelerations are not constrained, the effects in ΔLOD and C_{20} are much larger.

The last section of this paper deals with the secular effect of the relativistic accelerations due to the *Lense-Thirring* and *deSitter* effect in ΔLOD. Whereas the total effect due to these accelerations in ΔLOD is 0.0088 ms, the effect of the partial derivatives is very small ($\delta(\Delta\text{LOD}) < 1.3\ \mu s$ after the first iteration).

Declaration of individual contribution

The idea of investigating the reasons for the spurious systematic signals in SLR derived LOD values was of M. Bloßfeld (as a consequence of P-I). Furthermore, M. Bloßfeld suggested to analyze the impact of relativistic accelerations on the LOD values. The implementation of the relativistic accelerations in DOGS-OC was done by M. Bloßfeld with help of M. Gerstl. U. Hugentobler derived the formula for the secular effect of the once-per-revolution cross-track acceleration and supported significantly the understanding of the compensation of the secular precession of ω and M through variations in the semi-major axis a. The conception of the paper, the creation of figures and the writing of the first manuscript version was done by M. Bloßfeld. H. Müller and D. Angermann helped to improve the SLR-related content. Furthermore, the three anonymous reviewers and the associated editor improved the publication through comments on content and linguistic issues.

5.3 P-III: Second-degree Stokes coefficients from multi-satellite SLR

Bloßfeld M., Müller H., Gerstl M., Štefka V., Bouman J., Göttl F., Horwath M. (2015) Second-degree Stokes coefficients from multi-satellite SLR. In: J Geodesy, in review

Copyright

Summary of publication III

This paper presents reliable weekly and monthly estimates of the second-degree Stokes coefficients of the Earth's gravitational field. They are derived from the iterative VCE-based combination of NEQs of up to ten satellites (equipped with RRA) with different orbit characteristics between 2000.0 and 2014.0. The diversity of orbit altitudes, inclinations, cross-section-to-mass ratios and orbital resonances with the Earth's gravitational field allows to decorrelate the second-degree Stokes coefficients and the orbital parameters. Since the correlation of C_{20} and the right ascension of the ascending node Ω is the largest one, various satellite constellations are tested to what extend each satellites contributes to the decorrelation. A significant contribution has been found for LAGEOS 1 and 2, Ajisai, Stella, Starlette and LARES. No significant contribution on the decorrelation has been found for Etalon 1 and 2, BLITS and Larets. The solution setup and the computation procedure are presented in detail in order to give the user of this publicly available time series the opportunity to obtain reliable interpretations of their final results.

In order to validate the solutions, the internal precision is assessed by comparing the obtained formal errors in terms of second-degree geoid errors. The formal errors of the monthly DGFI multi-satellite solutions are about four times smaller than the CSR ReLease04 (RL04) or RL05 errors. This fact is caused by the different orbit modeling and the higher number of observations in the DGFI solution than in the CSR solution. Whereas the CSR computes monthly arcs, the DGFI monthly solution comprises four weekly arcs that are stacked to one monthly arc. This means that four initial sets of orbit elements remain in the DGFI monthly NEQ. Nevertheless, the DGFI second-degree geoid errors show a much smaller variation in the standard deviations than the CSR errors. This fact is caused by the stabler long-term observation geometry since the variation in the global network coverage is reduced due to the incorporation of up to ten satellites. The obtained monthly DGFI time series of second-degree Stokes coefficients has nearly constantly the same formal errors which allows a better comparison of the obtained coefficients at different epochs. Therefore, time-variable geophysical phenomena might be interpreted more reliable.

The external accuracy is validated by comparing the mass-related equatorial excitation functions $\chi_{1,2}^{\text{mass}}$ (derived from the different C_{21}, S_{21}) among themselves and with respect to external geophysical model combinations and reduced geodetic excitation functions. Thereby, large differences in amplitudes and phases between the different solutions can be seen. For χ_1^{mass}, the DGFI monthly solution fits better to three of four model combinations than the CSR time series. The highest agreement is achieved between the DGFI solution and the NEG$^{\text{mass}}$ model combination, where the mass-related excitation function is derived from a combination of the atmospheric (NCEP), the oceanic (ECCO) and the hydrological (GLDAS) model. For χ_2^{mass}, the annual amplitudes and phases of the DGFI, both CSR and the CSR GRACE solution show only small differences ($\Delta < 10$ %).

In addition to the internal and external validation, a geophysical application of the derived Stokes coefficients is presented. Since C_{20} dominates the estimation of the Antarctic ice mass loss, C_{20}-induced ice mass changes in Antarctica, estimated from different C_{20} time series, are compared. If the long-term trends (2003.0 until 2013.0) of the GRACE solutions (C_{20} replaced using CSR RL05 and monthly DGFI values) are compared, a difference of about 12.3 Gt/y is found. This difference has a magnitude of about 13 % of the total ice mass loss in Antarctica.

The results presented in this paper emphasize the importance of accurately determined second-degree Stokes coefficients. The presented SLR solution allows a validation of results obtained with the CSR RL05 SLR time series. Comparing at least two independent SLR solutions provides the ability to assess their impact on geophysical investigations.

Declaration of individual contribution

The idea for the computation of a multi-satellite solution was of M. Bloßfeld and V. Štefka. The reprocessing of the various satellites and their combination using VCE was done by M. Bloßfeld and supported by H. Müller. The software developments, necessary for the processing of the LEOs was developed primarily by V. Štefka and implemented in DOGS-OC by M. Bloßfeld and M. Gerstl. The VCE algorithm was implemented in an external routine by M. Bloßfeld. The geophysical application of the Stokes coefficients (Antarctic ice mass trends) was based on the idea of J. Bouman. F. Göttl helped to validate the obtained Stokes coefficients and the CSR time series through equatorial excitation functions. M. Horwath provided the GRACE solution. The conception of the paper, the creation of figures and the writing of the first manuscript version was done by M. Bloßfeld. The co-authors helped to improve the manuscript through comments on content and linguistic issues.

5.4 P-IV: Epoch reference frames as short-term realizations of the ITRS

Bloßfeld M., Seitz M., Angermann D. (2015) Epoch reference frames as short-term realizations of the ITRS. In: IAG Symposia Series 143, in press

Copyright

Summary of publication IV

This paper studies the effect of an enlarged sampling interval for the ERFs on the geodetic datum of the obtained TRFs and on their ability to monitor non-linear station motions. Therefore, the sampling interval is varied from one to four weeks. To evaluate the datum stability, the obtained ERF time series are transformed on a combined MRF using a common subnet of GNSS stations. In order to obtain interpretable results, all TRF solutions are based on identical input models and data.

The longer the sampling interval is, the more stable is the geodetic datum. The scatter of the four-weekly transformation parameter time series is reduced by up to 50 % compared to the weekly time series. However, the annual variations in the parameter time series are not damped. The increase of the ERF datum can be explained with the larger number of LT in the longer sampling intervals and the more stable ground station network.

The trade-off for the higher datum stability is the decreased ability to monitor short-term non-linear station motions. Signals with periods below twice the sampling interval cannot be sampled correctly. As an example, the paper presents a time series of Yakutsk (Russia) and discusses the ability of the different ERF solutions to approximate a spurious signal between 2005.6 and 2006.1 (maybe due to snow coverage). The best approximation can be achieved with the 7- and 14-day ERFs where the 14-day ERFs already cause an error of about 10 mm in the east and height component. The error increases to 20 mm for the 28-day ERFs.

At the end of this paper, the properties of the MRF and the different ERFs are summarized. The major finding of the paper is that the optimal sampling interval of the ERFs depends on their application. Whereas the 28-day ERFs are suitable to monitor annual variations or post-seismic deformations, the main application for the 7- and 14-day ERFs would be to monitor abrupt changes or short-term local environmental effects. The main application of the MRFs are the monitoring of long-term changes, sea level rise or plate tectonics.

Declaration of individual contribution

The idea of enlarging the sampling interval was of M. Bloßfeld. The used data was equal to the data used for paper P-I. The conception of the paper, the creation of figures and the writing of the first manuscript version was done by M. Bloßfeld. The co-authors M. Seitz and D. Angermann helped to improve the manuscript through discussions of the results and proof reading. Finally, the three reviewers and the editor improved the paper with their corrections about content and linguistic issues.

5.5 P-V: Satellite Laser Ranging – A tool to realize GGOS?

Bloßfeld M., Štefka V., Müller H., Gerstl M. (2015) Satellite Laser Ranging – A tool to realize GGOS? In: IAG Symposia Series 143, in press

Copyright

Summary of publication V

This paper focuses on the intra-technique combination of SLR satellites with different orbit altitudes, inclinations, and satellite characteristics. It discusses the ability of SLR to contribute to GGOS by estimating station coordinates, EOP and Stokes coefficients of degree two to twenty in one common adjustment. The satellites are relatively weighted using VCE. In total, three different solution types are computed: (i) estimating only station coordinates, (ii) estimating station coordinates and EOP and (iii) estimating station coordinates, EOP and Stokes coefficients.

In a first step, the different obtained relative weights of the satellites w.r.t. the estimated parameters are discussed. Whereas the relative weights for LAGEOS 1/2 and Etalon 1/2 nearly do not change, the relative weights of the LEOs increase significantly when Stokes coefficients are estimated. This fact can be explained with the high sensitivity of the LEOs on the Earth's gravitational field. Furthermore there exist large differences between the LEO weights which are caused by orbit and/or satellite characteristics.

The major part of this paper studies the different parameters obtained from a common adjustment. Therefore, three different solution types are computed: (i) only observations to LAGEOS 1/2 are considered, (ii) observations to LAGEOS 1/2 and LARES are considered (this solution setup is tested since the ILRS plans to include LARES in its official product computation) and (iii) the observations to up to ten satellites are considered. In the following, the results are summarized:

- The stability of the geodetic datum can be improved by including more satellites into the solution. Especially the Root Mean Square (RMS) of the z-translation is reduced when up to ten satellites are considered (reduction of about 30 %). The station repeatability is also improved. When ten satellites are used, the horizontal WRMS is reduced by about 35 %. The scatter of the height component only slightly improves since the observation geometry does not change significantly (only satellites in the hemisphere above the station are observed).
- As it was the case for the station coordinates, also the EOP are improved significantly when more satellites are considered. The systematics in the LOD values nearly totally disappear and the scatter of the terrestrial pole coordinates w.r.t. the IERS08C04 time series is reduced by about 67 % in comparison to a single-satellite solution.
- The Stokes coefficients with degree two to twenty are significantly decorrelated and their standard deviations are decreased. If the standard deviations of the two satellite solution (only LAGEOS 1/2) are compared to the standard deviations of the ten satellite solution, an improvement of especially the degrees greater than five can be seen. This fact is caused by the incorporation of LEOs in the multi-satellite solution.

In summary, several advantages of a multi-satellite SLR solution are found. Due to the mix of various orbit and satellite characteristics, the obtained multi-satellite solutions provide reliable estimates of the parameters associated to the three pillars of GGOS, the station coordinates, EOP and Stokes coefficients.

Declaration of individual contribution

The idea for using a multi-satellite SLR solution to estimate station coordinates, EOP and Stokes coefficients in one common adjustment was of M. Bloßfeld. The software developments, necessary for the processing of the LEOs was developed primarily by V. Štefka and implemented in DOGS-OC by M. Bloßfeld and M. Gerstl. The VCE algorithm was implemented in an external routine by M. Bloßfeld. H. Müller supported the reprocessing.

The conception of the paper, the creation of figures and the writing of the first manuscript version was done by M. Bloßfeld. The co-authors helped to improve the manuscript through comments on content and linguistic issues. Furthermore, the three anonymous reviewers and the editor improved the manuscript with their corrections about content and linguistic issues.

5.6 Co-author publications

In the following, the four co-author publications are briefly described. Since they are not directly part of this thesis, they are not attached to this thesis.

5.6.1 P-A: The 2008 DGFI Realization of the ITRS: DTRF2008

Seitz M., Angermann D., Bloßfeld M., Drewes H., Gerstl M. (2012) The 2008 DGFI Realization of the ITRS: DTRF2008. In: J Geodesy 86(12), pp: 1097–1123, DOI: 10.1007/s00190-012-0567-2

Copyright

This publication is available at link.springer.com.

Summary of publication A and declaration of own contribution

This publication presents in detail the methodology for the inter-technique combination at NEQ level applied at DGFI which is one of the ITRS CCs. The derived algorithm is used in order to compute a realization of the ITRS using input data of the IAG Services IGS, ILRS, IVS and IDS. The computed global TRF is named DTRF2008. The obtained station coordinates are compared with the second (official) realization of the ITRS, the ITRF2008. In addition, the commonly estimated EOP are compared with the IERS 08 C04 time series.

The processing of the ILRS input data, including the time series analysis, introduction of discontinuities and the accumulation of NEQs was done by M. Bloßfeld. In addition, several analysis done by M. Bloßfeld helped to validate the DTRF2008 solution. Finally, M. Bloßfeld helped to improve the paper through comments and corrections on content and linguistic issues.

5.6.2 P-B: Reducing the draconitic errors in GNSS geodetic products

Rodriguez-Solano C. J., Hugentobler U., Steigenberger P., Bloßfeld M., Fritsche M. (2014) Reducing the draconitic errors in GNSS geodetic products. In: J Geodesy, 88(6), pp 559–574, DOI: 10.1007/s00190-014-0704-1

Copyright

This publication is available at springer.link.com.

Summary of publication B and declaration of own contribution

This publication investigates the impact of orbit modeling deficiencies due to solar radiation pressure on GNSS-derived geodetic products such as station coordinates and EOP. The paper shows that using the adjustable box-wing model derived by Rodriguez-Solano et al. (2012) clearly improves the GNSS orbit during non-eclipse seasons. In addition, different non-nominal yaw attitude models are tested and the GNSS orbit could be further improved during eclipse seasons. These improvements result in a nearly completely decreased draconitic error in the geocenter Z-component. The draconitic errors in the rates of the terrestrial pole coordinates and LOD are not conclusively reduced. In the case of the station coordinates, the draconitic errors are reduced but still visible in the obtained time series.

The idea of testing the impact of the new solar radiation pressure and altitude models on the EOP (especially on the y-pole rates) was of M. Bloßfeld. Finally, M. Bloßfeld helped to improve the paper through comments and corrections on content and linguistic issues.

5.6.3 P-C: Combined estimation of the Earth's gravity field using SLR and GRACE data

Haberkorn C., Bloßfeld M., Bouman J., Fuchs M., Schmidt M. (2015) Combined estimation of the Earth's gravity field using SLR and GRACE data. In: IAG Symposia Series 143, in press

Copyright

This publication is available at rd.springer.com.

Summary of publication C and declaration of own contribution

Nowadays, it is recommended to replace the Stokes coefficient C_{20} in temporal gravitational field models derived from GRACE observations. In this study, we investigate the impact of a rigorous combination of an SLR NEQ and a GRACE NEQ on a combined NEQ in order to quantify the improvement due to a rigorous combination. The SLR NEQ (test month is January 2007) is obtained from a multi-satellite SLR solution which takes into account observations to up to 8 different satellites. The analysis shows that the impact of SLR on the GRACE NEQ in minor, but positive. Improvements (lower standard deviations) of the combined NEQ w.r.t. the GRACE NEQ can be found in the very low degree, sectoral and near-sectoral, as well as in resonance-order Stokes coefficients.

The computation of the SLR input NEQ was done by M. Bloßfeld. Furthermore, M. Bloßfeld helped to improve the paper through comments and corrections on content and linguistic issues.

5.6.4 P-D: Separation of atmospheric, oceanic and hydrological polar motion excitation mechanisms by a combination of geometric and gravimetric space observations

Göttl F., Schmidt M., Seitz F., Bloßfeld M. (2015) Separation of atmospheric, oceanic and hydrological polar motion excitation mechanisms by a combination of geometric and gravimetric space observations. In: J Geodesy, online first, DOI: 10.1007/s00190-014-0782-0

Copyright

This publication is available at link.springer.com.

Summary of publication D and declaration of own contribution

In this publication, observations to various geodetic space techniques such as GNSS, SLR, VLBI and DORIS, satellite altimetry and satellite gravimetry are combined to separate geophysical excitation mechanisms of the Earth rotation. In the case of the atmospheric and oceanic mass effect, good agreements with the geodetic solutions and model estimates are found. In contrast to this, the hydrological and integral mass effect differ significantly from the model estimates. In comparison to RMS differences of the solutions which are based on geophysical models, the formal errors of the adjusted geodetic results are significantly smaller which means a step forward w.r.t. the understanding of individual contributions of the subsystems to Earth rotation variations.

The computation of the SLR input time series was done by M. Bloßfeld. Parts of the analysis published here have been addressed in P-III.

Abbreviations and Nomenclature

Abbreviations

LOD_R	"regularized" Length Of Day (LOD corrected for tidal signals)	19
$UT1_R$	"regularized" Universal Time 1 (UT1 crrected for tidal signals)	19
AC	Analysis Center	28, 33, 39–41, 47, 63
APKIM	Actual Plate KInematic and crustal deformation Model	41
AWG	Analysis Working Group	49
BCRS	Barycentric Celestial Reference System	46
BIH	Bureau International de l'Heure	38, 46
BKG	Bundesamt für Kartographie und Geodäsie	35, 36, 44, 45
BLITS	Ball Lense In The Space	49, 53, 58, 64
CATREF	Combination and Analysis of Terrestrial REference Frames	31
CC	Combination Center	29, 38, 41, 67
CHAMP	CHAllenging Minisatellite Payload	8
CIO	Celestial Intermediate Origin	45, 46, 74, 75
CIP	Celestial Intermediate Pole	45–47, 52, 55, 75
CIRS	Celestial Intermediate Reference System	46, 74
CS-TRAFO	TRAnsFOrmation routine of DOGS-CS	16, 35, 36
CS-TRASI	TRAnsformation with SIngluar transformation matrix routine of DOGS-CS	17, 36
CSR	Center for Space Research	53, 58, 59, 64, 65
DFG	Deutsche Forschungsgemeinschaft	35, 44, 45, 52, 59
DGFI	Deutsches Geodätisches Forschungsinstitut	11, 12, 29, 31, 33, 35, 36, 38, 43–45, 52, 53, 59, 64, 67
DOGS	DGFI Orbit and Geodetic parameter estimation Software	10, 33
DOGS-CS	Combination and Solution library of DOGS	10, 11, 15, 17, 33, 35, 36, 62, 69
DOGS-OC	Orbit Computation library of DOGS	10, 11, 33–35, 63, 65, 66, 76
DOGS-RI	Radio Interferometry library of DOGS	33
DORIS	Doppler Orbithography and Radiopositioning Integrated by Satellite	8, 11, 14, 29, 37–39, 41, 60, 62, 68
DTRF	DGFI Terrestrial Reference Frame	36, 38, 39, 41, 43, 61, 63, 67, 76
EOP	Earth Orientation Parameters	3, 4, 8–10, 17–21, 26, 36–38, 43–49, 54–59, 62, 66, 67, 76

ERA	Earth Rotation Angle	45, 46
ERF	Epoch Reference Frame	3, 4, 9, 10, 36, 42–44, 48, 55–59, 61, 62, 65, 76
FCN	Free Core Nutation	47
FESG	Forschungseinrichtung Satellitengeodäsie	52
FGS	Forschungsgruppe Satellitengeodäsie	59
FK5	Fifth Fundamental Catalogue	46
FOR 1503	Forschergruppe “Space-time reference systems for monitoring global change and for precise navigation in space”	35, 44, 45, 52, 59
FOR584	Forschergruppe “Earth Rotation and Global Dynamic Processes”	45
GAST	Greenwich Apparent Sideral Time	45, 46
GCRS	Geocentric Celestial Reference System	34, 38, 45–47, 74
GGOS	Global Geodetic Observing System	3, 4, 8, 9, 37, 54, 57, 59, 60, 66, 76
GGOS-D	Global Geodetic Observing System – Deutschland	8, 62
GNSS	Global Navigation Satellite Systems	3, 4, 8, 10, 11, 14, 31, 36–39, 41, 43, 49, 55, 57, 59–62, 65, 67, 68
GOCE	Gravity field and steady-state Ocean Circulation Explorer	8, 52
GPS	Global Positioning System	18, 19, 29, 30, 76, 79
GRACE	GRAvity recovery and Climate Experiment	8, 11, 36, 52–54, 64, 65, 68
GTRS	Geocentric Terrestrial Reference System	38
IAG	International Association of Geodesy	3, 4, 8, 45, 59, 67
IAPG	Institut für Astronomische und Physikalische Geodäsie, Technische Universität München, Germany	59
IAU	International Astronomical Union	45
ICGEM	International Center for Global Gravity Field Models	52
ICRF	International Celestial Reference Frame	47
ICRS	International Celestial Reference System	46, 76
IDS	International DORIS Service	29, 41, 67
IERS	International Earth Rotation and Reference Systems Service	29, 35, 38, 39, 41, 45–47, 49, 58, 66, 67
IGN	Institute Nationale de l’Information Géographique et Forestière	31, 38, 43
IGS	International GNSS Service	29, 67
ILRS	International Laser Ranging Service	29, 33, 49, 57, 59, 63, 66, 67
ITRF	International Terrestrial Reference Frame	8, 29, 38–43, 47, 55, 63, 67
ITRS	International Terrestrial Reference System	34, 38–43, 45, 46, 50, 52, 55, 67, 75, 76
IUGG	International Union of Geodesy and Geophysics	8
IVS	International VLBI Service for Geodesy and Astrometry	29, 36, 60, 67

JPL	Jet Propulsion Laboratory	47
JWG	Joint Working Group	45
LAGEOS	LAser GEOdynamics Satellite	41, 44, 49, 52, 53, 56–59, 63, 64, 66
LARES	LAser RElativity Satellite	44, 49, 53, 58, 59, 64, 66
LEO	Low Earth Orbiter	41, 44, 58, 65, 66
LLR	Lunar Laser Ranging	8
LOD	Length Of Day	3, 4, 9, 10, 18, 19, 35, 37, 39, 47–49, 54–56, 58, 62, 63, 66, 67
LT	Local Ties	42–44, 56, 57, 59, 60, 62, 65
MRF	multi-year reference frame	9, 37, 39, 43, 44, 48, 57–59, 61, 62, 65
NASA	National Aeronautics and Space Administration	60
NEQ	Normal EQuation	10–19, 21, 22, 24, 25, 27–32, 35, 36, 43, 53, 54, 57, 64, 67, 68, 72, 74–76
NNR	No-Net-Rotation	28, 36, 38, 41, 43, 44, 55, 57
NNS	No-Net-Scale	28, 36
NNT	No-Net-Translation	28, 36, 51
NRO	Non Rotating Origin	45
O-C	‘observed’ minus ‘computed with a priori values’	12, 29, 73, 74
PCO	Phase Center Offset	41
PLATO	Performance simuLations and Architectural Trade-Offs	60
POD	Precise Orbit Determination	44
pwl	piece-wise linear	18, 42, 48, 49
RMS	Root Mean Square	49, 66, 68
RRA	Retro-Reflector-Array	33, 64
SINEX	Solution INdependent EXchange format	11, 14, 29, 30, 42
SLR	Satellite Laser Ranging	3, 4, 8–12, 14, 18, 19, 29, 30, 36–39, 41, 43, 44, 48, 49, 52–64, 66, 68, 76
TAI	Temps Atomique International (engl.: International Atomic Time)	47
TC	Technique Center	29, 38
TCB	Temps Coordonné Barycentrique (engl.: Barycentric Coordinate Time)	46
TCG	Temps Coordonné Geocentrique (engl.: Geocentric Coordinate Time)	38, 39, 46

TDB	Temps Dynamique Barycentrique (engl.: Barycentric Dynamical Time)	46
TIO	Terrestrial Intermediate Origin	46, 75
TIRS	Terrestrial Intermediate Reference System	45, 46, 74, 75
TRF	Terrestrial Reference Frame	3, 4, 8–10, 20, 29, 36–40, 42–44, 48, 49, 52, 54–61, 65, 67
TT	Temps Terrestre (engl.: Terrestrial Time)	39
TUM	Technische Universität München	52
UT1	Universal Time 1	18, 19, 39, 46–49, 54, 56
UTC	Universal Time Coordinated	39, 46–49, 54, 56
VCE	Variance Component Estimation	11, 32, 59, 64–66
VLBI	Very Long Baseline Interferometry	3, 4, 8, 10, 11, 14, 18, 19, 29, 37–39, 41, 43, 48, 55–57, 59–62, 68, 76

Nomenclature

$\Delta\rho$	*scalar*	range bias of measurement [m]	33, 34
Δr	*scalar*	bias of tropospheric refraction [-]	33, 34
Δt	*scalar*	time bias of measurement [s]	33, 34
$\boldsymbol{\Delta x}$	$[u \times 1]$	vector of first order correction terms to $\boldsymbol{x_0}$	11
$\boldsymbol{\Delta \hat{x}}$	$[u \times 1]$	vector of estimated first order correction terms to $\boldsymbol{x_0}$	13
$\boldsymbol{\Delta x_k}$	$[u_k \times 1]$	vector of first order correction terms to $\boldsymbol{x_0}$ of the k-th equation system	30
$\dot{\Omega}$	*scalar*	rate of the right ascension of the ascending node Ω	48
Υ	*scalar*	Vernal Equinox	46
ϵ	*scalar*	measurement error	33, 34
λ_k	*scalar*	individual weighting factor of the k-th equation system	31
ω	*scalar*	frequency of linear-trigonometric station motion model	22
ρ	*scalar*	one-way range measurement	33, 34
σ_0^2	*scalar*	a priori variance factor	13, 14
$\boldsymbol{\sigma_c}$	$[n_c \times 1]$	vector of standard deviations of pseudo observations $\boldsymbol{c}$	27
$\hat{\sigma}_0^2$	*scalar*	a posteriori variance factor	13, 14
$\sigma_{0,k}^2$	*scalar*	a priori variance factor of the k-th equation system	30
ϑ	*scalar*	geographic latitude	50
$\boldsymbol{A}$	$[n \times u]$	(Jacobian) matrix with first derivatives of $f(\boldsymbol{x_0})$ at the point $\boldsymbol{x_0}$ (design matrix of the NEQ system)	12, 14
$\boldsymbol{a}_{\mathrm{DG}}$	$[3 \times 1]$	direct 3-dimensional gravitational acceleration (direct effect on the satellite)	34
$\boldsymbol{a}_{\mathrm{GE}}$	$[3 \times 1]$	3-dimensional gravitational acceleration caused by the Earth (Stokes coefficients C_{nm}, S_{nm} with $n, m \in \mathbb{N}^+$ and $m \leq n$	34
$\boldsymbol{a}_{\mathrm{GM}}$	$[3 \times 1]$	3-dimensional gravitational acceleration caused by the Moon	34
$\boldsymbol{a}_{\mathrm{GNT}}$	$[3 \times 1]$	3-dimensional gravitational acceleration caused by mass variations due to non-tidal loading effects (e.g., atmospheric, hydrological, oceanic)	34
$\boldsymbol{a}_{\mathrm{GP}}$	$[3 \times 1]$	3-dimensional gravitational acceleration caused by the Sun and other planets	34

$\boldsymbol{a}_{\mathrm{GT}}$	$[3 \times 1]$	3-dimensional gravitational acceleration caused by mass variations due to solid Earth and ocean tides	34
$\boldsymbol{a}_{\mathrm{IG}}$	$[3 \times 1]$	indirect 3-dimensional gravitational acceleration (indirect effect on the satellite via the Earth)	34
$\boldsymbol{A_k}$	$[n_k \times u_k]$	(Jacobian) matrix of the k-th equation system	30
$\boldsymbol{a}_{\mathrm{KEP}}$	$[3 \times 1]$	3-dimensional gravitational acceleration caused by the point-concentrated mass of the Earth (Stokes coefficient C_{00})	34
$\boldsymbol{a}_{\mathrm{NG}}$	$[3 \times 1]$	3-dimensional non-gravitational acceleration (e.g., due to solar radiation pressure, atmospheric drag)	34
$\bar{\boldsymbol{A}}_{\boldsymbol{1}}^{+}$	$[u_r \times n]$	pseudoinverse of matrix $\bar{\boldsymbol{A}}_{\boldsymbol{1}}$ with $rg(\bar{\boldsymbol{A}}_{\boldsymbol{1}}) = u_r$	25
$\tilde{\boldsymbol{A}}$	$[n \times u]$	matrix with constrained/transformed first derivatives	16, 25
$\boldsymbol{b}$	$[n \times 1]$	vector of observations	11
$\boldsymbol{C}$	$[n_c \times u]$	Jacobian matrix of pseudo observations	28
$\boldsymbol{c}$	$[n_c \times 1]$	vector of pseudo observations (constraints)	27, 72
$\boldsymbol{CF}$	$[3 \times 1]$	Center of Figure	62
$\boldsymbol{c_j}$	$[3 \times 1]$	3-dimensional cosine amplitudes of linear-trigonometric motion model of station j (named $\boldsymbol{c}_{\mathrm{ITRF}}$ in Section 3.1.6b)	22
$\boldsymbol{C_k}$	$[n_{c,k} \times u_k]$	Jacobian matrix of pseudo observations of the k-th equation system	31
$\boldsymbol{CM}$	$[3 \times 1]$	Center of Mass of the whole Earth (solid Earth plus its non-rigid envelope)	38, 40, 41, 51, 57, 62
c_{masc}	*scalar*	satellite-specific center of mass correction (difference between reflector and center of mass of the satellite in measurement direction) [m]	33, 34
c_{mesc}	*scalar*	SLR array-dependent correction (e.g., phase center offset in measurement direction) [m]	33, 34
C_{nm}	*scalar*	Harmonic cosine (Stokes) coefficient of degree n and order m	50
$\overline{C}_{nm}$	*scalar*	normalized Stokes (cosine) coefficient of degree n and order m	50
c_{rel}	*scalar*	relativistic range correction [m]	33, 34
c_{sta}	*scalar*	station-dependent SLR correction [m]	33, 34
c_{trop}	*scalar*	tropospheric range correction [m]	33, 34
$\boldsymbol{D}$	$[3 \times 3]$	3-dimensional rotation matrix around the Cardan angles with $\boldsymbol{D} = \boldsymbol{D_1}(\alpha)\boldsymbol{D_2}(\beta)\boldsymbol{D_3}(\gamma)$	23
$\boldsymbol{d}$	$[u \times 1]$	transformation (translation) vector of affine transformation	15
$\boldsymbol{d_t^c}(t_i)$	$[3 \times 1]$	3-dimensional translations common to all stations at epoch t_i	40
GM	*scalar*	Geocentric gravitational constant $GM = GM_{\oplus} = 3.986004418 \cdot 10^{14}\ \frac{m^3}{s^2}$	50
$\boldsymbol{H_j^{14}}$	$[6 \times 14]$	$(u_a = 14)$-parameter similarity transformation matrix for the j-th station	24
$\boldsymbol{H_j^7}$	$[3 \times 7]$	$(u_a = 7)$-parameter similarity transformation matrix for the j-th station	23
$\boldsymbol{I}$	$[u \times u]$	(quadratic) identity matrix ($\boldsymbol{I}_{[u]}$ has the dimension $[u \times u]$)	17
i	*scalar*	inclination of orbital plane of a satellite	48
k	*scalar*	index for k-th equation system with $1 \leq k \leq m$	30
$\hat{\boldsymbol{K}}_{\hat{\boldsymbol{q}}\hat{\boldsymbol{q}}}$	$[7/14 \times 7/14]$	variance-covariance matrix of the 7/14 datum parameters	30
$\hat{\boldsymbol{K}}_{\hat{\boldsymbol{x}}\hat{\boldsymbol{x}}}$	$[u \times u]$	variance-covariance matrix of the corrected unknowns	13
$\boldsymbol{K_{ll}}$	$[n \times n]$	variance-covariance matrix of the observations	13
$\boldsymbol{K_{ll,k}}$	$[n_k \times n_k]$	variance-covariance matrix of the observations of the k-th equation system	30
$\boldsymbol{l}$	$[n \times 1]$	vector of O-C	12, 14

L_C	*scalar*	scaling factor between TCG and TCB with TCG/TCB = $1 - L_C$ and $L_C = 1.48082686741 \cdot 10^{-8} \pm 2 \cdot 10^{-17}$	46
L_G	*scalar*	scaling factor between TT and TCG with $L_G = 1 - d(\mathrm{TT})/d(\mathrm{TCG}) = 6.969290134 \cdot 10^{-10}$	39
$\boldsymbol{l_k}$	$[n_k \times 1]$	vector of O-C of the k-th equation system	30
$\tilde{\boldsymbol{l}}$	$[n \times 1]$	vector of constrained/transformed O-C	16, 25
$\boldsymbol{M}$	$[u \times u]$	inverse matrix of $\boldsymbol{N}$	26
m	*scalar*	number of equation systems	30
N	*scalar*	number of parameter groups or stations ($1 \leq j \leq N$)	17
$\boldsymbol{N}$	$[u \times u]$	NEQ matrix	13, 14, 74
n	*scalar*	number of observation equations	11
$\boldsymbol{N_c}$	$[u \times u]$	combined NEQ matrix	31
n_c	*scalar*	number of pseudo observations (constraints)	27
$\boldsymbol{N_k}$	$[u_k \times u_k]$	k-th NEQ matrix	31
n_k	*scalar*	number of observation equations of the k-th equation system	30
N_{nm}	*scalar*	normalization factor of degree n and order m for Stokes coefficients	50
$\tilde{\boldsymbol{N}}$	$[u \times u]$	transformed NEQ matrix	16, 21
$p(t_i)$	*scalar*	parameter offset at epoch t_i	18
$\bar{p}(t_i)$	*scalar*	"regularized" parameter offset at epoch t_i	19
$\dot{\bar{p}}(t_i)$	*scalar*	"regularized" parameter drift at epoch t_i	19
$\boldsymbol{P_{cc}}$	$[n_c \times n_c]$	positive definite weight matrix of the pseudo observations	28
$\boldsymbol{P_{cc,k}}$	$[n_{c,k} \times n_{c,k}]$	positive definite weight matrix of the pseudo observations of the k-th equation system	31
$\dot{p}(t_i)$	*scalar*	parameter drift at epoch t_i	18
$\boldsymbol{P_{ll}}$	$[n \times n]$	positive definite weight matrix of the observations	13, 14
$\boldsymbol{P_{ll,k}}$	$[n_k \times n_k]$	positive definite weight matrix of the observations of the k-th equation system	30
$\tilde{\boldsymbol{P}}_{\boldsymbol{ll}}$	$[n \times n]$	constrained/transformed positive definite weight matrix of the observations	16, 25
P_{nm}	*scalar*	associated Legendre functions of degree n and order m	50
$\boldsymbol{Q}(t)$	$[3 \times 3]$	rotation matrix from the CIRS into the GCRS (using the "CIO-based transformation")	45
$\boldsymbol{q_0}$	$[u_a \times 1]$	vector of a priori values of the additional unknowns	20, 21
$\hat{\boldsymbol{q}}$	$[u_a \times 1]$	vector of corrected additional parameters	20, 75
$\boldsymbol{Q_{ll}}$	$[n \times n]$	positive definite weight coefficient (cofactor) matrix of the observations	12
$\boldsymbol{Q_{ll,k}}$	$[n_k \times n_k]$	positive definite weight coefficient (cofactor) matrix of the observations of the k-th equation system	30
$\boldsymbol{R}$	$[u \times u]$	transformation matrix of affine transformation	15, 75
$r(t_i)$	*scalar*	conventional "regularization" term r at the epoch t_i to account for effects due to zonal tides on Earth's rotation	19
r	*scalar*	redundancy (degree of freedom)	13
$r_{c,k}^{(j)}$	*scalar*	partial redundancy of the k-th NEQ system w.r.t. the combined NEQ system in the j-th iteration step	32
$\ddot{\boldsymbol{r}}_{\mathrm{sat}}$	$[3 \times 1]$	3-dimensional total acceleration acting on a near-Earth satellite	34
$\boldsymbol{r}_{\mathrm{sat}}$	$[3 \times 1]$	3-dimensional position of the satellite in the GCRS [m]	33, 34
$\boldsymbol{r}_{\mathrm{sta}}$	$[3 \times 1]$	3-dimensional position of the station in the ITRS [m]	33, 34
$\boldsymbol{R}(t)$	$[3 \times 3]$	rotation matrix from the TIRS into the CIRS (using the "CIO-based transformation")	45

$\boldsymbol{S}$	$[u \times u_a]$	transformation matrix of the additional unknowns $\hat{\boldsymbol{q}}$ to the unknown $\hat{\boldsymbol{x}}$	20
s	*scalar*	CIO locator: position of the CIO on the equator of the CIP	46
$\boldsymbol{s_j}$	$[3 \times 1]$	3-dimensional sine amplitudes of linear-trigonometric motion model of station j (named $\boldsymbol{s}_{\mathrm{ITRF}}$ in Section 3.1.6b)	22
S_{nm}	*scalar*	harmonic sine (Stokes) coefficient of degree n and order m	50
$\overline{S}_{nm}$	*scalar*	normalized Stokes (sine) coefficient of degree n and order m	50
s'	*scalar*	TIO locator: position of the TIO on the equator of the CIP	46
T	*scalar*	number of epochs ($1 \leq i \leq T$)	22
$\boldsymbol{T}$	$[u \times u]$	inverse of regular transformation matrix $\boldsymbol{R}$	16
$\boldsymbol{t}$	$[u \times 1]$	translation vector of a priori values	15
t_M	*scalar*	approximated epoch of reflection of the laser pulse at the satellite [s]	33, 34
u	*scalar*	number of unknowns	11
$\dot{u}_0$	*scalar*	rate of argument of latitude of a satellite at osculation epoch t_0	48
u_a	*scalar*	number of additional unknowns	20
u_e	*scalar*	number of eliminated unknowns	26
u_j	*scalar*	number of unknowns in j-th parameter group	17
u_k	*scalar*	number of unknowns of the k-th equation system	30
u_r	*scalar*	number of reduced unknowns	24, 73
u_t	*scalar*	number of transformed unknowns	17
V	*scalar*	gravitational potential	50
$\boldsymbol{v}$	$[n \times 1]$	vector of (observation and functional model) errors	11, 12
$\boldsymbol{v_c}$	$[n_c \times 1]$	vector of pseudo observation errors	28
$\hat{\boldsymbol{v}}$	$[n \times 1]$	vector of corrected (observation and functional model) errors	13
$\boldsymbol{v_k}$	$[n_k \times 1]$	vector of (observation and functional model) errors of the k-th equation system	30
$\tilde{\boldsymbol{v}}$	$[n \times 1]$	vector of transformed (observation and functional model) errors	16, 25
$\boldsymbol{W}(t)$	$[3 \times 3]$	rotation matrix from the ITRS into the TIRS	45
X_{CIP}	*scalar*	X-coordinate of celestial intermediate pole	46
$\boldsymbol{x}$	$[u \times 1]$	vector of unknowns	11
$\boldsymbol{x_0}$	$[u \times 1]$	vector of a priori values of the unknowns	11, 14
$\hat{\boldsymbol{x}}_{\boldsymbol{c}}$	$[u \times 1]$	vector of corrected parameters of the combined NEQ system	32
$\hat{\boldsymbol{x}}$	$[u \times 1]$	vector of corrected parameters	13, 14
$\boldsymbol{X}_{\mathrm{ITRF}}$	$[3 \times 1]$	ITRF station position	39
$\dot{\boldsymbol{X}}_{\mathrm{ITRF}}$	$[3 \times 1]$	ITRF station velocity	39
$\hat{\boldsymbol{x}}_{\boldsymbol{k}}$	$[u_k \times 1]$	vector of corrected parameters of the k-th equation system	31
$\boldsymbol{X_n}(t_i)$	$[3 \times 1]$	correction term n for $\boldsymbol{X_R}$ at epoch t_i	39
x_p	*scalar*	x-component of terrestrial pole coordinates (angles)	17, 46
$\boldsymbol{X_R}(t_i)$	$[3 \times 1]$	regularized station position at epoch t_i	39
$\boldsymbol{X}(t_i)$	$[3 \times 1]$	instantaneous station position at epoch t_i	39
$\tilde{\boldsymbol{x}}_{\boldsymbol{0}}$	$[u \times 1]$	vector of transformed a priori values	16
$\hat{\tilde{\boldsymbol{x}}}$	$[u \times 1]$	constrained/transformed vector of corrected parameters	18
$\tilde{\boldsymbol{X}}(t_i)$	$[3 \times 1]$	estimated station position offset at frequent epochs t_i	42
$\boldsymbol{y}$	$[u \times 1]$	right hand side of the NEQ system	13, 14
$\boldsymbol{y_c}$	$[u \times 1]$	right hand side of the combined NEQ system	31
Y_{CIP}	*scalar*	Y-coordinate of celestial intermediate pole	46
$\boldsymbol{y_k}$	$[u_k \times 1]$	right hand side of the k-th NEQ system	31
y_p	*scalar*	y-component of terrestrial pole coordinates (angles)	46
$\tilde{\boldsymbol{y}}$	$[u \times 1]$	right hand side of the transformed NEQ system	16, 21

List of Figures

All figures except Figure 2.2 have been compiled with Inkscape, version 0.48 or Generic Mapping Tools (GMT), version 4.5.8.

List of Tables

Bibliography

Altamimi Z., Sillard P., Boucher C. (2002) ITRF2002: a new release of the International Terrestrial Reference Frame for Earth Science Applications. In: J Geophys Res 107(10), DOI 10.1029/2001JB000561

Altamimi Z., Collilieux X., Legrand J., Garayt B., Boucher C. (2007) ITRF2005: A new release of the International Terrestrial Reference Frame based on time series of station positions and Earth orientation parameters. In: J Geophys Res 112(09), DOI 10.1029/2007JB004949

Altamimi Z., Collilieux X., Métivier L. (2011) ITRF2008: an improved solution of the international terrestrial reference frame. In: J Geodesy 85(8), pp: 457–473, DOI 10.1007/s00190-011-0444-4

Angermann D., Drewes H., Krügel M., Meisel B., Gerstl M., Kelm R., Müller H., Seemüller W., Tesmer V. (2004) ITRS Combination Center at DGFI: A Terrestrial Reference Frame Realization 2003. In: Deutsche Geodätische Kommission, B Series 313, Verlag der Bayerischen Akademie der Wissenschaften, München, ISBN: 3-7696-8593-8

Angermann D., Müller H. (2009) On the Strength of SLR Observations to Realize the Scale and Origin of the Terrestrial Reference System. In: Observing our Changing Earth, IAG Symposia Series 133, ed: Sideris M. G., pp: 21–29, DOI 10.1007/978-3-540-85426-5_3

Angermann D., Gerstl M., Sánchez L., Gruber T., Hugentobler U., Steigernberger P. (2014) GGOS Bureau for Standards and Conventions: Inventory of standards and conventions for geodesy. In: IAG Symposia Series 143, in press

Argus D. F., Gordon R. G. (1991) No-Net-Rotation model of current plate velocities incorporating plate motion model NUVEL-1. In: Geophys Res Lett 18(11), pp: 2039–2042, DOI 10.1029/91GL01532

Argus D. F., Gordon R. G., DeMets C. (2011) Geologically current motion of 56 plates relative to the no-net-rotation reference frame. In: Geochem Geophys Geosys 12(11), DOI 10.1029/2011GC003751

Arias E. F., Charlot P., Feissel M., Lestrade J. F. (1995) The extragalactic reference system of the International Earth Rotation Service, ICRS. In: Astron Astrophys 303, pp: 604–608

Bachmann S., Lösler M., Messerschmitt L., Schmid R., Bloßfeld M., Thaller D. (2014) BKG/DGFI Combination Center Annual Report 2013. In: International VLBI Service for Geodesy and Astrometry 2013 Annual Report, eds: Baver K. D., Behrend D., Armstrong K. L., pp: 257-260, NASA/TP-2014-217522

Bawden G. W., Thatcher W., Stein R. S., Hudnut K. W., Peltzer G. (2001) Tectonic contraction across Los Angeles after removal of groundwater pumping effects. In: Nature 412, pp: 812–815, DOI 10.1038/35090558

Beutler G. (2005a) Methods of Celestial Mechanics - I: Physical, Mathematical and Numerical Principles. In: Astronomy and Astrophysics Library, Springer-Verlag, Berlin Heidelberg New York, ISBN-3: 3-540-40749-9

Beutler G. /2005b) Methods of Celestial Mechanics - II: Application to Planetary System, Geodynamics and Satellite Geodesy. In: Astronomy and Astrophysics Library, Springer-Verlag, Berlin Heidelberg New York, ISBN-3: 3-540-40750-2, 2005b

Bevis M., Alsdorf D., Kendrick E., Fortes L. P., Forsberg B., Smalley R. Jr., Becker J. (2005) Seasonal fluctuations in the mass of the Amazon River system and Earth's elastic response. In: Geophys Res Lett 32(L16308), DOI 10.1029/2005GL023491

Bizouard C., Gambis D. (2009) The Combined Solution C04 for Earth Orientation Parameters Consistent with International Terrestrial Reference Frame 2005. In: Geodetic Reference Frames, pp: 265–270, IAG Symposia Series 134, eds: Drewes H. and Bosch W., Springer-Verlag, Berlin Heidelberg New York, DOI 10.1007/978-3-642-00860-3_41

Bizouard C., Gambis D. (2011) The combined solution C04 for Earth Orientation Parameters consistent with International Terrestrial Reference Frame 2008. In: Technical Note, URL: `http://hpiers.obspm.fr/iers/eop/eopc04/C04.guide.pdf`, (2014-07-18)

Blewitt G., Lavallée D. (2002) Effect of annual signals on geodetic velocity. In: J Geophys Res 107(7), DOI 10.1029/2001JB000570

Blewitt G (2003) Self-consistency in reference frames, geocenter definition, and surface loading of the solid Earth. In: J Geophys Res 108(B2), DOI 10.1029/2002JB008082

Bloßfeld M., Seitz M. (2012) The role of VLBI in the weekly inter-technique combination. In: Proceedings of the IVS 2012 General Meeting, pp: 319–323, eds: Behrend D. and Baver K. D., NASA/CP-2012-217504

Böckmann S., Artz T., Nothnagel S. (2010) VLBI terrestrial reference frame contributions to ITRF2008. In: J Geodesy 84(3), pp: 201–219, DOI 10.1007/s00190-009-0357-7

Böckmann S., Artz T., Nothangel A., Tesmer V. (2010) International VLBI Service for Geodesy and Astrometry: Earth orientation parameter combination methodology and quality of the combined products. In: J Geophys Res 115(B04404), DOI 10.1029/2009JB006465

Bouman J., Florberghagen R., Rummel R. (2013) More Than 50 Years of Progress in Satellite Gravimetry. In: EOS Transactions 94(31), pp: 269–276, American Geophysical Union, DOI 10.1002/2013EO310001

Bowman B., Tobiska K., Marcos F., Huang C., Lin C., Birke W. (2008) A New Empirical Thermospheric Density Model JB2008 Using New Solar and Geomagnetic Indices. In: AIAA/AAS Astrodynamics Specialist Conference and Exhibit, DOI 10.2514/6.2008-6438

Capitaine N. (2002) Comparison of "Old" and "New" Concepts: The Celestial Intermediate Pole and Earth Orientation Parameters. In: Proceedings of the IERS Workshop on the Implementation of the New IAU Resolutions, pp 35–44, eds: Capitaine N., Gambis D., McCarthy D. D., Petit G., Ray J., Richter B., Rothacher M., Standish M. and Vondrak J., IERS Technical Note 29, Frankfurt am Main, Verlag des Bundesamts für Kartographie und Geodäsie, ISBN: 3-89888-866-5

Capitaine N., Wallace P. T., Chapront J. (2003) Expressions for IAU 2000 precession quantities. In: Astron Astrophys 412, pp:567–586, DOI 10.1051/0004-6361:20031539

Chen J. L., Rodell M., Wilson C. R., Famiglietti J. S. (2005) Low degree spherical harmonic influences on Gravity Recovery and Climate Experiment (GRACE) water storage estimates. In: Geophys Res Lett 32(L14405), DOI 10.1029/2005GL022964

Cheng M. K., Ries J. C. (2012) GRACE Technical Note 05. `ftp://podaac.jpl.nasa.gov/allData/grace/docs/TN-05_C20_SLR.txt`

Cheng M. K., and Ries J. C. (2013) GRACE Technical Note 07. `ftp://podaac.jpl.nasa.gov/allData/grace/docs/TN-07_C20_SLR.txt`

Ciufolini I. (1987) The LAGEOS Lense-Thirring precession and the LAGEOS non-gravitational nodal perturbations - I. In: Celestial Mech 40(1), pp: 19–33, DOI 10.1007/BF01232322

Ciufolini I. (1989) LAGEOS 3 and the gravitomagnetic field. In: NASA Workshop on Relativistic Gravitation Experiments in Space, Annapolis, Maryland, June 1988, NASA,Conf. Publ.,3046, 126

Collilieux X., Altamimi Z., Ray J., van Dam T., Wu X. (2009) Effect of the satellite laser ranging network distribution on geocenter motion estimates. In: J Geophys Res 114(B4), DOI 10.1029/2008.JB005727

Combrinck L. (2010) Satellite Laser Ranging. In: Sciences of Geodesy - I: Advances and Future Directions, pp: 301–338, ed: Xu G., Springer-Verlag, Berlin Heidelberg New York, DOI 10.1007/978-3-642-11741-1_9

de Sitter W. (1916) On Einstein's theory of gravitation and its astronomical consequences. In: Monthly Notices of the Royal Astronomical Society 77, pp: 155–184

Dettmering D., Heinkelmann R., Schmidt M., Seitz M. (2010) Die Atmosphäre als Fehlerquelle und Zielgröße in der Geodäsie. In: ZfV 135(2), pp:100–105, (in German)

Dong D., Yunck T., Heflin M. (2003) Origin of the International Terrestrial Reference Frame. In: J Geophys Res 108(B4), DOI 10.1029/2002JB002035

Drewes H. (2009) The Actual Plate Kinematic and Crustal Deformation Model APKIM2005 as basis for a non-rotating origin. In: Reference Frames, IAG Symposia 134, ed; Drewes H., pp: 95–99, DOI 10.1007/978-3-642-00860-3_15

Dong D., Yunck T., Heflin M. (2003) Origin of the International Terrestrial Reference Frame. In: J Geophys Res 108(B4), DOI 10.1029/2002JB002035

Donovan H., Wetzel S., Ma C., Hase H., Behrend D., Pearlsman M., Noll C., Pavlis E., Long J., Stowers D., McCormick D., Emerson C. (2011) Global Geodetic Observing System (GGOS) - Site Requirements for GGOS Core Sites. http://cddis.gsfc.nasa.gov/docs/GGOS_SiteReqDoc.pdf

ESA (1999) Gravity field and steady-state ocean circulation mission. In: Reports for mission selection; the four candidate earth explorer core missions, ESA SP-1233(1)

Flechtner F., Dahle C., Gruber C., Sasgen I., König R., Michalak G., Neumayer K.-H. (2013) Status GFZ RL05 and RL05a GRACE L2 Products. In: GRACE Science Team Meeting, Austin, TX, USA, October 23-25, 2013

Förste C., Bruinsma S. L., Flechtner F., Marty J. C., Lemoine J. M., Dahle C., Abrikosov O., Neumayer K. H., Biancale R., Barthelmes F., Balmino G. (2012) A preliminary update of the Direct approach GOCE Processing and a new release of EIGEN-6C. Presented at the AGU Fall Meeting 2012, San Francisco, USA, 3-7 Dec, Abstract No. G31B-0923

Freymueller J. T. (2010) Active tectonics of plate boundary zones and the continuity of plate boundary deformation from Asia to North America. In: Curr Sci India 99(12), pp: 1719–1732

Gambis D., Bizouard C., Richard J. Y., Carlucci T., Becker O., Baudoin P. (2013) Reports of IERS components - Earth Orientation Centre. In: IERS Annual Report 2011. ed: Dick W. R., International Earth Rotation and Reference Systems Service, Verlag des Bundesamts für Kartographie und Geodäsie, Frankfurt am Main, pp: 70–83, ISBN: 978-3-86482-046-5

Gauß C. F. (1823) Theoria combinationis observationum. Henricus Dieterich, Gottingae, (in Latin)

Gerstl M. (1997) Parameterschätzung in DOGS-OC. In: DGFI Interner Bericht, MG/01/1996/DGFI, 2nd edition (in German)

Gerstl M., Kelm R., Müller H., Ehrensperger W. (2001) DOGS-CS Kombination und Lösung großer Gleichungssysteme. In: DGFI Interner Bericht, MG/01/1995 (in German)

Gross R., Beutler G., Plag H. P. (2009) Integrated scientific and societal user requirements and functional specifications for the GGOS. In: Global Geodetic Observing System - Meeting the Requirements of a Global Society on a Changing Planet in 2020, pp: 209–224, Springer Verlag, Berlin Heidelberg New York, eds: Plag H. P. & Pearlman M. R., DOI 10.1007/978-3-642-02686-7

Göttl F. (2013) Kombination geodätischer Raumbeobachtungen zur Bestimmung von geophysikalischen Anregungsmechanismen der Polbewegung. In: Deutsche Geodätische Kommission, C Series 741, Verlag der Bayerischen Akademie der Wissenschaften, München, ISBN: 978-3-7696-5126-3 (in German)

Heiskanen W. A., Moritz H. (1967) Physical Geodesy. W. H. Freeman and Company, San Francisco, ISBN-10: 0716702339

Hofmann-Wellenhof B., Moritz H. (2006) Physical Geodesy. Second edition, Springer, Wien, ISBN-10: 3-211-33544-7

Hugentobler U., Gruber T., Steigenberger P., Angermann D., Bouman J., Gerstl M., Richter B. (2012) GGOS Bureau for Standards and Conventions: Integrated Standards and Conventions for Geodesy. In: Geodesy for Planet Earth, pp: 995-998, IAG Symposia Series 136, eds: Kenyon S. C., Pacino M. C., Marti U. J., Springer Berlin Heidelberg, DOI 10.1007/978-3-642-20338-1_124

IAG Resolution 16 (1983). 16th General Assembly of the IAG, Hamburg

IAU Resolution B1.5 (2006) Extended relativistic framework for time transformations and realization of coordinate times in the solar system. http://www.iau.org/administration/resolutions/general_assemblies/, (2014-07-18)

IAU Resolution B1.8 (2006) Definition and use of Celestial and Terrestrial Ephemeris Origins. http://www.iau.org/administration/resolutions/general_assemblies/, (2014-07-18)

IAU Resolution B1.9 (2006) Re-definition of Terrestrial Time TT. http://www.iau.org/administration/resolutions/general_assemblies/, (2014-07-18)

Iorio L. (2002) The impact of the static part of the Earth's gravity field on some tests of general relativity with satellite laser ranging. In. Celest Mech Dyn Astr 86(3), pp: 277–294, DOI 10.1023/A:1024223200686

IUGG Resolution 3 (2003) Integrated Global Geodetic Observing System (IGGOS). http://www.iugg.org/assemblies/2003sapporo/, (2014-08-04)

IUGG Rsolution 2 (2007) Geocentric and International Terrestrial Reference Systems (GTRS and ITRS). http://www.iugg.org/assemblies/2007perugia/, (2014-07-23)

IUGG Rsolution 3 (2007) Global Geodetic Observing System (GGOS) of the International Association of Geodesy (IAG). http://www.iugg.org/assemblies/2007perugia/, (2014-08-04)

Kaplan G. H. (2005) Celestial pole offsets: Conversion from (dX,dY) to ($d\psi$, $d\epsilon$). In: U. S. Naval Observatory Tech. Note

Kaula W. M. (1966) Theory of Satellite Geodesy - Applications of Satellites to Geodesy. In: Blaisdell Publishing Company, Waltham, Massachusetts, ISBN: 0-486-41465-6, 1966

Koch K. R., Kusche J. (2002) Regularization of geopotential determination from satellite data by variance components. In: J Geodesy 76(5), pp: 259–268, DOI 10.1007/s00190-002-0245-x

Koch K. R. (2004) Parameterschätzung und Hypothesentests in linearen Modellen. Vierte, bearbeitete Auflage, *http://www.geod.uni-bonn.de*, Ehemals Ferd. Dümmlers Verlag, Bonn (in German)

Kovalevsky J., Mueller I. I. (1989) Introduction In: Reference Frames in Astronomy and Geophysics, eds: Kovalevsky J., Mueller I. I., Kolaczek B., Kluwer Academic Publishers, ISBN: 0-7923-0182-X

Lense J., Thirring H. (1918) Über den Einfluss der Eigenrotation

der Zentralkörper auf die Bewegung der Planeten und Monde nach der Einsteinschen Gravitationstheorie. In: Physikalische Zeitschrift 19(159), pp: 156–163 (in German)

Liu H. S., Chao B. F. (1991) The Earth's equatorial principal axis and moments of inertia. In: Geophys J Int 106(3), pp: 699–702, DOI 10.1111/j.1365-246X.1991.tb06341.x

Lucchesi D. M. (2001) Reassessment of the error modeling of non-gravitational perturbations on LAGEOS II and their impact in the Lense–Thirring determination. Part I. In: Planet Space Sci 49(5), pp: 447–463, DOI 10.1016/S0032-0633(00)00168-9

Lucchesi D. M. (2002) Reassessment of the error modeling of non-gravitational perturbations on LAGEOS II and their impact in the Lense–Thirring derivation-Part II. In: Planet Space Sci 50(10-11), pp: 1067–1100, DOI 10.1016/S0032-0633(02)00052-1

Mäkinen J, Ihde J. (2008) The Permanent Tide In Height Systems. In: Observing our Changing Earth, IAG Symposia 133, ed: Sideris M. G., pp: 81–87, DOI 10.1007/978-3-540-85426-5_10

Markov A. A. (1912) Wahrscheinlichkeitsrechnung. Zweite Auflage, Liebmann H. (Übers.), B. G. Teubner, Leipzig, Berlin

Mathews P. M., Herring T. A., Buffet B. A. (2002) Modeling of nutation and precession: New nutation series for nonrigid Earth, and insights into the Earth's interior. In: J Geophys Res 107(B4), DOI 10.1029/2001JB000390

Meisel B., Angermann D., Krügel M. (2009) Influence of Time Variable Effects in Station Positions on the Terrestrial Reference Frame. In: Geodetic Reference Frames, pp: 89-93, IAG Symposia Series 134, ed: Drewes H., Springer Berlin Heidelberg, DOI 10.1007/978-3-642-00860-3_14

Nothnagel A., Angermann D., Börger K., Dietrich R., Drewes H., Görres B., Hugentobler U., Ihde J., Müller J., Oberst J., Pätzold M., Richter B., Rothacher M., Schreiber U., Schuh H., Soffel M. (2010) Space-Time Reference Systems for Monitoring Global Change and for Precise Navigation. In: Mitteilungen des Bundesamtes für Karthographie und Geodäsie, Band 44, Verlag des Bundeamtes für Karthographie und Geodäsie, ISBN: 978-3-89888-920-9, (in German)

Pail R., Goiginger H., Schuh W. D., Höck E., Brockmann J. M., Fecher T., Gruber T., Mayer-Gürr T., Kusche J., Jäggi A., Rieser D. (2011) Combined satellite gravity field model GOCO01S derived from GOCE and GRACE. In: Geophys Res Lett 37(L20314), DOI 10.1029/2010GL044906

Petit G., Luzum B. (2010) IERS Conventions (2010). In: IERS Tech. Note 36, Verlag des Bundesamtes für Kartographie und Geodäsie, ISBN: 978-3-89888-989-6

Plag H. P., Pearlman R. (2009) Global Geodetic Observing System - Meeting the Requirements of a Global Society on a Changing Planet in 2020. In: Springer Verlag, Berlin Heidelberg New York, eds: Plag H. P. & Pearlman M. R., DOI 10.1007/978-3-642-02686-7

Ratcliff J. T., Gross R. S. (2013) Combinations of Earth Orientation Measurements: SPACE2011, COMB2011 and POLE2011. In: JPL Publication 13-5

Rebischung P. (2014) Can GNSS contribute to improving the ITRF definition?. Dissertation, l'Observatoire de Paris

Rodriguez-Solano C., Hugentobler U., Steigenberger P. (2012) Adjustable box-wing model for solar radiation pressure impacting GPS satellites. In: Adv Space Res 49(7), pp: 1113–1128, DOI 10.1016/j.asr.2012.01.016

Rothacher M., Beutler G., Herring T. A. (1999) Estimation of nutation using Global Positioning System. In: J Geophys Res 104(B3), pp: 4835–4859, DOI 10.1029/1998JB900078

Rothacher M., Angermann D., Artz T., Bosch W., Drewes H., Böckmann S., Gerstl M., Kelm R., König D., König R., Meisel B., Müller H., Nothnagel A., Panafidina N., Richter B., Rudenko S., Schwegmann W., Seitz M., Steigenberger P., Tesmer V., Thaller D. (2011) GGOS-D: homogeneous reprocessing and rigorous combination of space geodetic observations. In: J Geodesy 85(10), pp: 679–705, DOI 10.1007/s00190-011-0475-x

Rummel R., Rothacher M., Beutler G. (2005) Integrated Global Geodetic Observing System (IGGOS) - science rationale. In: J Geodyn 40(4-5), pp: 357–362, DOI 10.1016/j.jog.2005.06.003

Rummel R. (2014) Geodäsie in Zeiten des Wandels - Versuch einer Standortbestimmung. In: ZfV 139(4), pp: 211–216, DOI 10.12902/zfv-0034-2014, (in German)

Schuh H., Dill R., Greiner-Mai H., Kutterer H., Müller J., Nothnagel A., Richter B., Rothacher M., Schreiber U., Soffel M. (2003) Erdrotation und globale dynamische Prozesse. In: Mitteilungen des Bundesamtes für Kartographie und Geodäsie, Band 32, Verlag des Bundesamtes für Kartographie und Geodäsie, ISBN:3-89888-883-5, (in German)

Seitz M. (2009) Kombination geodätischer Raumbeobachtungsverfahren zur Realisierung eines terrestrischen Referenzsystems. In: Deutsche Geodätische Kommission, C Series 630, Verlag der Bayerischen Akademie der Wissenschaften, München, ISBN: 978-3-7696-5042-6 (in German)

Seitz F., Schuh H. (2010) Earth Rotation. In: Sciences of Geodesy - I: Advances and Future Directions, pp:185–227, Springer-Verlag, Berlin Heidelberg New York, ed: Xu G., DOI 10.107/978-3-642-11741-1_6

Seitz M. (2015) Comparison of Different Combination Strategies Applied for the Computation of Terrestrial Reference Frames and Geodetic Parameter Series. In: The 1st International Workshop on the Quality of Geodetic Observation and Monitoring Systems (QuGOMS'11) 2011, IAG Symposia Series 140, pp: 57–64, eds: Kutterer H., Seitz F., Alkhatib H., Schmidt M., DOI 10.1007/978-3-319-10828-5_9

Seitz M., Angermann D., Gerstl M., Bloßfeld M., Sánchez L., Seitz F. (2015) Geometrical Reference Systems. In: Handbook of Geomathematics (Second Edition), eds: Freeden W., Nashed M. Z., Sonar T., in press

Shepherd A. and 46 others (2012) A Reconciled Estimate of Ice-Sheet Mass Balance. In: Science, 338(6111), pp: 1183–1189, DOI 10.1126/science.1228102

Sillard P., Boucher C. (2001) A review of algebraic constraints in terrestrial reference frame datum definition. In: J Geodesy 75(2-3), pp: 63–73, DOI 10.1007/s001900100166

Springer T. (2009) NAPEOS Mathematical Models and Algorithms. `ftp://dgn6.esoc.esa.int/napeos/DOPS-SYS-TN-0100-OPS-GN-MathModels.pdf`

Sośnica K., Jäggi A., Thaller D., Dach R., Beutler G. (2014) Contribution of Starlette Stella and AJISAI to the SLR-derived global reference frame. In: J Geodesy 88(8), pp: 789-804, DOI 10.1007/s00190-014-0722-z

Sośnica K. (2014) Determination of Precise Satellite Orbits and Geodetic Parameters using Satellite Laser Ranging. Dissertation, ISBN: 978-83-938898-0-8, `http://www.bernese.unibe.ch/publist/publist.php#thesis`

Tapley B. D., Bettadpur S., Ries J. C., Thompson P. F., Watkins M. M. (2004) GRACE Measurements of Mass Variability in the Earth System. In: Science 305(5683), pp: 503–505, DOI 10.1126/science.1099192

Thaller D. (2008) Inter-technique combination based on homogeneous equation systems including station coordinates, Earth orientation and troposphere parameters. In: Scientific Technical Report STR 08/15, Deutsches GeoForschungsZentrum (GFZ), DOI 10.2312/GFZ.b103-08153

Torge W. (2001) Geodesy. 3rd edition, Berlin; New York, deGruyter, ISBN: 3-11-017172-8

Tregoning P., van Dam T. (2005) Effects of atmospheric pressure loading and seven-parameter transformations on esti-

mates of geocenter motion and station heights from space geodetic observations. In: J Geophys Res 110(B3), DOI 10.1029/2004JB003334

Willis P., Lemoine F. G., Moreaux G., Soudarin L., Ferrage P., Ries J., Otten M., Saunier J. Noll C., Biancale R., Luzum B. (2015) The International DORIS Service (IDS) - Recent developments in preparation for ITRF2013. In: IAG Symposia Series 143, in press

Wu X., Ray J., van Dam T. (2012) Geocenter motion and its geodetic and geophysical implications. In: J Geodyn 58, pp: 44–61, DOI 10.1016/j.jog.2012.01.007

Curriculum vitae

Name:	Mathis Bloßfeld
Geburtsdatum:	27. Dezember 1984
Geburtsort:	Leipzig
Nationalität:	Deutsch
Familienstand:	verheiratet

Mitgliedschaft in internationalen Forschergruppen

seit 09/2012	Mitglied der Joint Working Group 1.3 “Strategies for Epoch Reference Frames” der International Association of Geodesy (IAG)
seit 05/2011	Mitglied der Working Group “Combination on Observation Level (COL)” des International Earth Rotation and Reference Systems Service (IERS)
seit 01/2011	Mitglied der “Analysis Working Group” (AWG) des International Laser Ranging Service (ILRS)

Beruflicher Werdegang

seit 04/2009	Wissenschaftlicher Mitarbeiter am Deutschen Geodätischen Forschungsinstitut (DGFI)
10/2008 - 03/2009	Tutor für Numerical Modeling (Dozent: apl. Prof. Dr.-Ing. Michael Schmidt)
10/2008 - 03/2009	Tutor für Introduction to Satellite Navigation (Dozent: Univ.-Prof. Dr. Christoph Günther)
04/2008 - 09/2008	Tutor für Software Engineering (Dozent: Dr.-Ing. Thomas Gruber)
05/2007 - 03/2009	Studentische Hilfskraft am Deutschen Geodätischen Forschungsinstitut (DGFI)
03/2007 - 04/2007	Praktikum am Deutschen Geodätischen Forschungsinstitut (DGFI)

Ausbildung

10/2004 - 03/2009	Technische Universität München (TUM) Studiengang: Geodäsie und Geoinformation Vertiefungsrichtung: Erdmessung und Satellitennavigation Abschluss: Diplom-Ingenieur Geodäsie und Geoinformation
	Diplomarbeit: Eigenschwingungen der Erde aus Beobachtungen mit dem 30m Vertikalpendel in Berchtesgaden, Begutachter: apl. Prof. Dr.-Ing. Michael Schmidt
	Studienarbeit: Geographische Verteilung von mit der COSMIC-Satelliten-konstellation gemessenen GPS-Okkultationen, Begutachter: Univ.-Prof. Dr. phil. nat. Urs Hugentobler
09/1995 - 06/2004	Finsterwalder-Gymnasium Rosenheim Abschluss: allgemeine Hochschulreife (Abitur)
09/1991 - 08/1995	Grundschule Happing, Rosenheim

Auszeichnungen

2013	Best Presentation Award der International Association of Geodesy (IAG) (IAG Symposium 2013, Potsdam)
2013	Bernd-Rendel Preis der Deutschen Forschungsgemeinschaft (DFG)
2013	Young Scientist's Travel Award for European of the European Geosciences Union (EGU)
2012	Young Author Award (Ko-Autor) der International Association of Geodesy (IAG)
2009	Best Presentation Award (Geodätische Woche 2009, Karlsruhe)
2009	Habert-Buchpreis des Deutschen Vereins für Vermessungswesen e.V. für hervorragende Leistungen im Studium

Acknowledgments

An dieser Stelle möchte ich mich bei meinem Doktorvater, Herrn Univ.-Prof. Dr. phil. nat. Urs Hugentobler sehr herzlich für die Betreuung meiner Arbeit bedanken. Prof. Hugentobler begeisterte mich bereits als Student für die physikalische Geodäsie und hat großen Anteil daran, dass ich in diesem Arbeitsfeld meine berufliche Erfüllung gefunden habe. Durch zahlreiche Diskussionen über die Dynamik von Satellitenbahnen hat Prof. Hugentobler maßgeblich zum Gelingen dieser Arbeit beigetragen. Auch möchte ich mich bei meinem zweiten Gutachter, Herrn Univ.-Prof. Dr.-Ing. Florian Seitz bedanken, der mich zudem als Institutsdirektor des DGFI immer sehr unterstützt hat und es mir ermöglichte, durch zahlreiche Teilnahmen an wissenschaftlichen Konferenzen eine internationale Vernetzung mit anderen Wissenschaftlern aufzubauen. Herrn Univ.-Prof. phil. nat. Markus Rothacher möchte ich herzlich für die Begutachtung meiner Doktorarbeit danken.

Mein herzlicher Dank gilt allen Mitarbeiterinnen und Mitarbeitern des DGFI für ihren Beitrag zu einer durchgehend angenehmen und freundschaftlichen Atmosphäre an unserem Institut. Ganz besonders bedanken möchte ich mich bei Frau Dr.-Ing. Manuela Seitz, die mich sehr intensiv unterstützt hat und geduldig auf alle meine Fragen geantwortet hat. Herrn Dr.-Ing. Detlef Angermann möchte ich für die berufliche und freundschaftliche Unterstützung und die Freiheit danken, meine Forschungsschwerpunkte weitgehend selbst nach meinen Interessen wählen zu dürfen. Herrn Dipl.-Ing. Horst Müller und Herrn Dr. rer. nat. Michael Gerstl möchte ich für die geduldige Einführung und Unterstützung in unsere Software danken, ohne die ich niemals diese Arbeit hätte bewältigen können. Herrn apl. Prof. Dr.-Ing. Michael Schmidt möchte ich danken, dass er mich durch die Betreuung meiner Diplomarbeit ans DGFI gelotst hat und mir jederzeit mit Rat und Tat zur Seite steht.

Diese Arbeit ist im Rahmen der Forschergruppe "Erdrotation und globale dynamische Prozesse" der Deutschen Forschungsgemeinschaft (DFG) entstanden, bei der meine Untersuchungen durch zahlreiche konstruktive Diskussionen an Klarheit gewonnen haben.

Zuletzt möchte ich meiner Familie und allen voran meiner Frau Julia danken, die mich immer unterstützt hat und mich stets ermutigte, diesen Weg weiter zu gehen.